PROPAGATION AND INSTABILITIES OF OBLIQUELY PROPAGATING WHISTLER MODE WAVES IN A HOT MAGNETOSPHERIC PLASMA

by

Kozo HASHIMOTO

May 1980

Department of Electrical Engineering

Kyoto University, Kyoto, Japan

PROPAGATION AND INSTABILITIES OF OBLIQUELY PROPAGATING WHISTLER MODE WAVES IN A HOT MAGNETOSPHERIC PLASMA

by

Kozo HASHIMOTO

May 1980

Department of Electrical Engineering

Kyoto University, Kyoto, Japan

ACKNOWLEDGEMENTS

The author wishes to express his sincere and hearty appreciation to Professor Iwane Kimura for his continual guidance, inspiration and stimulating supervision throughout the present work and for his careful reading of the manuscript.

The author is deeply indebted to Dr. Hiroshi Matsumoto for his useful guidance, critical discussion and careful reading of the manuscript.

The author also wishes to express his deep appreciation to Emeritus Professor Ken-ichi Maeda for his useful advices and encouragement, and to Professors Susumu Kato, Toru Ogawa, Ryohei Itatani, and Hiromu Momota, now Professor of Nagoya University,for their valuable discussion and encouragement.

The author is deeply grateful to Professor Hiroshi Oya of Tohoku University for his valuable advice at the biginning of the present work and his useful comments.

The author is grateful to Drs. Kazuaki Takao, Tsutomu Yabuzaki, Shoichiro Fukao, Takehiko Aso, Isamu Nagano, and Masaharu Fujita and Messrs. Minoru Tsutsui and Sadao Miyatake for their discussion and useful suggestions. He also indebted to Mr. Hiroshi Kumagai for his discussion and co-works in Chapter 5.

Thanks are also due to discussion with colleagues in Kimura's Laboratory of the Department of Electrical Engineering and the Ionosphere Research Laboratory of Kyoto University.

All numerical computations were performed at the Data Processing Center, Kyoto University, Kyoto, Japan.

PREFACE

There have been many kinds of very low frequency (VLF) wave phenomena observed by satellites and on the ground. Generation mechanisms and propagation of these waves in the magnetosphere are greatly affected by thermal or nonthermal characteristics of the plasmas. The "whistlers" which are produced by ordinary lightning discharges and the "VLF emissions" which are originated in the magnetosphere are a couple of well-known VLF electromagnetic wave phenomena. Generation mechanisms of these emissions are not yet thoroughly understood. The propagation of these waves in the magnetosphere is classified into two types: ducted and non-ducted propagation. The former is the propagation in an enhanced ionization duct which lies along a geomagnetic field line. The latter is the propagation without assistance of the ducts. Its ray paths are calculated by "ray tracing" i.e. by numerically integrating the differential euqations for the ray. Both types of propagation can be observed by satellites, although non-ducted VLF waves can not always be observed on the ground. The electrostatic wave phenomena in the VLF range are observed only by satellites.

The causes of the VLF emissions have been thought to be due to a cyclotron instability, Cerenkov radiation, or Cerenkov instability. The cyclotron instability occurs in the whistler mode by an anisotropy of plasmas, or by an interaction of the wave with a counter-streaming electron beam. The cyclotron instability of whistler mode waves has been studied mainly for propagation along the geomagnetic field lines i.e. for ducted propagation.

The present author's study has an emphasis on instabilities for obliquely propagating (or non-ducted) whistler mode in a bi-Maxwellian hot plasma and on the quasi-electrostatic whistler mode instabilities as well.

A microscopic theory derived from the collisionless Boltzmann equation and an electrostatic approximation are applied to the analysis of these instabilities. The growth rate and polarizations of these modes are studied and an interpretation of some narrow-band VLF emissions above the local half cyclotron frequency is attempted.

In order to calculate whistler mode ray paths in hot plasmas, the ray tracing technique in cold plasmas is extended by a warm plasma approximation. The results are applied to a method of estimation of the electron temperature from wave damping during the propagation in the magnetosphere.

New approximated equations for growth rates in a two-component (cold + bi-Maxwellian) plasma are derived and the net growth along non-ducted paths is calculated. Effects of the Landau damping on the growth rates are also discussed.

In order to consider the effect of beam a comparison between the cyclotron instability caused by a temperature anisotropy and that by a counter-streaming electron beam is studied. From a transition analysis between them their essential energy sources are found to be identical.

CONTENTS

CHAPTER 1

GENERAL INTRODUCTION

1-1 Introduction

VLF emissions are one of very interesting wave phenomena in the magnetosphere. Some of these emissions have been explained mainly by an instability due to a wave-particle cyclotron interaction of spiraling energetic electrons with whistler mode waves propagating along the geomagnetic field. Less attention has been paid to propagation and instability in obliquely propagating whistler mode waves in a hot plasma. The main purpose of the present thesis is mainly to investigate these two items in more detail. A cyclotron instability of the obliquely-propagating whistler mode waves is analysed in both electromagnetic and electrostatic regions. The electrostatic nature is discussed in relation to the Harris instability.

Another topic to be dealt with is the ray paths of whistler mode waves in the inhomogeneous magnetospheric plasma. A ray tracing computer program is developed for the waves in the media consisting of both cold and hot and hot plasmas. This chapter is devoted to a brief review of related basic theories.

Sections 1-2 to 5 of this chapter are concerned with wave phenomena in a homogeneous hot plasma; the whistler mode cyclotron instability, the microscopic theory of the dispersion relation in a bi-Maxwellian plasma, the warm plasma approximation and the electrostatic approximation, respectively. In section 1-2, the dispersion relation of longitudinally

propagating whistler mode waves and their growth rate are derived. In section 1-3, the dispersion relation in a bi-Maxwellian hot plasma is derived according to Stix (1962).

In sections 1-6 to 8, the whistler mode propagation in a cold homogeneous plasma and in an enhanced ionization (called duct) along the static magnetic field and related basic theories which are actually applicable to the propagation in the magnetosphere are reviewed. In section 1-6, the dispersion relation of the whistler mode, group velocity and propagation in the duct are stated. Section 1-7 introduces the ray tracing algorithm which is a method of calculation of ray paths in inhomogeneous media such as the magnetosphere. A magnetospheric model used in this thesis is given in section 1-8. A review of the related works and contribution of the present work are given in sections 1-9 and 10, respectively.

1-2 Whistler Mode Cyclotron Instability

In this section, we consider waves in a homogeneous unbounded plasma with a uniform static magnetic field B_o along the z axis, and assume the first order quantities to vary as $\exp\{i(kz-\omega t)\}$, where k, ω and t are the wave number, the angular frequency of the wave, and time. The dispersion relation is derived from the linearlized collisionless Boltzmann equation and the Maxwell equations (Bell and Bunemann, 1964). We consider only right-hand circular-polalized waves propagating along the z. The first-order collisionless Boltzmann equation for electrons is given by

$$\frac{\partial f_1}{\partial t} + \vec{v}\frac{\partial f_1}{\partial \vec{r}} - \frac{e}{m}(\vec{v} \times \vec{B}_o)\frac{\partial f_1}{\partial \vec{v}} = \frac{e}{m}(\vec{E} + \vec{v} \times \vec{B}_1)\frac{\partial f_o}{\partial \vec{v}} \qquad (1.1)$$

$\vec{E}$, $\vec{B}$, f, $\vec{r}$, $\vec{v}$, e and m are the electric field, the magnetic field,

the velocity distribution function, the position vector, the velocity vector, the charge of electrons, and the electron mass, respectively. The suffices o and 1 denote the zeroth and the first-order quantities. The zeroth-order distribution function f_o can be described as $f_o(v_\perp, v_{||})$, where $v_\perp$ and $v_{||}$ are the velocities of electrons perpendicular and parallel to the static magnetic field. From Eq.(1.1) and the Maxwell equations, one obtains the following dispersion relation,

$$c^2k^2 - \omega^2 = \Pi_e^2 \iint \frac{(\omega - kv_{||})\frac{\partial f_o}{\partial v_\perp} + kv_\perp \frac{\partial f_o}{\partial v_{||}}}{(\omega - kv_{||} - \Omega_e)} \pi v_\perp^2 dv_\perp dv_{||} \tag{1.2}$$

where $\Pi_e^2 \equiv N_e e^2/\varepsilon_o m$ is the electron plasma frequency and $\Omega_e \equiv eB_o/m$ is the electron cyclotron frequency. Integrating Eq. (1.2) by parts, we obtain

$$c^2k^2 - \omega^2 = -\Pi_e^2 \iint \left[\frac{\omega - kv_{||}}{\omega - kv_{||} - \Omega_e} + \frac{\frac{1}{2}k^2v_\perp^2}{(\omega - kv_{||} - \Omega_e)^2} \right] 2\pi v_\perp f_o dv_\perp dv_{||} \tag{1.3}$$

The velocity satisfying the condition for the denominator to be zero,

$$v_{||} = V_R \equiv (\omega - \Omega_e)/k \tag{1.4}$$

is called a "resonance velocity". The Doppler-shifted wave frequency seen by an electron is equal to the frequency of gyration Ω_e of the electron, if the electron velocity satisfies the condition (1.4).

For a cold plasma, f_o can be expressed as

$$f_o(v_\perp, v_{||}) = \frac{1}{2\pi v_\perp} \delta(v_\perp)\delta(v_{||}) \tag{1.5}$$

Substituting Eq.(1.5) into Eq.(1.3), we obtain the cold plasma dispersion relation for the whistler mode,

$$n^2 \equiv \frac{c^2k^2}{\omega^2} = 1 - \frac{\Pi_e^2}{\omega(\omega - \Omega_e)} \tag{1.6}$$

where n is the refractive index.

For a hot plasma distribution, the solution ω of Eq.(1.3) becomes complex, i.e., $\omega = \omega_r + i\gamma$ for a given k due to the thermal effect. If the resonance velocity V_R is much greater than the thermal velocity of the plasma and $\gamma << \omega_r$, then an explicit form of the growth rate γ is derived (Kennel and Petschek, 1966) as

$$\gamma = \pi\Omega_e(1 - \frac{\omega_r}{\Omega_e})^2\eta(V_R)\{A(V_R) - \frac{1}{\Omega_e/\omega_r - 1}\} \tag{1.7}$$

where

$$\eta(V_R) = 2\pi \frac{\Omega_e - \omega_r}{k} \int_0^\infty v_\perp f_o(v_\perp, v_\parallel = V_R)\, dv_\perp \tag{1.8}$$

and

$$A(V_R) = \frac{\int_0^\infty \frac{v_\perp}{v_\parallel}(v_\parallel \frac{\partial f_o}{\partial v_\perp} - v_\perp \frac{\partial f_o}{\partial v_\parallel})\, v_\perp dv_\perp}{2\int_0^\infty f_o v_\perp dv_\perp}\Bigg|_{v_\parallel = V_R} \tag{1.9}$$

For example, for a bi-Maxwellian distribution represented by

$$f_o(v_\perp, v_\parallel) = \frac{m}{2\pi\kappa T_\perp}\left(\frac{m}{2\pi\kappa T_\parallel}\right)^{\frac{1}{2}} \exp\left(-\frac{mv_\perp^2}{2\kappa T_\perp} - \frac{mv_\parallel^2}{2\kappa T_\parallel}\right) \tag{1.10}$$

$A(V_R)$ becomes independent of V_R and reduces to

$$A = (T_\perp - T_\parallel) / T_\parallel \,. \tag{1.11}$$

Hereafter, the quantity A is called an "anisotropy factor".

Since η is always positive, the condition of wave growth ($\gamma > 0$) for $\omega_r < \Omega_e$ is given by

$$A > \frac{1}{(\Omega_e/\omega_r) - 1} \tag{1.12}$$

Therefore, the frequency range in which the waves grow is given by

$$\omega_r < \frac{A}{A + 1} \Omega_e \tag{1.13}$$

An example of the solution to Eq.(1.3) for the bi-Maxwellian plasma is shown in Fig.1.1 (Scharer and Trivelpiece, 1967).

In the rest of this section an instability due to an interaction of whistler mode waves with a gyrating electron stream (beam) is reviewed(Bell and Bunemann, 1964). It has been proved that no whistler mode excitation in a cold plasma can be achieved by any electron beam, streaming along the external magnetic field i.e. without any transverse velocity component. However, a beam with comsiderable transverse velocity components leads to a whistler mode instabiltiy in the beam plasma system. The transverse, gyrating energy of electrons becomes the energy source of the wave growth. In the following the distribution of a beam will be expressed by

$$f(v_\perp, v_\parallel) = \frac{1}{2\pi} \delta(v_\parallel - V_B) h_\perp(v_\perp) \tag{1.14}$$

where $h_\perp(v_\perp)$ indicates a transverse velocity distribution function and V_B is the beam velocity. In the medium consisting of the beam represented by Eq.(1.14)and the background cold plasma expressed by Eq.(1.5), the dispersion relation (1.3) becomes

$$c^2k^2 - \omega^2 + \frac{\Pi_c^2 \omega}{\omega - \Omega_e} = - \frac{\Pi_b^2(\omega - kV_B)}{\omega - kV_B - \Omega_e} - \frac{\frac{1}{2} k^2 \langle v_\perp^2 \rangle \Pi_b^2}{(\omega - kV_B - \Omega_e)^2} \tag{1.15}$$

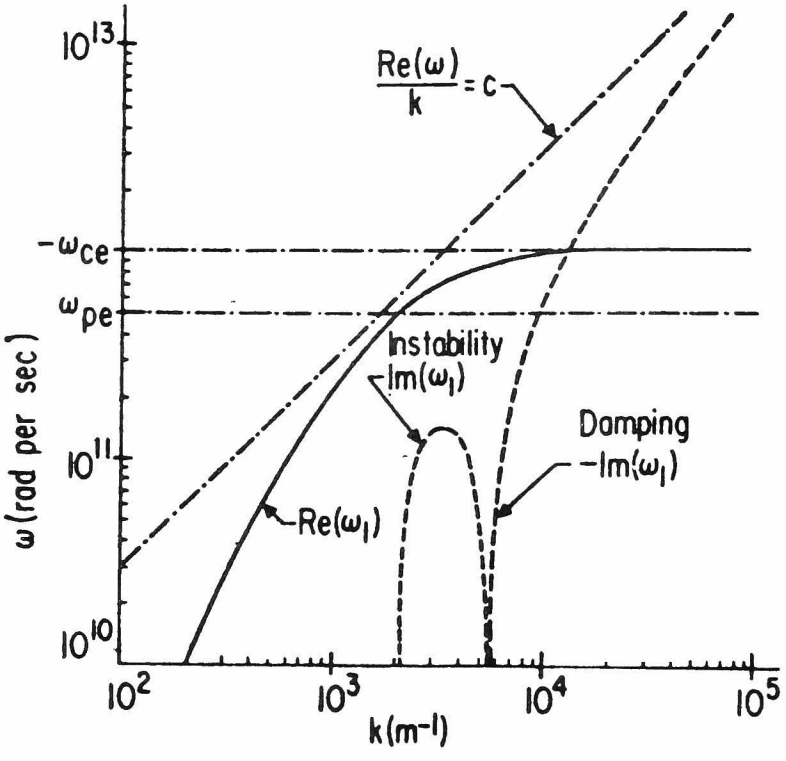

Fig. 1.1. Damping and instabilities for whistler mode in an anisotropic Maxwellian plasma. In the figure, $\omega_{ce} = -\Omega_e$, $\omega_{pe} = \Pi_e$, and $\omega_1 = \omega$ (after Scharer and Trivelpiece, 1967).

where Π_c and Π_b are the plasma frequency of the cold plasma and that of the beam, respectively, and

$$< v_\perp^2 > = \int_0^\infty h_\perp(v_\perp) v_\perp^2 \, 2\pi v_\perp dv_\perp \tag{1.16}$$

A tenuous beam ($\Pi_b^2 << \Pi_c^2$) causes an instability when the denominators on the right hand side of (1.15) are small, i.e., near the resonance condition ($V_B \simeq V_R$) ,

$$\omega_r - kV_B - \Omega_e \simeq 0 \tag{1.17}$$

Because $\omega_r < \Omega_e$, this equation requires $kV_B < 0$, so that it is necessary for the resonance that the wave and the beam are encountering each other from opposite directions. An example of the solutions of Eq.(1.15) for a given real k is shown in Fig.1.2 (Kimura, 1967).

1-3 Dispersion Relation in a bi-Maxwellian Hot Plasma (Microscopic Theory)

In this section, a dielectric tensor for a bi-Maxwellian hot plasma (1.10) is introduced according to Chs.8 and 9 of Stix (1962). The mobility tensor $\overleftrightarrow{M}^{(j)}$ is defined as

$$< \vec{v}^{(j)} > \equiv \int \vec{v} \, f_1^{(j)} \, dv_x dv_y dv_z = \frac{1}{B_o} \overleftrightarrow{M}^{(j)} \vec{E} \tag{1.18}$$

where $f_1^{(j)}$ is the first-order velocity distribution function for particles of type j. $\overleftrightarrow{M}$ is determined from the Maxwell equations and the first-order Boltzmann equation. A wave normal vector $\vec{k}$ is assumed to be in x-z plane and to make an angle θ with a constant magnetic field $\vec{B}_o = \hat{z}B_o$ in the z direction. Then, $k_y = 0$ and each element of $\overleftrightarrow{M}$ is shown as follows.

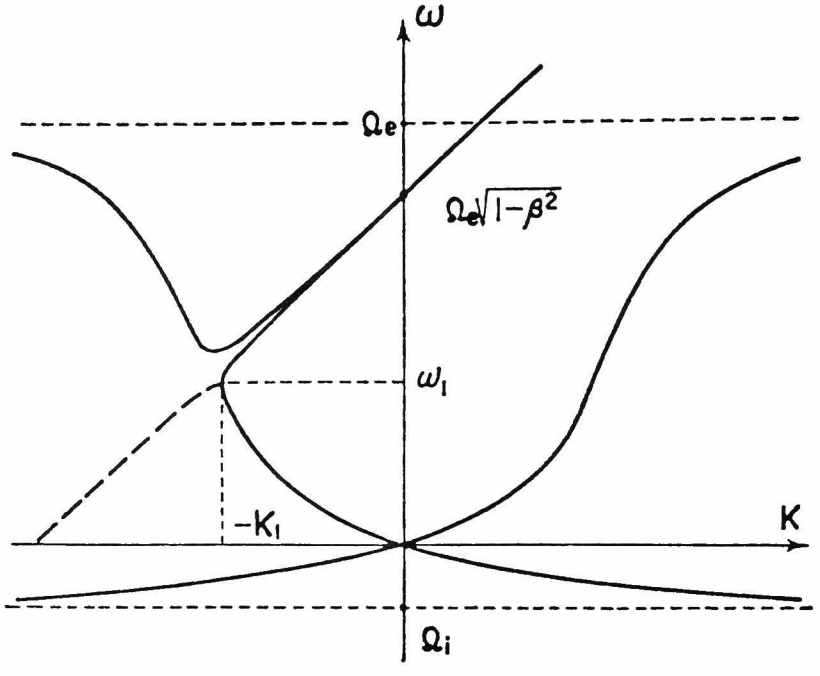

Fig. 1.2. Transverse interaction of a whistler mode with an electron beam which has finite transverse velocity resulting in cyclotron instability for ω less than ω_1 and k smaller than $-k_1$. The factor $\beta = V_B/c$ and it is neglected in Eq.(1.15) (after Kimura, 1967).

$$
\begin{aligned}
M_{xx} &= \frac{-\Omega\varepsilon e^{-\lambda}}{mk_z}\frac{\kappa T_\perp}{} \sum_{n=-\infty}^{\infty} \frac{n^2}{\lambda} I_n[\langle\Theta\rangle_n] \\
M_{xy} &= \frac{-\Omega e^{-\lambda}}{mk_z}\frac{\kappa T_\perp}{} \sum_{n=-\infty}^{\infty} i\, n(I_n - I_n')[\langle\Theta\rangle_n] \\
M_{xz} &= \frac{-\varepsilon e^{-\lambda}}{mk_z}\frac{\kappa T_\perp}{} \sum_{n=-\infty}^{\infty} \frac{nk_x}{\lambda} I_n[n\langle\Phi\rangle_n - \langle\Psi\rangle_n] \\
M_{yx} &= \frac{-\Omega e^{-\lambda}}{mk_z}\frac{\kappa T_\perp}{} \sum_{n=-\infty}^{\infty} -i\, n(I_n - I_n')[\langle\Theta\rangle_n] \\
M_{yy} &= \frac{-\Omega\varepsilon e^{-\lambda}}{mk_z}\frac{\kappa T_\perp}{} \sum_{n=-\infty}^{\infty} \left(\frac{n^2}{\lambda} I_n + 2\lambda I_n - 2\lambda I_n'\right)[\langle\Theta\rangle_n] \\
M_{yz} &= \frac{-e^{-\lambda}}{mk_z}\frac{\kappa T_\perp}{} \sum_{n=-\infty}^{\infty} -i\, k_x(I_n - I_n')[n\langle\Phi\rangle_n - \langle\Psi\rangle_n] \\
M_{zx} &= \frac{-\varepsilon e^{-\lambda}}{mk_z}\frac{\kappa T_\perp}{} \sum_{n=-\infty}^{\infty} \frac{-nk_x}{\lambda} I_n[\langle v_z\Theta\rangle_n] \\
M_{zy} &= \frac{-\ e^{-\lambda}}{mk_z}\frac{\kappa T_\perp}{} \sum_{n=-\infty}^{\infty} -i\, k_x(I_n - I_n')[\langle v_z\Theta\rangle_n] \\
M_{zz} &= \frac{\Omega\varepsilon e^{-\lambda}}{k_z} \sum_{n=-\infty}^{\infty} I_n[n\langle v_z\Phi\rangle_n - \langle v_z\Psi\rangle_n]
\end{aligned}
\tag{1.19}
$$

where I_n and I_n' are the modified Bessel function of the n-th order and its derivative respectively and the argument of them is

$$\lambda = \frac{k_x^2\,\kappa T_\perp}{\Omega_e^2\, m} \tag{1.20}$$

The terms of the form $\langle Q \rangle_n$ in Eq.(1.19) are

$$
\begin{aligned}
\langle v_z^p\,\Theta\rangle_n &= 2\left(\frac{m}{2\kappa T_\parallel}\right)^{\frac{3}{2}}\left[-\frac{T_\parallel}{T_\perp}F_p + \frac{k_z}{\omega}\left(\frac{T_\parallel}{T_\perp}F_{p+1} - F_{p+1}\right)\right] \\
\langle v_z^p\,\Phi\rangle_n &= 2\left(\frac{m}{2\kappa T_\parallel}\right)^{\frac{3}{2}}\left[-\frac{\Omega}{\omega}\left(\frac{T_\parallel}{T_\perp}F_{p+1} - F_{p+1}\right)\right] \\
\langle v_z^p\,\Psi\rangle_n &= -2\left(\frac{m}{2\kappa T_\parallel}\right)^{\frac{3}{2}} F_{p+1}
\end{aligned}
\tag{1.21}
$$

for p = 0, 1, or 2, where F_p can be derived as

$$F_p = \frac{ik_z}{\pi^{\frac{1}{2}}}\int_{-\infty}^{\infty} \frac{v_z^p}{\omega - k_z v_z + n\Omega}\exp\left(-\frac{mv_z^2}{2\kappa T_\parallel}\right) dv_z \tag{1.22}$$

For p = 0,

$$F_0 = \pi^{\frac{1}{2}} \frac{k_z}{|k_z|} \exp(-\alpha_n^2) + 2i\, S(\alpha_n) \tag{1.23}$$

where

$$S(\alpha) \equiv e^{-\alpha^2} \int_0^{\alpha} e^{t^2} dt \tag{1.24}$$

and

$$\alpha_n = \frac{\omega + n\Omega}{k_z} \left(\frac{m}{2\kappa T_{\parallel}} \right)^{\frac{1}{2}} \tag{1.25}$$

F_0 is related to the plasma dispersion function as

$$Z(\alpha_n) = i\, F_0 \tag{1.26}$$

which is tabulated by Fried and Conte (1961). F_1 and F_2 can be expressed in terms of F_0 from Eq.(1.22)

$$\begin{aligned} F_1 &= -i \left(\frac{2\kappa T_{\parallel}}{m} \right)^{\frac{1}{2}} + \left(\frac{\omega + n\Omega}{k_z} \right) F_0 \\ F_2 &= -i \left(\frac{\omega + n\Omega}{k_z} \right) \left(\frac{2\kappa T_{\parallel}}{m} \right)^{\frac{1}{2}} + \left(\frac{\omega + n\Omega}{k_z} \right) F_0 \end{aligned} \tag{1.27}$$

Substituting Eqs.(1.26) and (1.27) into (1.21), we obtain

$$\begin{aligned} \langle \Theta \rangle_n &= \frac{2T_{\parallel}}{T_{\perp}} \left(\frac{m}{2\kappa T_{\parallel}} \right)^{\frac{3}{2}} iZ + \frac{2ik_z}{\omega T_{\perp}} \left(\frac{m}{2\kappa T_{\parallel}} \right) (T_{\perp} - T_{\parallel}) (1 + \alpha_n Z) \\ \langle v_z \Theta \rangle_n &= \frac{2i}{\omega T_{\perp}} \left(\frac{m}{2\kappa T_{\parallel}} \right) (\omega T_{\perp} + n\Omega T_{\perp} - n\Omega T_{\parallel}) (1 + \alpha_n Z) \\ \langle \Phi \rangle_n &= \frac{-2i\Omega}{\omega T_{\perp}} \left(\frac{m}{2\kappa T_{\parallel}} \right) (T_{\perp} - T_{\parallel}) (1 + \alpha_n Z) \\ \langle v_z \Phi \rangle_n &= \frac{-2i\Omega}{k_z \omega T_{\perp}} \left(\frac{m}{2\kappa T_{\parallel}} \right) (\omega + n\Omega) (T_{\perp} - T_{\parallel}) (1 + \alpha_n Z) \\ \langle \Psi \rangle_n &= 2i \left(\frac{m}{2\kappa T_{\parallel}} \right) (1 + \alpha_n Z) \\ \langle v_z \Psi \rangle_n &= \frac{2i}{k_z} \left(\frac{m}{2\kappa T_{\parallel}} \right) (\omega + n\Omega) (1 + \alpha_n Z) \end{aligned} \tag{1.28}$$

where Z has an argument α_n. Each element of $\overleftrightarrow{M}$ is determined by substituting Eq. (1.28) into Eq.(1.19). The following symmetries can also be derived.

$$\begin{aligned} M_{xy} &= -M_{yx} \\ M_{xz} &= M_{zx} \\ M_{yz} &= -M_{zy} \end{aligned} \tag{1.29}$$

The equivalent dielectric tensor is defined by the vector notation

$$\vec{D} = \varepsilon_o \overleftrightarrow{K} \cdot \vec{E} = \varepsilon_o \left(\vec{E} + \frac{i}{\varepsilon_o \omega} \vec{j} \right) \tag{1.30}$$

and the current density $\vec{j}$ is given by

$$\vec{j} = \sum_j N_j Z_j e \varepsilon_j < \vec{v}^{(j)} > \tag{1.31}$$

where N_j, Z_j, and ε_j are the zeroth-order density, the charge number and the sign of charge, ± 1 for particles of type j. $< \vec{v}^{(j)} >$ is expressed in terms of mobility tensor by Eq. (1.18). The above relations may be combined to give

$$\overleftrightarrow{K} = \overleftrightarrow{1} + \frac{ie}{\varepsilon_o \omega B_o} \sum_j N_j Z_j \varepsilon_j \overleftrightarrow{M}^{(j)} \tag{1.32}$$

or equivalent for electrons

$$\overleftrightarrow{K} = \overleftrightarrow{1} - i \sum_j \frac{\Pi_j^2}{\omega \Omega_j} \overleftrightarrow{M}^{(j)} \tag{1.33}$$

where $\overleftrightarrow{1}$ is the unit dyad.

Fourier analysis of Maxwell's equations in time and space gives the dispersion relation for plasma waves,

$$\vec{n} \times (\vec{n} \times \vec{E}) + \overleftrightarrow{K} \cdot \vec{E} = 0 \tag{1.34}$$

where $\vec{n}$ is a refractive index vector defined by

$$\vec{n} \equiv c\vec{k}/\omega \tag{1.35}$$

In matrix form, with $k_y = 0$, this equation becomes

$$\begin{pmatrix} -n_z^2 + K_{xx} & K_{xy} & n_x n_z + K_{xz} \\ K_{yx} & -n_x^2 - n_z^2 + K_{yy} & K_{yz} \\ n_x n_z + K_{zx} & K_{zy} & -n_x^2 + K_{zz} \end{pmatrix} \begin{pmatrix} E_x \\ E_y \\ E_z \end{pmatrix} = 0 \tag{1.36}$$

The determinant of this vector equation gives the dispersion relation.

$$D(\omega) = \begin{vmatrix} -n_z^2 + K_{xx} & K_{xy} & n_x n_z + K_{xz} \\ K_{yx} & -n_x^2 - n_z^2 + K_{yy} & K_{yz} \\ n_x n_z + K_{zx} & K_{zy} & -n_x^2 + K_{zz} \end{vmatrix} = 0 \tag{1.37}$$

1-4 Warm Plasma Approximation (Full Adiabatic Theory)

In case of low temperature ($\lambda << 1$) and in a condition far from resonance ($|\alpha_n| >> 1$), a warm plasma approximation can be used (Sitenko and Stepanov, 1957). We can use an asymptotic expression of $S(\alpha)$ in the right hand side of Eq. (1.23). $S(\alpha)$ i.e., Eq. (1.24) for $|\alpha| >> 1$ and $|I_m\alpha| << 1$ becomes

$$S(\alpha) = \frac{1}{2\alpha}\left(1 + \frac{1}{2\alpha^2} + \frac{3}{4\alpha^4} + \cdots\right) \tag{1.38}$$

The higher terms are negligible. The dielectric tensor is expanded to the first-order in ascending powers of a small parameter $\tau \equiv k^2\kappa T/m\omega^2$ (Aubry et al., 1970);

$$\overleftrightarrow{K} = \overleftrightarrow{K}^{(0)} + \tau\overleftrightarrow{K}^{(1)} \tag{1.39}$$

where $\overleftrightarrow{K}^{(0)}$ is the cold plasma dielectric tensor

$$\overleftrightarrow{K}^{(0)} = \begin{pmatrix} 1 - \frac{X}{1 - Y^2} & + \frac{iXY}{1 - Y^2} & 0 \\ - \frac{iXY}{1 - Y^2} & 1 - \frac{X}{1 - Y^2} & 0 \\ 0 & 0 & 1 - X \end{pmatrix} \tag{1.40}$$

and $\overleftrightarrow{K}^{(1)}$ expresses the warm plasma correction. Its elements are:

$$\begin{aligned}
K_{xx}^{(1)} &= - \frac{X}{1 - Y^2} \left[\frac{3\sin^2\theta}{1 - 4Y^2} + \frac{1 + 3Y^2}{(1 - Y^2)^2} \cos^2\theta \right] \\
K_{yy}^{(1)} &= - \frac{X}{1 - Y^2} \left[\frac{1 + 8Y^2}{1 - 4Y^2} \sin^2\theta + \frac{1 + 3Y^2}{(1 - Y^2)^2} \cos^2\theta \right] \\
K_{zz}^{(1)} &= - X \left[3\cos^2\theta + \frac{\sin^2\theta}{1 - Y^2} \right] \\
K_{xy}^{(1)} &= -K_{yx}^{(1)} = i \frac{XY}{1 - Y^2} \left[\frac{6\sin^2\theta}{1 - 4Y^2} + \frac{3 + Y^2}{(1 - Y^2)^2} \cos^2\theta \right] \\
K_{xz}^{(1)} &= K_{zx}^{(1)} = - \frac{2X}{(1 - Y^2)^2} \sin\theta\cos\theta \\
K_{yz}^{(1)} &= -K_{zy}^{(1)} = -i \frac{XY}{(1 - Y^2)^2} (3 - Y^2) \sin\theta\cos\theta
\end{aligned} \tag{1.41}$$

where $X = (\Pi_e^2 / \omega^2)$ and $Y = \Omega_e / \omega$. The substitution of Eqs. (1.40) and (1.41) into Eq. (1.37) gives the dispersion relation in the warm plasma approximation:

$$q\alpha_1 n^6 + (\alpha_0 + q\beta_1) n^4 + (\beta_0 + q\gamma_1) n^2 + \gamma_0 = 0 \tag{1.42}$$

where $q = \kappa T / mc^2$, α_0, β_0, γ_0 are coefficients of the cold plasma dispersion equation

$$\begin{aligned}
\alpha_0 &= K_{xx}^{(0)} \sin^2\theta + K_{zz}^{(0)} \cos^2\theta \\
\beta_0 &= - \left[K_{xx}^{(0)} K_{yy}^{(0)} + (K_{xy}^{(0)})^2 \right] \sin^2\theta \\
&\quad - K_{zz}^{(0)} \left[K_{xx}^{(0)} + K_{yy}^{(0)} \cos^2\theta \right]
\end{aligned} \tag{1.43}$$

$$\gamma_0 = K_{zz}^{(0)} \left[(K_{xy}^{(0)})^2 + K_{xx}^{(0)} K_{yy}^{(0)} \right]$$

and α_1, β_1, γ_1 contains the temperature effect

$$\begin{aligned}
\alpha_1 &= K_{xx}^{(1)} \sin^2\theta + K_{zz}^{(1)} \cos^2\theta + 2K_{xz}^{(1)} \sin\theta\cos\theta \\
\beta_1 &= -[K_{xx}^{(1)} K_{yy}^{(0)} + K_{yy}^{(1)} K_{xx}^{(0)} + 2K_{xy}^{(0)} K_{xy}^{(1)}] \sin^2\theta \\
&\quad - K_{zz}^{(1)} [K_{xx}^{(0)} + K_{yy}^{(0)} \cos^2\theta] \\
&\quad - K_{zz}^{(0)} [K_{xx}^{(1)} + K_{yy}^{(1)} \cos^2\theta] \\
&\quad + 2\sin\theta\cos\theta \left[K_{xy}^{(0)} K_{yz}^{(1)} - K_{xz}^{(1)} K_{yy}^{(0)} \right] \\
\gamma_1 &= K_{zz}^{(1)} \left[(K_{xy}^{(0)})^2 + K_{xx}^{(0)} K_{yy}^{(0)} \right] \\
&\quad + K_{zz}^{(0)} \left[2K_{xy}^{(0)} K_{xy}^{(1)} + K_{xx}^{(0)} K_{yy}^{(1)} + K_{xx}^{(1)} K_{yy}^{(0)} \right]
\end{aligned} \tag{1.44}$$

1-5 Electrostatic Approximation

The electric field of electrostatic waves may be derived from a potential,

$$\vec{E} = -\nabla\phi = -i\vec{k}\phi \tag{1.45}$$

so that $\vec{E}$ is parall to $\vec{k}$. If we dot the dispersion relation for plasma waves Eq. (1.34) with $\vec{n}$, we have

$$\vec{n} \cdot \overleftrightarrow{K} \cdot \vec{E} = 0 \tag{1.46}$$

Taking Eq. (1.45) and $\vec{n} \,//\, \vec{k}$ into account, we obtain the dispersion relation for the electrostatic approximation as

$$\vec{k} \cdot \overleftrightarrow{K} \cdot \vec{k} = 0 \tag{1.47}$$

Using $k_y = 0$ and $K_{xz} = K_{zx}$ from Eqs. (1.29) and (1.33), we can write Eq. (1.47) in the form(Stix, 1962)

$$k_x^2 K_{xx} + 2k_x k_z K_{xz} + k_z^2 K_{zz} = 0 \tag{1.48}$$

Evaluating the elements of $\overleftrightarrow{K}$ from Eqs. (1.19), (1.21), and (1.33), we obtain

$$\begin{aligned} k_x^2 + k_z^2 + \sum_j \sum_{n=-\infty}^{\infty} \frac{\Pi_j^2 m e^{-\lambda} I_n(\lambda)}{\kappa T_\perp} A_{nj} &= 0 \\ A_{nj} = \frac{T_\perp}{T_{||}} + \left[\frac{(\omega + n\Omega)T_\perp - n\Omega T_{||}}{k_z T_{||}} \left(\frac{m}{2\kappa T_{||}} \right)^{\frac{1}{2}} \right] Z(\alpha_n) & \end{aligned} \tag{1.49}$$

We consider an instability in this situation. Bernstein (1958) has shown that there is no instability if the plasma is in thermal equilibrium $T_\perp = T_{||}$. It has been shown by Harris (1961) that an instability occurs for sufficiently anisotropic velocity distributions and there can be no instability for either $k_\perp = 0$ or $k_{||} = 0$. Shima and Hall (1965) have shown that marginally unstable solutions ($I_m\omega = 0^+$) of the dispersion equation can occur only if both

$$\ell + \frac{1}{2} < \frac{\omega_r}{\Omega_e} < \ell + 1 - \frac{T_{||}}{T_\perp} \quad \text{and} \quad \frac{\omega_r}{\Omega_e} < \frac{T_\perp}{T_{||}} - 1 \tag{1.50}$$

where ℓ is an integer. Gitomer et al. (1972) have calculated (1.49) in the frequency range $0 < \omega_r < \Omega_e$ for an electron plasma and have shown maximum growth rate (Fig.1.3).

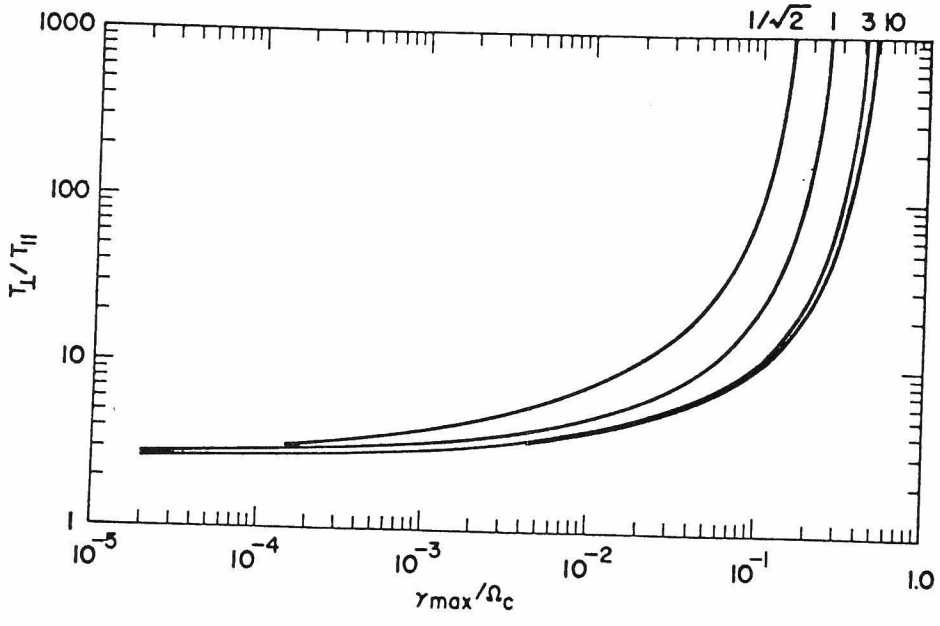

Fig. 1.3. Maximum growth rate ω_{max}/Ω_e as a function of $T_\perp/T_\parallel$ for four values of Π_e/Ω_e. In the figure $\Omega_c = \Omega_e$ (after Gitomer et al., 1972).

1-6 Whistler Mode Propagation in a Cold Plasma

We summarize a whistler mode wave propagation in a cold homogeneous plasma permeated by a static magnetic field. At frequencies much higher than an ion cyclotron frequency, effects of ions can be neglected. Then for a wave normal angle θ with respect to the direction of the background magnetic field, the square of refractive index is given by Appleton Hartree's equations (Helliwell, 1965):

$$n^2 = 1 - \frac{X}{1 - \frac{\frac{1}{2}Y^2\sin^2\theta}{1 - X} \pm \frac{1}{1-X}\sqrt{\frac{1}{4}Y^4\sin^4\theta + Y^2\cos^2\theta\,(1 - X)^2}} \tag{1.51}$$

where $X = f_p^2/f^2$, $Y = f_H/f$; f_p and f_H are the electron plasma frequency and the electron cyclotron frequency, respectively. Collisional effects are neglected. The propagation under the condition $Y > 1$ ($f < f_H$) is called a whistler mode. When the following condition

$$Y^2\sin^4\theta << 4\cos^2\theta\,(1 - X)^2 \tag{1.52}$$

is satisfied the quasi-longitudinal(QL) approximation can be applied. Then Eq. (1.51) is approximated by

$$n^2 = 1 - \frac{X}{1 \pm Y\cos\theta} \tag{1.53}$$

In the ionosphere, generally X exceeds $Y\cos\theta + 1$. Then only the minus sign is selected in Eq. (1.53) and we obtain

$$n^2 = 1 + \frac{f_p^2}{f\,(f_H\cos\theta - f)} \tag{1.54}$$

The direction of energy flow in lossfree media is along the group-velocity vector $\vec{v}_g$ (Stix, 1962):

$$\vec{v}_g = \frac{\partial \omega}{\partial \vec{k}} = \hat{k} \frac{\partial \omega}{\partial k} + \hat{\theta} \frac{1}{k} \frac{\partial \omega}{\partial \theta} = \frac{\partial \omega}{\partial k} \left(\hat{k} - \hat{\theta} \frac{1}{k} \frac{\partial k}{\partial \theta} \right) \tag{1.55}$$

where $\hat{k}$ is the unit vector in the wave normal direction and $\hat{\theta}$ is the unit vector normal to $\hat{k}$ and coplanar with $\vec{v}_g$ and $\hat{k}$. The angle α between $\vec{v}_g$ and $\hat{k}$ is determined by

$$\tan \alpha = -\frac{1}{k} \frac{\partial k}{\partial \theta} = -\frac{1}{n} \frac{\partial n}{\partial \theta} \tag{1.56}$$

As is geometrically demonstrated in Fig.1.4, this equation indicates that the ray direction is directed normal to the n-θ surface. When $f_p^2 >> f_H f$, the second term on the right hand side of Eq. (1.54) is much larger than unity. If we disregard the unity, Eq. (1.54) becomes (Helliwell, 1965),

$$n = f_p / f^{1/2} (f_H \cos\theta - f)^{1/2} \tag{1.57}$$

Let us consider a propagation in a particular type of inhomogeneous medium, i.e., a propagation along an enhanced ionization (so-called duct) aligned with the geomagnetic field. General nature of a ray path in this case is shown in Fig.1.5 for f being negligible as compared with $f_H \cos\theta$ (Smith et al., 1960). Assume that the ray is started at a point on the line of maximum ionization with an initial wave normal angle θ_o. Snell's law demands that n $\cos\theta$ is constant. The wave normal direction always rotates toward the direction of increasing refractive index or increasing ionization. For $0 < f < f_H/2$, a wave is called to be trapped in the duct because the ray path is always confined within a field aligned enhanced ionization. For such a trapping, the initial wave normal angle θ_o must be less than $\cos^{-1} 2f/f_H$. For $f > f_H/2$, waves can not be trapped by the enhanced ionization, but are instead trapped by a field aligned

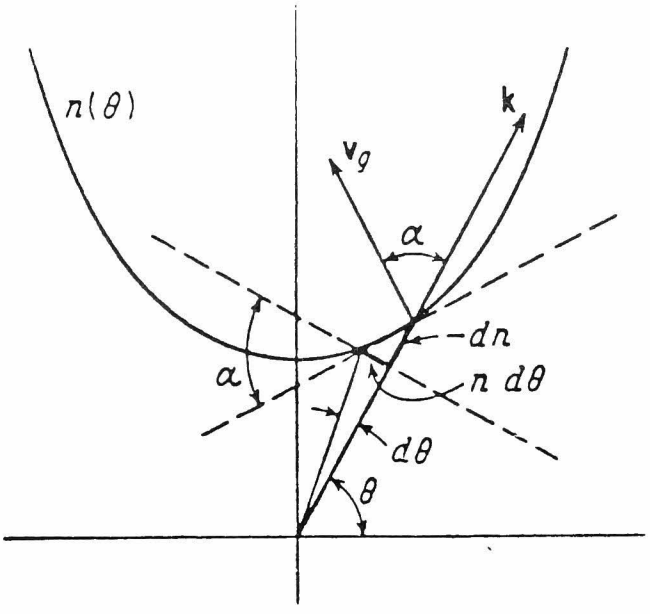

Fig. 1.4. n-θ surface, illustrating direction of $\vec{v}_g$ (after Stix, 1962).

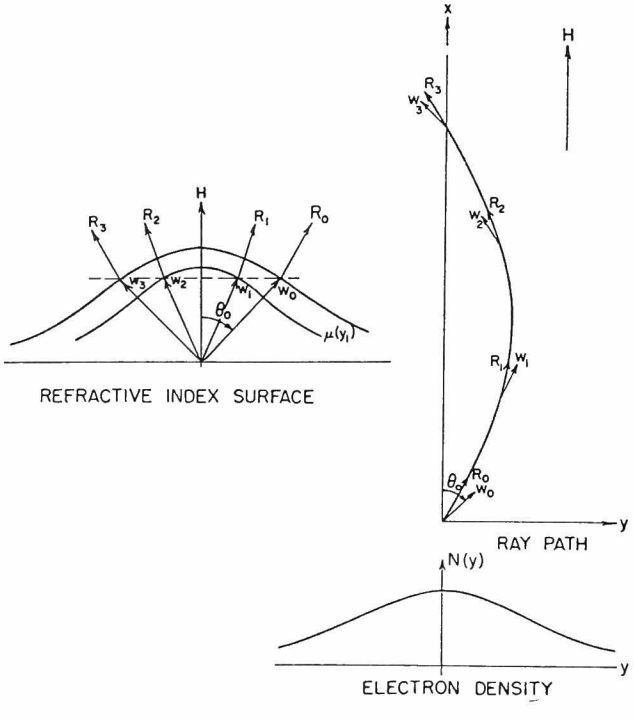

Fig. 1.5. Ray tracing in an enhancement of ionization aligned with the magnetic field (after Smith et al., 1960).

depressed ionization.

Let us introduce the resonance cone angle θ_{res}, where the refractive index n becomes infinite. This angle is, therefore, defined in such a way that the denominator in Eq. (1.51) becomes zero, i.e.,

$$\theta_{res} = \tan^{-1}\{ - \frac{(1 - X)(1 - Y^2)}{1 - X - Y^2} \} \tag{1.58}$$

or

$$\theta_{res} = \tan^{-1}\{ \frac{(f_P^2 - f^2)(f_H^2 - f^2)}{f^2 (f_p^2 + f_H^2 - f^2)} \}$$

where the minus sign is selected in Eq. (1.51). At an angle higher than θ_{res}, n^2 becomes negative and waves can not propagate and become evanescent.

1-7 Ray Tracing

Generally in anisotropic media, the ray direction of a wave is different from its wave normal direction and the direction of the ray varies in inhomogeneous media as the wave propagates. The magnetospheric plasma is such an inhomogeneous and anisotropic medium. The ray tracing is a technique to obtain the ray paths in such a medium. Here, we derive basic equations in a 2-dimensional ray tracing.

The locus of the tip of the refractive index vector $\vec{n}(\rho_r, \rho_\phi)$ forms a refractive index surface, where ρ_r and ρ_ϕ are the r- and the ϕ- components of a refractive index vector $\vec{n}$ in two dimensional polar coordinates (r, ϕ). The refractive index $\vec{n}$ is obtained from Appleton-Hartree's equation (1.51) and $\vec{n}$ can be written as $\vec{n}(r, \phi, \rho_r, \rho_\phi)$ where ρ_r and ρ_ϕ appear only in the form of the direction cosine of the wave normal;

$$\frac{\rho_r}{(\rho_r^2+\rho_\phi^2)^{1/2}}, \frac{\rho_\phi}{(\rho_r^2+\rho_\phi^2)^{1/2}} \tag{1.59}$$

Then, the equation of the refractive index surface can be written by (Budden, 1961)

$$G(r, \phi, \rho_r, \rho_\phi) \equiv \frac{(\rho_r^2 + \rho_\phi^2)^{1/2}}{n(r, \phi, \rho_r, \rho_\phi)} = 1 \tag{1.60}$$

As the equation of a tangent to the refractive index surface is represented by $d\rho_r / d\rho_\phi$, direction cosines of the ray direction which is normal to the refractive index surface is then, given by

$$\left(\frac{1}{\sqrt{1+\left(\frac{d\rho_r}{d\rho_\phi}\right)^2}}, \frac{-\frac{d\rho_r}{d\rho_\phi}}{\sqrt{1+\left(\frac{d\rho_r}{d\rho_\phi}\right)^2}}\right) = \left(\frac{\partial G}{\partial \rho_r}, \frac{\partial G}{\partial \rho_\phi}\right) \tag{1.61}$$

On the other hand, the ray velocity is $\vec{dr} / dt$ and its direction cosines are proportional to

$$\left(\frac{dr}{dt}, r\frac{d\phi}{dt}\right) \tag{1.62}$$

Naturally Eq. (1.62) must be proportional to Eq. (1.61). In the case of $\rho_\phi = 0$, $\partial G / \partial \rho_r = 1/n$ while the wave normal component of the ray velocity $dr/dt = c/n$ (where t is the time of phase travel). Hence the proportionality factor is equal to c.

Namely,

$$\frac{dr}{dt} = c\frac{\partial G}{\partial \rho_r} \quad \text{and} \quad r\frac{d\phi}{dt} = c\frac{\partial G}{\partial \rho_\phi} \tag{1.63}$$

Here we obtain

$$\frac{dr}{dt} = c\frac{\partial G}{\partial \rho_r} = \frac{c}{n^2}\left(\rho_r - n\frac{\partial n}{\partial \rho_r}\right) \tag{1.64}$$

and

$$r \frac{d\phi}{dt} = c \frac{\partial G}{\partial \rho_\phi} = \frac{c}{n^2}\left(\rho_\phi - n \frac{\partial n}{\partial \rho_\phi}\right) \tag{1.65}$$

The differentiation of G along the ray path i.e., $dG/dr = 0$, that is

$$\frac{dG}{dr} = \frac{\partial G}{\partial r} + \frac{\partial G}{\partial \rho_r} \frac{\partial \rho_r}{\partial r} + \frac{\partial G}{\partial \rho_\phi} \frac{\partial \rho_\phi}{\partial r} = 0 \tag{1.66}$$

When the WKB approximation can be applied, we have $\nabla \times \vec{\rho} = 0$, i.e.

$$\frac{1}{r} \frac{\partial}{\partial r} (r\rho_\phi) - \frac{1}{r} \frac{\partial \rho_r}{\partial \phi} = 0$$

or

$$\frac{\partial \rho_\phi}{\partial r} + \frac{\rho_\phi}{r} - \frac{1}{r} \frac{\partial \rho_r}{\partial \phi} = 0 \tag{1.67}$$

Substituting Eqs. (1.63) and (1.67) into Eq. (1.66), we obtain

$$c\frac{\partial G}{\partial r} + \frac{\partial \rho_r}{\partial r} \frac{dr}{dt} + \frac{\partial \rho_r}{\partial \phi} \frac{d\phi}{dt} - \rho_\phi \frac{d\phi}{dt} = 0 \tag{1.68}$$

Therefore

$$\frac{d\rho_r}{dt} = - \frac{\partial G}{\partial r} + \rho_\phi \frac{d\phi}{dt} = \frac{c}{n} \frac{\partial n}{\partial r} + \rho_\phi \frac{d\phi}{dt} \tag{1.69}$$

Similarly

$$\frac{d\rho_\phi}{dt} = - \frac{\partial G}{\partial \phi} - \frac{\rho_\phi}{r} \frac{dr}{dt} = \frac{1}{r} \left(\frac{c}{n} \frac{\partial n}{\partial \phi} - \frac{dr}{dt} \right) \tag{1.70}$$

Eqs. (1.64), (1.65), (1.69) and (1.70) are the basic equation of the ray tracing derived by Haselgrove (1954).

The group delay time t_g is defined as

$$\frac{dt_g}{dt} = \frac{c}{nv_{gk}} = 1 + \frac{f}{n} \frac{\partial n}{\partial f} \tag{1.71}$$

where v_{gk} is the wave normal component of the group velocity (Kimura, 1966)

In the application to the ray tracing in the ionosphere and in the magnetosphere, r and ϕ should be the geocentric radius and the geomagnetic latitude, respectively.

1-8 Magnetospheric Model

In this section a description is given on a magnetospheric electron density model to be used for ray tracing in this thesis. The geomagnetic field can be expressed by a dipole field within 6 ∿ 7 earth radii. The electron cyclotron frequency f_H at a point (r, ϕ) is given by (Helliwell, 1965)

$$f_H = f_{Heq}\left(\frac{R_E}{r}\right)^3(1 + 3\sin^2\phi)^{1/2} \tag{1.72}$$

where f_{Heq} is a cyclotron frequency at the equator (880kHz) and R_E is the mean earth radius (6370km). Defining Λ as geomagnetic latitude of the field line at $r = R_E$, we obtain

$$\frac{r}{R_E} = \frac{\cos^2\phi}{\cos^2\Lambda} \tag{1.73}$$

a field line is identified by either Λ which is called the "invariant latitude" or the "L value" defined by

$$L = \frac{r}{R_E \cos^2\phi} = \frac{1}{\cos^2\Lambda} \tag{1.74}$$

We have basically used a computer program of ray tracing based on Kimura's paper (1966). To calculate electron and ion densities, according to Aikyo and Ondoh (1971), the diffusive equilibrium model (Angerami and Thomas, 1964) is used inside the plasmapause ($L \leq 4$), and the collisionless model (Eviatar et al., 1964) is used in the trough region ($L > 4$ and $h >$ 3000km in altitude). The diffusive equilibrium model used is

$$N_{de} = N_o \left[\sum_i \eta_i \exp(-z/H_i)\right]^{\frac{1}{2}}$$
$$N_{di} = N_{de}\frac{\eta_i \exp(-z/H_i)}{\sum_i \eta_i \exp(-z/H_i)} \tag{1.75}$$

$$z = \frac{r_o}{r}(r - r_o) , \quad H_i = \kappa T/M_i g_o$$

where N_{de}, N_{di} = the electron and the i-th ion densities,

$N_o = 10^4$/cc, the electron density at the reference level r_o = 7370km (h = 1000km in altitude),

z = the geopotential height ,

H_i, η_i = the scale height and the percentage of the i-th ion at the reference level r_o,

M_i = the ion mass of the i-th ion,

κ, T, g_o = the Boltzmann constant, the temperature (= 1000K, same for electrons and ions), and the gravity at r_o respectively.

In our model, ions are composed of O^+ , H_e^+ and H^+, and $\eta_o = 0.025$, η_{He} = 0.823, and $\eta_H = 0.152$ at r_o.

The collisionless model used is

$$N_{ce} = N_{ci} = N_{de}\left[1 - (1 - \frac{B}{B_o})^{\frac{1}{2}} \exp\left(- \frac{z}{2H_p} \frac{B}{B_o - B} \right)\right] \tag{1.76}$$

where H_p is the scale height of H^+ defined by Eq. (1.75), B is the geomagnetic field at a given point, and B_o is the geomagneic field at the bottom (r = 9370km) of collisionless region in the same field line as B. In higher altitudes where H^+ is dominant, we use

$$N_{de} = N_o \exp(-z/2H_p) \tag{1.77}$$

By linearly combining Eqs. (1.75) and (1.76), the following density model are deduced (Aikyo and Ondoh, 1971)

$$\begin{aligned} N_j &= \{\tfrac{1}{2} - f(L)\} N_{dj} + \{\tfrac{1}{2} + f(L)\} N_{cj} \\ f(L) &= \frac{1}{\pi} \tan^{-1}\frac{L - \varepsilon_L}{\varepsilon_L} \\ j &= e, H^+, He^+, \text{ and } O^+ \end{aligned} \tag{1.78}$$

where L, ξ_L, and ε_L are the L value at a given point, the plasmapause position, and the half-width of the transition region. In our later calculation $\xi_L = 4.0$ and $\varepsilon_L = 0.05$ are used, which correspond to Aikyo and Ondoh's model I (1971). The electron density profile of this model is shown in Fig.1.6. The plasmapause is recognized at $L = 4$ in the figure. Latitude dependence at the reference level is neglected.

1-9 Review of Previous Works

We briefly review previous works related with this thesis, especially on the hot plasma theory and ray tracing and describe the background of the present work.

The warm plasma approximation (full adiabatic theory) was first derived by Sitenko and Stepanov (1957) for a low temperature Maxwellian plasma. Aubry et al. (1970) used this approximation to examine the characteristics of wave propagation for frequencies around the plasma frequency f_p and the upper hybrid frequency (f_{UHR}). They confirmed the validity of this theory in comparison with the microscopic theory for the wave normal angles $\theta = 0°$ and 90° with respect to the static magnetic field. Bitoun et al. (1970) applied it to the ray tracing in a plane stratified ionosphere to interpret a topside resonance at f_{UHR}. Hamelin and Beghin (1976) examined the dispersion near the lower hybrid resonance frequency f_{LHR} by this approximation, comparing with the electrostatic approximation at $\theta = 90°$.

The dispersion relation for longitudinal waves can be described by the electrostatic approximation. Bernstein (1958) showed that the longitudinal wave propagating at $\theta = 90°$ has no Landau damping. Crawford (1965)

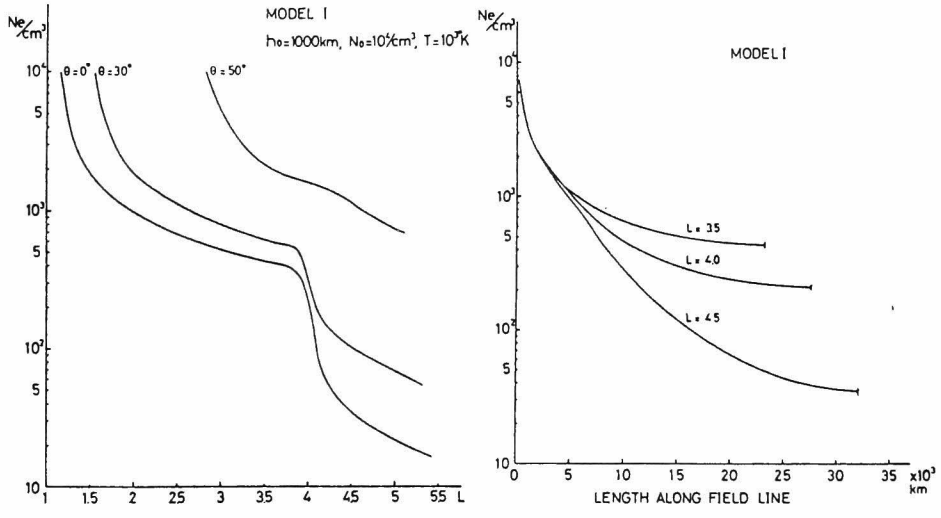

Fig. 1.6. Electron density model. θ indicates latitude in the figure (after Aikyo and Ondoh, 1971).

obtained numerically the dispersion relation for this "Bernstein mode". Harris (1959 and 1961) found growing longitudinal waves in an anisotropic bi-Maxwellian plasma. It was also shown that there is no instability for either $\theta = 0°$ or $\theta = 90°$. This is called "Harris instability". Ozawa et al. (1962) tabulated the unstable regions for variation of parameters, $T_\perp / T_\parallel$, θ, and B_o. The criteria for this instability were obtained by Shima and Hall (1965). Extensive results of the dispersion curves and instability domains were presented by Oya (1971 b) in a range of $f > f_H$. Contour plots of the linear growth rate were obtained by Gitomer et al. (1972). They calculated the refractive index for frequencies $f < f_H$ which are the most unstable frequency range. They studied the nonlinear aspects of the mode by the two dimensional numerical simulation as well. Jacquinot and Leloup (1970) compared the growth rate with that of the whistler mode ($\theta = 0°$) in the frequency range $f < f_H$ under the existence of a cold plasma. As to loss-cone distribution (mirror-confined plasma);

$$f(v_\perp, v_\parallel) = \frac{1}{\pi^{\frac{3}{2}} \alpha_\perp^2 \alpha_\parallel j!} \left(\frac{v_\perp}{\alpha_\perp}\right)^{2j} \exp\left(- \frac{v_\perp^2}{\alpha_\perp^2} - \frac{v_\parallel^2}{\alpha_\parallel^2} \right) \tag{1.79}$$

$$\alpha_\perp = \frac{m}{2\kappa T_\perp}, \qquad \alpha_\parallel = \frac{m}{2\kappa T_\parallel}$$

Dory et al. (1965) indicated that unstable waves can exist even for $\theta = 90°$. Guest and Dory (1965) studied obliquely propagating mode of this kind. Young et al. (1971 and 1973) extensively studied this mode. Young (1974) studied the electrostatic mode in plasmas which consist of cold, bi-Maxwellian, and mirror-confined plasmas in order to interpret electrostatic waves near $f = f_H/2$ in space plasmas.

The microscopic theory (kinetic theory) has been studied by many authors, which was summarized by Stix (1962) for a bi-Maxwellian plasma.

This theory can treat both electromagnetic and electrostatic waves. Oya (1971 a) obtained the dispersion relation numerically over the both waves and discussed conversion of electrostatic plasma waves into electromagnetic waves around f_p and f_{UHR}. When a collisional effect can not be neglected, Lewis and Keller (1962) derived a dispersion relation in a Maxwellian plasma. This case was numerically calculated by Muldrew and Estabrooks (1972). They also compared it with Bitoun et al.'s (1970) results of the warm plasma approximation. Muldrew and Gonfalone (1974) used this dispersion relation to explain an interference between electrostatic waves and electromagnetic field observed in an afterglow plasma in the range of $0.5\ f_H \leq f \leq 1.5\ f_H$.

The ray paths of whistlers in the magnetosphere were first calculated graphically by Maeda and Kimura (1956) and more exactly by Yabroff (1961) using Haselgrove's (1954) equations for ray tracing. Kimura (1966) carried out more realistic ray tracing including the effect of ions. By satellites Angerami (1970) could observe ducted whistlers and some leakage of them from the ducts, which were interpreted by ray tracing in the medium including a field aligned duct. By taking account of a structure of the plasmapause in the electron density profile, Aikyo and Ondoh (1971) computed nonducted VLF wave paths in the vicinity of the plasmapause.

Net amplification of ducted whistlers by the cyclotron instability along field lines was calculated by Liemohn (1967). Analytical ray paths for low frequency ($f << f_H$) nonducted whistlers were obtained by Thorne and Kennel (1967) and growth rates along the paths were calculated by Kennel and Thorne (1967).

Relations between the present thesis and the above-mentioned previous works are as follows. A warm plasma approximation is applied to ray

tracing in warm plasmas (Ch. 5). The electrostatic approximation is compared with the microscopic theory and is used to evaluate the electrostatic nature of waves of large wave number (Ch. 2). The microscopic theory is fundamental in this thesis. This is used not only to calculate, growth rates and polarizations (especially Ch. 3) from dispersion relations but also to comfirm the approximated equations (Chs.4 and 5). A ray tracing computer program is used under a model magnetosphere shown in section 1-8 (Ch. 4), which is extended to the ray tracing in the warm plasma (Ch. 5). Net amplification is calculated for nonducted waves (Ch. 4). As for section 1-2, more detailed analysis is performed in Ch. 6.

1-10 Contribution of the Present Work

In chapter 2, an instability of obliquely propagating whistler mode waves in a single component electron plasma of a bi-Maxwellian distribution is analysed. The dispersion equation (1.37) is solved in a range of $f < f_H$. A large growth rate is obtained in a large wave number region. The electrostatic nature of this mode is clarified in comparison with a calculation of the electrostatic dispersion equation (1.49)(Hashimoto and Kimura, 1973).

In chapter 3, the instability shown in chapter 2 has been examined in more detail. A spatial growth rate and polarization of the mode are calculated as well. This instability with large wave numbers and large wave normal angles is clarified to be quasi-electrostatic, which has both electrostatic and electromagnetic nature and has non-zero magnetic field component. Growth regions are limited to $f > f_H/2$. These characteristics are essential in interpreting the mechanism of the band-limited hiss (Hashimoto and Kimura, 1980).

Chapter 4 is concerned with instabilities in a 2-component plasma which consists of an ambient cold plasma and a dilute bi-Maxwellian hot plasma. Assuming that a real part of the dispersion relation in this plasma is identical with that in the cold plasma, we derive approximate equations for the growth rate of obliquely propagating whistler mode waves in the plasma. These equations consist of a Landau damping term and a cyclotron instability term in a explicit form. The validity of these approximation is confirmed in comparison with solutions of the microscopic theory without approximation. The method is applied to calculate the net growth along ray paths obtained from the ray tracing in a cold plasma (Hashimoto and Kimura, 1977).

In chapter 5, ray paths in a warm plasma in the magnetosphere are calculated. The plasma is assumed to be an isotropic Maxwellian distribution. The warm plasma theory is confirmed in comparison with the microscopic theory at oblique wave normal angles. A ray tracing computer program of Kimura (1966) is modified into the one in a warm plasma, where the refractive index is calculated from the warm plasma approximation. The spatial Landau damping is calculated with the aid of the microscopic theory. A method of estimation of the electron temperature in the magnetosphere from this damping is proposed (Hashimoto et al., 1977).

Chapter 6 is devoted to examine the characteristics of two different types of whistler mode cyclotron instabilities. Waves propagating along the magnetic field are assumed. A temperature anisotropy type instability is compared with a beam type instability. As an extention of the work on electrostatic beam and Landau instabilities of O'Neil and Malmberg (1968) to electromagnetic whistler mode, a transition from the one to the other type is also discussed. It is clarified that the essential energy source of both types of instabilities are the same. (Hashimoto and Matsumoto, 1976)

Chapter 7 gives concluding remarks.

CHAPTER 2

OBLIQUE WHISTLER MODE INSTABILITIES IN ONE-COMPONENT HOT PLASMA

2-1 Introduction

One of the mechanisms frequently used to explain VLF and ELF emissions generated in the magnetosphere is the cyclotron instability. In a hot plasma, the instability caused by a non-Maxwellian distribution is prominent. For longitudinally propagating whistler mode waves,i.e., for the wave normal angle $\theta = 0°$, this instability has been throughly studied by many authors (e.g., Kennel and Petschek, 1966 or Schaler and Trivelpiece, 1967).

In the magnetosphere, generally, whistler mode waves propagate in a direction $\theta \neq 0°$, except when they propagate through the ducts. It is also necessary to consider radiation emitted in an oblique direction. The oblique propagation in a cold plasma permeated by a dilute energetic electron population, is discussed by Kennel (1966) and Brinca (1972). They assumed that the real part of the dispersion relation is derived from that in the cold plasma. Kennel (1966) has shown that the growth rate of the whistler mode becomes smaller as θ becomes larger if ω is low. Brinca (1972) has pointed out that the growth rate becomes maximum or minimum at $\theta = 0°$ according to plasma parameters. In a hot plasma, however, the real part of the dispersion relation differs from that in the cold plasma. Oya (1971 a) has studied the dispersion relation in a hot plasma for waves whose frequencies are higher than the gyrofrequency. In this paper, we will discuss the dispersion of obliquely propagating

whistler mode waves, that is, for frequencies less than the cyclotron frequency, and the instability due to the temperature anisotropy in a bi-Maxwellian velocity distribution.

In the next section, we will describe how to solve the dispersion equation and will discuss the frequency dependence and angular dependence of the dispersion curves, and will finally show that the growth rate becomes maximum at $\theta \simeq 50°$. In section 2-3, we will compare these findings with those derived from the electrostatic approximation and discuss these results in section 2-4.

2-2 Dispersion Equation for All Wave Lengths

The dispersion equation of electromagnetic waves in a magnetoactive hot plasma can be obtained from Eq.(1.37) for a plasma of a bi-Maxwellian distribution (1.10). Complex solutions of Eq. (1.37)i.e.,

$$\omega = \omega_r + i\gamma \tag{2.1}$$

will be solved for real k. In Eq. (2.1), ω_r is the angular frequency and γ is the growth rate ($\gamma > 0$ for instability). In order to obtain the roots of Eq. (1.37), Newton's method is applied, by using $\partial D/\partial\omega$ which is calculated analytically.

Figs. 2.1 and 2.2 show the frequency characteristics of the growth rate γ. The parameters shown in the figures are $P = \Pi_e/\Omega_e$ (Π_e and Ω_e are the electron plasma frequency and the cyclotron frequency), $A = (T_\perp / T_\parallel) - 1$, and $V_{T_\parallel} = \sqrt{2\kappa T_\parallel / m}$ (electron thermal velocity of the parallel temperature $T_\parallel$). The electron temperature is equal to 25eV and 1eV in

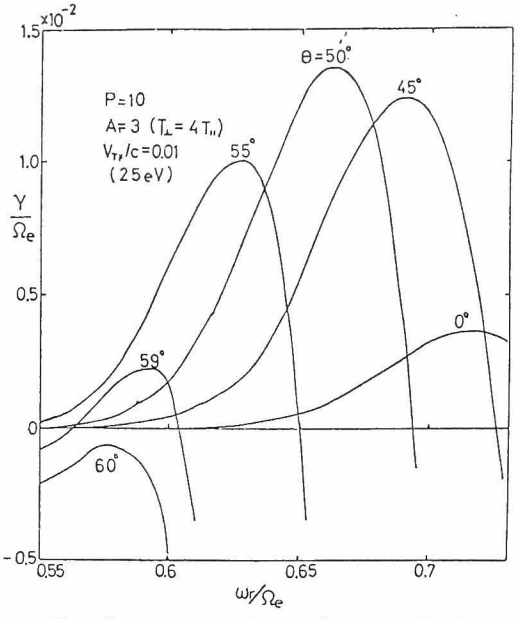

Fig. 2.1. The frequency dependence of the growth rate γ ($T_{\parallel}$ = 25 eV).

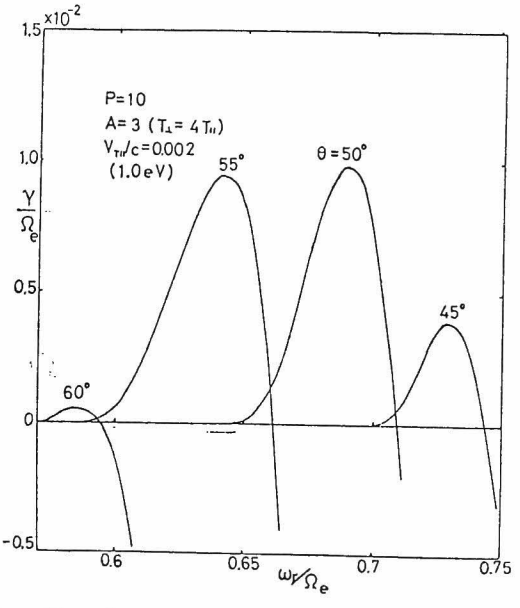

Fig. 2.2. The frequency dependence of the growth rate γ ($T_{\parallel}$ = 1 eV).

Figs. 2.1 and 2.2 respectively. The curve for $\theta = 0°$ is shown in Fig. 2.1 but is not shown in Fig. 2.2 because γ/Ω_e in the latter case is less than 10^{-40}. When $\theta \simeq 60°$ (see the curve $\theta = 59°$ in Fig. 2.1, for example), the growth rate varies first from negative(damping) to positive(growing), and goes to a large negative value as ω_r increases. If θ is fixed, the frequency range in which the growth rate is positive becomes wider as the temperature rises.

In Fig. 2.3 the maximum growth rate γ_{max} and the corresponding frequency ω_{max} at which γ reaches γ_{max} are shown for various θ. The peak value of γ_{max} does not so much depend on temperature, but the range of the wave normal angle corresponding to the large growth rate is narrower when the temperature is lower or P is smaller.

An important fact is that the wave number k corresponding to the large growth rate shown above is so large that these results can be obtained from the electrostatic approximation as shown in the next section.

2-3 Electrostatic Approximation

For electrostatic waves, the electric field is determined from the gradient of a potential. The dispersion relation can, then, be obtained by simpler equations(1.49), instead of Eq. (1.37). These equations are shown in section 1-5.

We compare the ω_r-k diagrams calculated from the dispersion equation of Eq. (1.37) with those calculated from Eq. (1.49), as shown in Figs. 2.4 (a) $\sim$ (c), where the wave number k is normalized by Ω_e/c. The solid lines in the figures correspond to Eq. (1.37), and the broken lines correspond to Eq. (1.49), and the chain lines to the dispersion equation in the cold plasma for $\theta = 50°$.

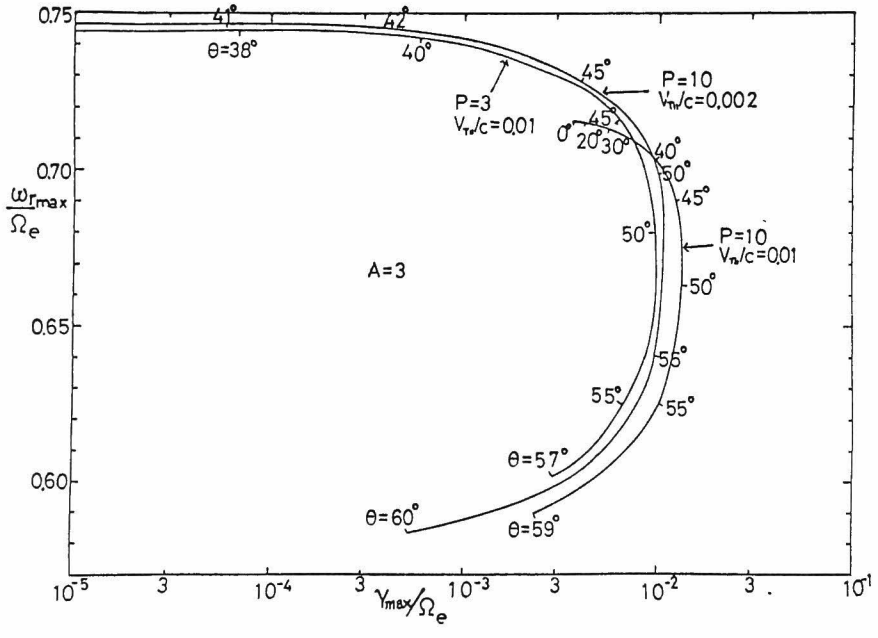

Fig. 2.3. The relationship between γ_{max} and ω_{max} with the wave normal direction θ as a parameter.

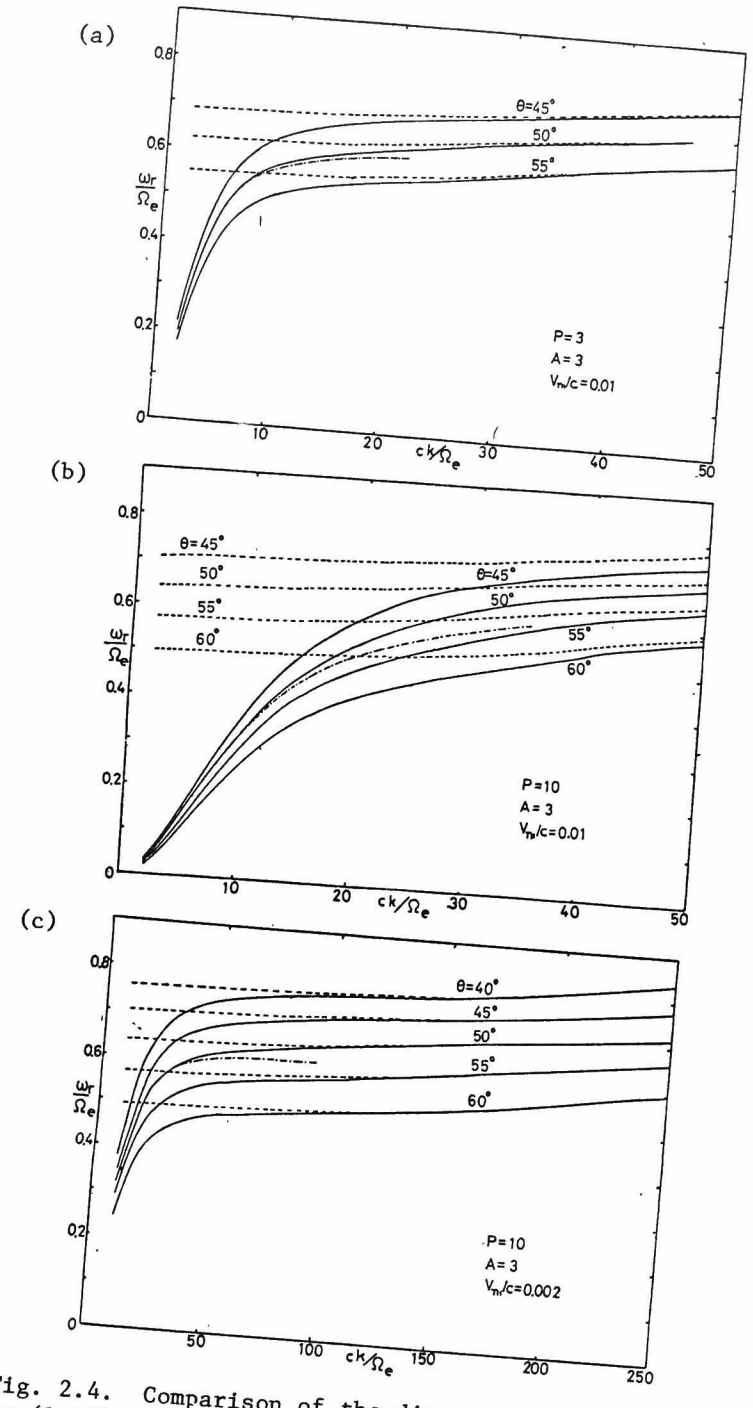

Fig. 2.4. Comparison of the dispersion curves of Eq.(1.37) with those of Eq.(1.49).

As the wave number k increases, the solid line (Eq. (1.37))departs from those of the cold plasma case and approaches to the electrostatic case , where the waves can be treated as electrostatic. When $\theta = 0°$, the propagation mode becomes purely transverse, so that it can not be electrostatic.

From Fig. 2.4(a) and (b), it is shown that waves become electrostatic at a smaller k as P decreases. The plasma parameters used to draw these figures are the same as those of Figs.2.1 and 2.2, respectively. The wavelength for a fixed frequency becomes shorter at a lower temperature, therefore the waves becomes more electrostatic. In Fig. 2.4(c), $V_{T_{\parallel}}/c$ is equal to one fifth of that of Fig. 2.4(b), but the scale of the abscissa is reduced to one fifth of Fig. 2.4(b), because in this scale (Fig.2.4(c))the broken lines(electrostatic approximation) become identical to those in Fig.2.4(b). This is easily understood from the fact that in Eqs.(1.25) and (1.49) the product of k and thermal velocity becomes an independent variable if θ and $T_{\perp}/T_{\parallel}$ are constant. However, the dispersion equation of Eq. (1.37) has the temperature dependence and has generally a larger growth rate in higher temperature. On the other hand, the relation between γ_{max} and ω_{max} in the electrostatic approximation has almost the same characteristics as the curve of $V_{T_{\parallel}}/c$ = 0.002 in Fig. 2.3.

2-4 Discussion and Conclusion

Section 1-5 has discussed the electrostatic instability by a temperature anisotropy. There is no instability at $\theta = 0°$ or 90° and the condition of this instability is

$$\ell + \frac{1}{2} < \frac{\omega_r}{\Omega_e} < \ell + 1 - \frac{T_{\parallel}}{T_{\perp}} \qquad (2.2)$$

where ℓ is an integer. It is found from this result that the instability exists in the oblique direction i.e. at an angle between 0° and 90° for $\omega_r < \Omega_e$ if $\ell = 0$. In the case of Fig.2.4, for example, the instability region of the electrostatic mode exists between $\omega_e/\Omega_e = 0.5$ and $\omega_r/\Omega_e = 0.75$ (in this case $T_{\perp}/T_{\parallel} = 4$). The electrostatic instability discussed in this chapter clearly satisfies the condition specified by Eq. (2.2).

In the region where ω_r is larger than Ω_e, Oya(1971 a) has discussed the mode conversion from Bernstein mode to electromagnetic waves through the upper hybrid frequency. In the present case, i.e., ω_r being less than Ω_e, ω_r departs from its value in the cold plasma due to a thermal effect as wave number increases and approaches that of the electrostatic approximation. The frequency ω_{max} corresponding to the maximum growth rate can exceed the resonance frequency for the whistler mode in the cold plasma.

The emissions excited by this electrostatic instability in the oblique direction can then propagate as the electromagnetic wave mode(whistler mode) over a wide range of the wave normal direction. A point to be stressed is that the emissions thus excited may be very intense, because the growth rate is fairly large, and can reach the earth in the whistler mode.

In conclusion, the whistler mode waves propagating obliquely in the magnetoactive hot plasma are highly unstable, having a large growth rate at relatively large wave normal angles and large wave numbers and it can be considered one manifestation of electrostatic instabilities. The emissions excited by this instability are radiated in the wave normal direction at a large angle to the geomagnetic field, though the ray direction can be directed close to the geomagnetic field.

CHAPTER 3

A GENERATION MECHANISM OF NARROW BAND HISS EMISSIONS ABOVE ONE HALF THE ELECTRON CYCLOTRON FREQUENCY IN THE OUTER MAGNETOSPHERE

3-1 Introduction

VLF emissions in the vicinity of the sub-harmonic cyclotron frequency ($f_H/2$), have been detected near the geomagnetic equator. For example, Burtis and Helliwell (1976) observed by OGO-3 a narrow band hiss above $f_H/2$ in frequency and chorus which consists of two frequency bands near $f_H/2$ with a missing in-between gap at $f_H/2$ (see Fig.3.1). Maeda (1976) reported similar emissions observed by S^3-A satellite, which had both AC-electric and magnetic field components. Among these emissions those especially observed in frequency above $f_H/2$ are generally stronger and more continuous than those below $f_H/2$.

Coroniti et al.(1971) reported extremely narrow band (Bandwidth $\sim 0.02f_H$) emissions at frequencies slightly above $f_H/2$ observed by OGO-5. Young (1974) explained the emission by electrostatic waves in a multi-component plasma which is composed of a cold plasma and a warm plasma with a temperature anisotropy, $A \sim 1.5$. He obtained the real part of dispersion relation from a electrostatic dispersion relation in a cold plasma limit which is equivalent to a resonance condition of a cold plasma dispersion relation. He deduced a plasma distribution function which was able to account for the emissions observed by Coroniti et al. (1971).

The present paper is concerned with the above mentioned emissions appearing in a frequency range above $f_H/2$. We suppose that the chorus

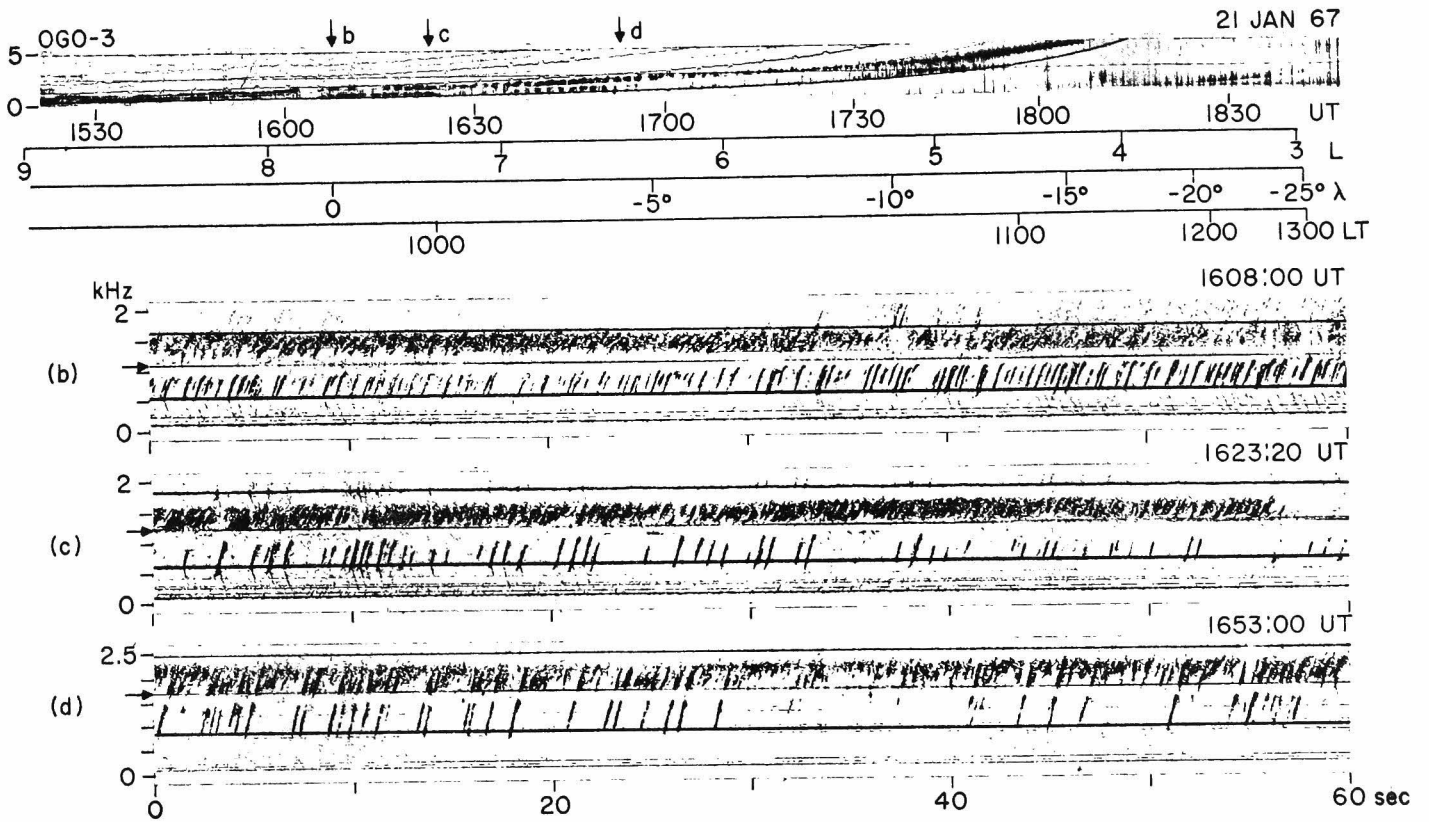

Fig. 3.1. (See caption in page 43).

observed at the same time with the hiss as reported by Burtis and Helliwell (1976) is considered to be generated by a different mechanism, and we now propose a generation mechanism of the hiss. The proposed mechanism is ascribed to a kind of the Harris type electrostatic instabilities in a single component bi-Maxwellian hot plasma. The mode concerned is an extension of the whistler mode in a shorter wavelength range (Hashimoto and Kimura, 1973). We call it a quasi-electrostatic whistler mode, which has both electrostatic and electromagnetic wave properties. The narrow-band emissions reported by Coroniti et al.(1971) may also be of the same category of the hiss.

We will describe, in section 3-2, on the quasi-electrostatic whistler mode and on its growth rate, polarization and propagation characteristics. In section 3-3, we will discuss the hiss, reported by Burtis and Helliwell (1976), the emissions reported by Maeda (1976),and the narrow-band emissions reported by Coroniti et al. (1971).

3-2 Quasi-electrostatic Whistler Mode

For a frequency f, less than the electron cyclotron frequency f_H, it is clarified in chapter 2 that a large growth rate is expected at relatively large wave normal angles and large wave numbers. Figure 3.2 shows a contour map of the growth rate of the instability as a function of frequency and wave normal angle θ, calculated from Eq. (1.37) for $f < f_H$, for in the plasma frequency $f_p = 8f_H$ and a parallel electron temperature of 2.5 eV (26000K) which are the plasma parameters at $L \sim 6$ in the equatorial plane in the magnetosphere. (Serbu and Maier, 1966 and Decreau et al., 1978). A small temperature anisotropy factor $A = T_\perp/T_\parallel - 1 = 2$

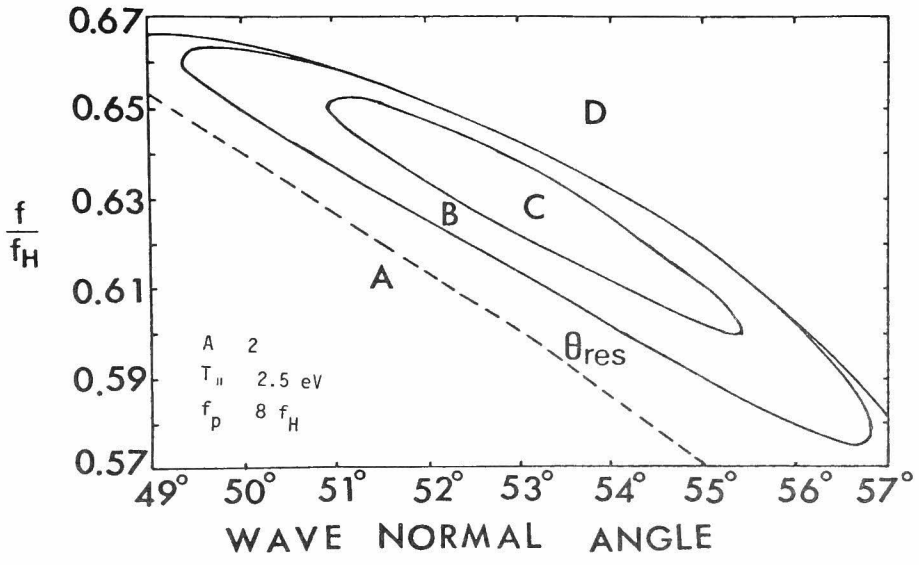

Fig. 3.2. Contour of growth rate as a function of frequency and wave normal angle.

Caption for Fig. 3.1.

Equatorial chorus detected with the electric antenna; dipole coordinates of the satellite are shown. Top panel: compressed spectrum showing double band of chorus increasing in frequency (magnetometer lines inserted at $f_H/4$ and harmonics). Panel b (geomagnetic latitude $\lambda \cong 0°$): arrow indicates 0.5 f_H; note absence of chorus between 0.45 and 0.55 f_H. Panel c ($\lambda = -2°$): note low correlation of emissions between upper and lower band. Panel d ($\lambda = -5°$): here is an unusual degree of correlation between bands; the upper band now begins near $f = 0.49\ f_H$ (after Burtis and Helliwell, 1976).

is assumed where $T_\perp$ and $T_\parallel$ are the temperatures of the bi-Maxwellian electron distribution perpendicular and parallel to the geomagnetic field lines, respectively. Solid lines divide the figure into four regions, A, B, C, and D. Region A is specified as $0 < \gamma < 10^{-4}\Omega_e$, B as $\gamma > 10^{-4}\Omega_e$, C as $\gamma > 5 \times 10^{-4}\Omega_e$ (grow) and D as $\gamma < 0$(damp), where $\Omega_e = 2\pi f_H$. In region D ($\gamma < 0$) the waves are heavily damped by the Landau and cyclotron dampings. Region C is the most growing region for a rather wide range of wave normal angles and for frequancies less than f_H. In the figure, a dashed line indicates the cold plasma resonance cone angle θ_{res} as a function of frequency. This line is equivalent to the so-called electrostatic dispersion relation in a cold plasma limit (e.g., Guest and Sigmar, 1971)

Although in a cold plasma, whistler mode waves can not propagate if $\theta > \theta_{res}$, the temperature effect enables them to propagate even for $\theta > \theta_{res}$. Actually, in the growing region, say $\gamma > 10^{-4}\Omega_e$, the wave normal angle θ is larger than θ_{res}.

The waves in this region are well approximated by the electrostatic approximation (1.49). The mode approximated by Eq.(1.49) for $f < f_H$ is the whistler mode with electrostatic properties. We will therefore call it " quasi-electrostatic whistler mode". In the following, we will discuss the magnetic field component of this mode.

Generally, the wave electric filed $\vec{E}$ is composed of two components;

$$\vec{E} = \vec{E}_\parallel + \vec{E}_\perp \tag{3.1}$$

where $\parallel$ and $\perp$ denote the longitudinal and transverse components with respect to the wave normal direction, respectively. Nontrivial solutions of Eq.(1.37) give the wave polarization. For example,

$$\frac{E_\parallel}{E} = \frac{E_x}{E}\sin\theta + \frac{E_z}{E}\cos\theta \tag{3.2}$$

Therefore, the ratio of the transverse component to the total electric field is given by

$$\frac{|\vec{E}_\perp|}{|\vec{E}|} = \sqrt{1 - \left(\frac{E_\parallel}{E}\right)^2} \tag{3.3}$$

On the other hand, the wave magnetic field $\vec{B}$ has only a transverse component $\vec{B}_\perp$. According to Maxwell's equations,

$$c\,\vec{B} = \vec{n} \times \vec{E}_\perp \tag{3.4}$$

i.e.,

$$c\,|\vec{B}| = n\,|\vec{E}_\perp| \tag{3.5}$$

Figure 3.3 shows a wave normal angle dependence of n, $|\vec{E}_\perp|/|\vec{E}|$, and $c|\vec{B}|/|\vec{E}|$, where the plasma parameters adopted in the calculation are the same as those of Fig.3.2 and $f = 0.63f_H$. When $\theta = 0°$, $|\vec{E}_\perp|/|\vec{E}|$ is unity, and $|\vec{E}_\perp|/|\vec{E}|$ decreases remarkably as θ increases. The ratio $|\vec{E}_\perp|/|\vec{E}|$ becomes about 10^{-2} at $\theta \sim 52°$, where waves are nearly electrostatic. However, $c|\vec{B}|/|\vec{E}|$ decreases down to only one tenth of that of $\theta = 0°$ because of the increase of the refractive index n. It will suggest that the magnetic field component of the waves of this mode is observable as well as the electric field component.

The spatial growth rate $-k_i$ of this mode is given by the relation

$$\gamma = -\vec{k}_i \cdot \vec{v}_g = -k_i v_{gk} \tag{3.6}$$

where $\vec{v}_g$ and v_{gk} are the group velocity and its component in the wave normal direction . Considering $v_{gk} = \partial\omega_r/\partial k_r$, we obtain (see Appendix A)

$$k_i = -\gamma/v_{gk} = -\gamma/(\partial\omega_r/\partial k_r) \tag{3.7}$$

The normalized temporal growth rate (γ/Ω_e; solid line) and spatial growth rate ($-ck_i/\Omega_e$; dashed line) are shown as a function of the wave normal angle in Fig.3.4. The parameters are the same as those of Fig.3.3. The peak of γ/Ω_e corresponds to the maximum growth rate in region D of Fig.

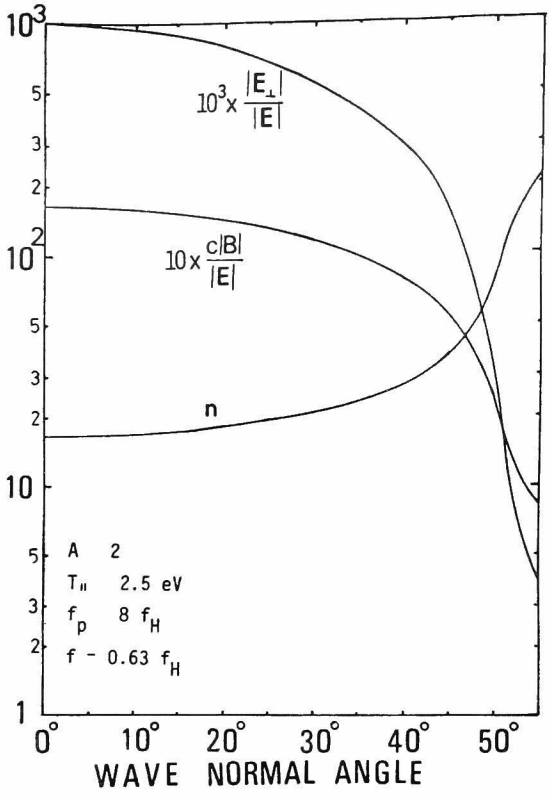

Fig. 3.3. Wave normal angle dependence of refractive index, transverse electric and magnetic field components of the wave.

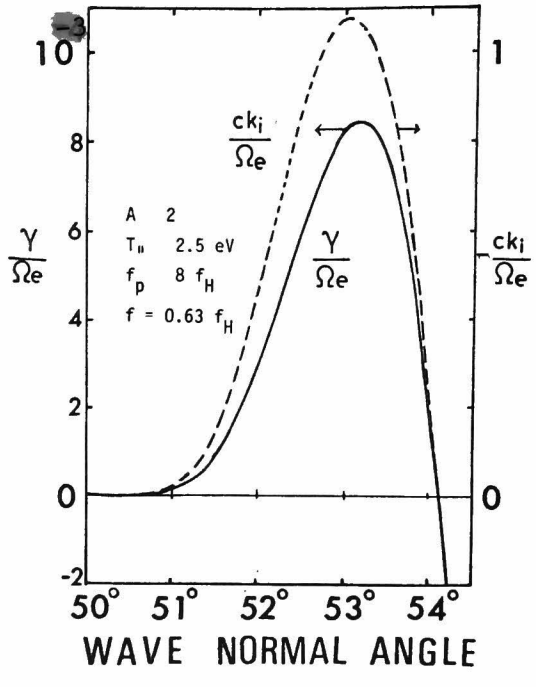

Fig. 3.4. Temporal and spatial growth rate as a function of wave normal angle.

3.2. Now, let us consider an actual situation in the magnetosphere. In Fig.3.3, $\gamma_{max} = 8 \times 10^{-4}\Omega_e$. The required time by γ_{max} to have the wave amplitude amplified by e-fold times at $L \simeq 6.6$ in the equatorial region is about 66 msec at $f_H = 3$kHz. The path length required for this amount of growth $\lambda_i = -2\pi/k_{imax}$ is 100 km at $-ck_{imax}/\Omega_e \simeq 1$ in Fig.3.4.

The mode becomes nearly electrostatic as k increases, and for a smaller k as f_p decreases or the temperature decreases (chapter 2). The unstable region of electrostatic waves described by Eq. (1.49) is limited in the following range from Eq.(1.50),

$$\frac{A}{A+1} f_H > f > \frac{1}{2} f_H \tag{3.8}$$

The growth rate of this instability and a frequency limit, below which waves grow are strictly dependent on the anisotropy factor A. Figure 3.5 shows the dependence of the growing region on the anisotropy factor A. Parameters other than A are the same as those of Fig.3.2. Solid lines show a boundary above which the wave is damped and points indicate the positions of the maximum growth rate for A = 2, 1.9, and 1.8, respectively. The maximum growth rates are $8.4 \times 10^{-4}\Omega_e$, $4.8 \times 10^{-4}\Omega_e$, and $2.4 \times 10^{-4}\Omega_e$ in case of A = 2, 1.9, and 1.8, respectively. The smaller the factor A, the narrower the growth region. A wave which grows when e.g. A = 2.0 in the region between the two lines corresponding to A = 2.0 and 1.8 must be damped when A is reduced to 1.8. Thus a small change of A seriously affects the propagation characteristics. The quasi-electrostatic mode has only a small growth rate or is in a marginal state for $f < \frac{1}{2}f_H$, the fact being different from the electrostatic case by Eq. (1.49).

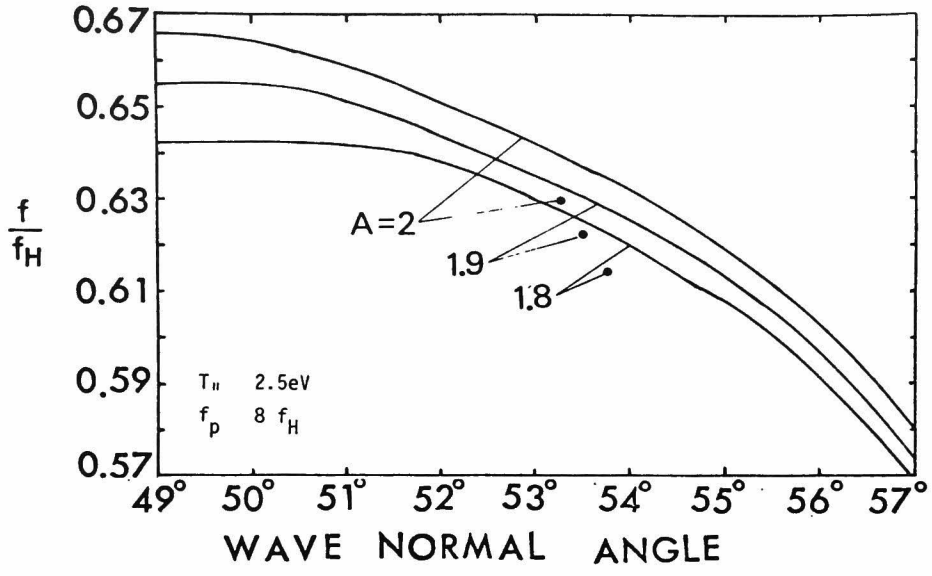

Fig. 3.5. Upper limits of wave growth and positions of the maximum growth rate.

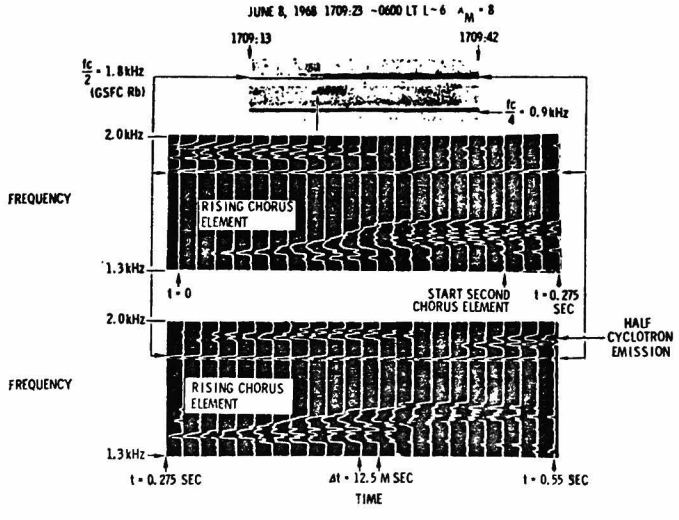

Fig. 3.6. Ogo 5 electric field ampligram of the 2 VLF banded chorus elements shown in the f-t diagram; note the narrowband emission slightly above the half-electron cyclotron frequency rubidium vapor magnetometer interference line (after Coroniti et al., 1971).

3-3 Application of Quasi-electrostatic Instability

The hiss above the half electron cyclotron frequency, $f_H/2$ observed by OGO-3 satellite near the geomagnetic equator shown in Fig.3.1 is thought to be an example of emissions caused by the quasi-electrostatic whistler mode instability as shown in Fig.3.2. Although there was also chorus in frequency below $f_H/2$ in the above case, we pay special attention only to the hiss. Then, the above-mentioned mode well explains the band limited nature and existence of lower cutoff in frequency above $f_H/2$ of the hiss. This chorus must be interpreted by a different mechanism, such as those by Burtis and Helliwell (1976).

Similar emissions were also observed by S^3-A satellite on an equatorial orbit (Fig.2 of Maeda, 1976). In this case, their magnetic field component was also found with a considerable intensity as well as electric field, although the absolute intensity could not be determined from the spectra. As was previously discussed, the "quai-electrostatic whistler mode" can possess the magnetic field component, as shown in Fig. 3.3, the fact being consistent with the observed results.

We have assumed that the emissions are observed near the source in the above two cases. A narrow band hiss is considered to be generated in a region where anisotropy factor A is maximum. When this hiss propagates toward outside of the source region, the band of frequency becomes narrower because the upper limit frequency decreases due to a decrease of A as shown in Fig.3.5. These situations will explain the extremely narrow band emissions slightly above $f_H/2$ ($0.53f_H$) observed by the OGO-5 satellite at $L \simeq 6$ at a geomagnetic latitude of 8° as shown in Fig.3.6 (Coroniti et al.,1971). In this case, it is thought that the emission was generated near the equator and propagate towards the earth. During the propagation, an increase of f_H also causes a decrease of f/f_H, resulting in the band-

width becoming narrower.

3-4 Discussion and Conclusion

We have calculated the whistler mode dispersion in the quasi-electrostatic conditions in a background hot plasma with a small anisotropy factor (A = 2) in the outer magnetosphere. There is almost no growth for $f > f_H$ in the above plasma conditions. Although larger anisotropies will cause wave growth even for $f > f_H$ (Oya, 1971 b), such a bi-Maxwellian plasma is generally most unstable for $f < f_H$ in a linear regime, as in the case of the Harris type pure electrostatic instability treated by Gitomer et al. (1972). For this reason, the VLF emissions often observed in frequency near $\frac{3}{2}f_H$ which were well correlated with enhanced magnetospheric electrons (e.g. Anderson and Maeda,1977) must be attributed to other mechanisms.

Recently, Coroniti et al., (1980) observed Jovian whistler mode chorus and $f_H/2$ emissions by Voyager 1 (see Fig.3.7). In order to explain a generation mechanism of the observed chorus, they suggest that a bi-Maxwellian ($T_\perp \simeq 2T_\parallel \simeq 2$keV) electron distribution should exist by 1% of the background plasma density. If the background plasma has an anisotropic temperature of the order of few eV, the $f_H/2$ emissions may also be explained by the quasi-electrostatic instability.

The hiss and the narrow band emissions, above $f_H/2$ observed in the vicinity of the equatorial plane may be explained by the quasi-electrostatic whistler mode. This mode has the following characteristics. (1) growing region is essentially band-limited above $f_H/2$, (2) wave magnetic field is not negligible, and (3) waves can propagate as an extention of the oblique whistler mode branch. The first characteristic

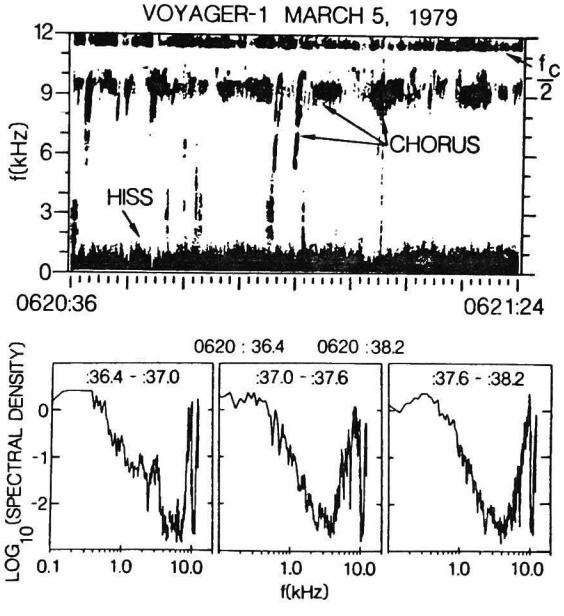

Fig. 3.7. The top panel contains frequency versus time display showing unstructured hiss, structured chorus, a half-cyclotron frequency gap, and an $f_H/2$ emission. The bottom panel contains successive 0.6-second spectral density averages made up from the high resolution waveform link which provides one 50 Hz to 12 kHz spectral sweep every 60 milliseconds. The plasma frequency $f_p \simeq 6f_H$. f_H is shown as f_c in the figure (after Coroniti et al., 1980).

(1) is important to explain the lower cut off above $f_H/2$, whereas the electromagnetic cyclotron instability does not limit the frequencies of emissions only above $f_H/2$. The observed magnetic field of quasi-electrostatic waves can be explained by (2). Characteristic (3) and decrease of f/f_H and anisotropic factor A during the propagation account for the extremely narrow band emissions. Ray tracing and calculation of the growth rate in a hot plasma with temperature anisotropy may be necessary for a more exact check.

CHAPTER 4

OBLIQUELY PROPAGATING WHISTLER MODE WAVES IN COLD PLASMAS PERMEATED BY DILUTE HOT PLASMA

4-1 Introduction

Recently the wave normal angle of VLF emissions was observed by OGO-5 satellite and it was found that the chorus was often non-ducted and was thus propagating obliquely to the geomagnetic field (Thorne et al., 1973; Burton and Holzer, 1974). Cerenkov radiation is known to be mainly radiated in the direction close to the resonance cone angle, which is another example of oblique propagation (Taylor and Shawhan, 1974). Papers which have dealt with oblique whistler mode propagation in a hot plasma are few. Kennel (1966) has studied the problem of obliquely propagating low-frequency waves in a cold plasma permeated by a dilute energetic population of a power law $(\text{energy})^{-n}$ spectrum.

Kennel and Thorne (1967) have estimated the wave growth along the non-ducted low-frequency whistler path. Brinca (1972) has analysed the growth rate for oblique propagation in a cold plasma permeated by hot electrons of a mathematically tractable distribution and has shown that the growth rate does not necessarily become a maximum for propagation along the static magnetic field in comparison with propagation at an arbitrary wave normal direction.

In this paper, we deal with a similar problem of oblique propagation in which we choose a bi-Maxwellian distribution function of hot electrons permeating a cold plasma. We then assume that the real part of the

frequency ω_r as a solution of the dispersion relation for a real k is identical with that in the cold plasma, as assumed by the above authors. In section 4-3, approximate equations composed of elementary functions are derived for the growth rate calculation, and the accuracy is discussed in section 4-4. Conditions for minimal parallel growth are derived as was done by Brinca (1972) and are compared with his results in section 4-5. The contribution of Landau damping to the oblique propagation is also examined. In section 4-6, we try to apply this method of growth rate calculation to the accumulation of the growth rate along ray paths of non-ducted whistler mode waves in a model magnetosphere.

4-2 Dispersion Relation

The dispersion equation of electromagnetic waves in the 2-component plasma (cold and dilute hot plasma) is shown in Eq. (1.37). Each element of $\overleftrightarrow{K}$ is the sum of the cold plasma component (S, D, and P) and the hot plasma component (M_{ij}) as follows

$$\begin{aligned} &K_{xx} = S + iqM_{xx}, \quad K_{yx} = iD + iqM_{yx}, \quad K_{zx} = iqM_{zx} \\ &K_{yy} = S + iqM_{yy}, \quad K_{zy} = iqM_{zy}, \quad K_{zz} = P + iqM_{zz}, \\ &K_{xy} = -K_{yx}, \quad K_{xz} = K_{zx}, \quad K_{yz} = -K_{zy} \end{aligned} \tag{4.1}$$

where $q = \Pi_h^2/\omega\Omega_e$, and Π_h and Ω_e are the plasma frequency of the hot electrons and the electron cyclotron frequency, respectively. S, P and D are the familiar Stix (1962) notations,

$$S = 1 + \frac{\Pi_c^2}{\Omega_e^2 - \omega^2}, \quad D = \frac{-\Pi_c^2\Omega_e}{\omega(\omega^2 - \Omega_e^2)}, \quad P = 1 - \frac{\Pi_c^2}{\omega^2}, \tag{4.2}$$

where Π_c is the plasma frequency of the cold electrons. Each element of $\overleftrightarrow{M}$ is shown by Eq. (1.19). The solutions of Eq. (1.37) will be compared with those of the approximated equations derived in the next section in

order to examine the accuracy of the approximation.

4-3 Approximate Equations

In this section, we summarize the assumptions to be made in the present paper.

(i) The hot electron density N_h is δN_c where N_c is the cold plasma density and δ is a constant which is much less than unity.

(ii) The dispersion relation $D = 0$ may be expanded into the lowest order determinant D^c and a higher-order complex determinant D^h. D^c corresponds to the cold plasma and consists of real elements. D^h corresponds to the hot plasma correction, and then, $D \equiv D^c + D^h = 0$. D^h is calculated only by the first-order term in λ and in the real and imaginary corrections for the cold plasma solutions. Therefore, we use D^1 instead of D^h and neglect its higher-order corrections.

(iii) The growth rate is so small that $\gamma << \omega_r$ and ω_r is derived from the cold plasma dispersion relation, i.e. $D^c = 0$. γ is considered to be a correction due to the existence of the hot plasma, and a correction to ω_r is neglected.

(iv) In each term of D^1, we take the zero- and first-order terms in λ of Eq. (1.20) and neglect the higher-order terms.

(v) The plasma dispersion function (1.26) is approximated as

$$Z(\alpha_n) = Z_r + i\pi^{1/2}\exp(-\alpha_n{}^2). \tag{4.3}$$

Because $\gamma << \omega_r$, we can use $\mathrm{Re}[\alpha_n]$ instead of α_n and Z_r is the real part of Z.

(vi) We consider the Landau resonance α_0 and the fundamental cyclotron resonance α_{-1} only, and neglect the other terms.

Here, we derive one example of the approximated elements of $\overleftrightarrow{M}$ based on the above assumptions. When λ is small, the modified Bessel function of the n-th order $I_n(\lambda)$ becomes,

$$I_0(\lambda) \simeq 1, \quad I_{\pm 1}(\lambda) \simeq \lambda/2 \quad \text{and} \quad \exp(-\lambda) \simeq 1 - \lambda \tag{4.4}$$

According to the assumptions (iv) to (vi), for example, M_{xx} of Eq. (1.19) and $\langle\theta\rangle_n$ of Eq. (1.28) are approximated by

$$M_{xx} = \frac{\Omega_e \kappa T_\perp}{mk_z} \frac{1-\lambda}{2} \langle\theta\rangle_{-1}, \tag{4.5}$$

$$\mathrm{Re}[\theta_n] = -\frac{2\pi^{1/2} T_\parallel}{T_\perp} \left(\frac{m}{2\kappa T_\parallel}\right)^{3/2} \left[1 + \frac{\omega + n\Omega_e}{\omega}\left(\frac{T_\perp}{T_\parallel} - 1\right)\exp(-\alpha_n^2)\right]. \tag{4.6}$$

The thermal correction $\omega^1 + i\gamma$ is found by the Taylor expansion about the cold plasma solution (Kennel 1966),

$$D^1(\omega_r, k) + (\omega^1 + i\gamma)\partial D^c(\omega_r)/\partial\omega = 0 \tag{4.7}$$

The growth rate γ is obtained by taking the imaginary part of Eq.(4.7)

$$\omega^1 = -\mathrm{Re}[D^1]/(\partial D^c/\partial\omega), \quad \gamma = -\mathrm{Im}[D^1]/(\partial D^c/\partial\omega). \tag{4.8}$$

$\mathrm{Re}[D^1]$ and $\mathrm{Im}[D^1]$ depend on $\mathrm{Re}[Z]$ ($\equiv Z_r$) and $\mathrm{Im}[Z]$ respectively. γ is a function of $\mathrm{Im}[Z]$. ω^1 is a function of Z_r and it is much smaller than ω_r. Z_r is not used in our calculation, because we can neglect ω^1, this being confirmed <u>a posteriori</u> by comparing with the exact solution of Eq. (1.37). Finally, we can derive the following approximated equations,

$$D^c = (P - n_x^2)\{(S - n_z^2)(S - n^2) - D^2\} + (S - n^2)n_x^2 n_z^2,$$

$$\begin{aligned}\mathrm{Im}[D^1] = {} & \chi_1[(P - n_x^2)\{(S - n_z^2) + (S - n^2) - 2D\} - n_x^2 n_z^2] \\ & -2\phi_1 n_x n_z (S - n^2 - D) - 2\phi_0 n_x n_z D + \psi_0\{(S - n_z^2)(S - n^2) - D^2\} \\ & + 4\lambda\chi_0\{(P - n_x^2)(S - n_z^2) - n_x^2 n_z^2\} + \lambda\chi_1[(P - n_x^2)\{4D - (S - n^2)\end{aligned}$$

$$- 3(S - n_x^2)\} + 3n_x^2 n_z^2] + \lambda(\psi_1 - \psi_0)\{(S - n_x^2)(S - n^2) - D^2\}, \tag{4.10}$$

where $n_x = n\sin\theta$, $n_z = n\cos\theta$,

$$\chi_j = \frac{\pi^{1/2}\Pi_h^2}{k_z\omega}\left(\frac{m}{2\kappa T_{\parallel}}\right)^{1/2}\left\{1 + \frac{\omega - j\Omega_e}{\omega}\left(\frac{T_{\perp}}{T_{\parallel}} - 1\right)\right\}\exp(-\alpha_{-j}^2),$$

$$\phi_j = \chi_j\left(\frac{\omega}{\Omega_e} - j\right)\tan\theta, \tag{4.11}$$

$$\psi_j = \frac{2\pi^{1/2}\Pi_h^2}{\omega k_z^3}\left(\frac{m}{2\kappa T_{\parallel}}\right)^{3/2}(\omega - j\Omega_e)^2\left(1 - \frac{\Omega_e}{\omega}\frac{jA}{A+1}\right)\exp(-\alpha_{-j}^2)$$

θ is the angle between the wave normal and the static magnetic field (z axis), and $A = (T_{\perp}/T_{\parallel}) - 1$ the temperature anisotropy factor. χ_j of Eq.(4.11) obeys the following relation,

$$\chi_j = -\frac{\Pi_h^2 \kappa T_{\perp}}{2\omega m k_z}\mathrm{Re}[\langle\theta\rangle_{-j}]. \tag{4.12}$$

From Eqs.(4.8), (4.10) and (4.11) we can calculate the growth rate with a fairly high accuracy. This method has the following merits. (a) The growth rate is obtained in the explicit form for a given k or ω_r. (b) Equations are represented by the elementary functions only. (c) Calculations can be performed quickly. (d) The growth rate (or damping rate) due to the cyclotron instability and that due to Landau damping are calculated separately. We can therefore easily understand the physical meaning of the results.

4-4 Accuracy of the Approximation

We discuss the accuracy of the approximation before considering the physical aspects. Figures 4.1 and 4.2 show the wavenumber vs.growth rate

characteristics. In the figures, A is the temperature anisotropy factor and $V_{T_{\parallel}}$ is the thermal velocity defined by $(2\kappa T_{\parallel}/m)^{1/2}$. γ_{exact} (solid lines) is the growth rate obtained by the numerical solution of Eq. (1.37) as follows:

(i) we have carried out the summations for so long as $I_n(\lambda)$ is greater than 10^{-10},

(ii) when $\theta = 0°$, only the $n = -1$ term survives for the whistler mode,

(iii) the plasma dispersion function Z was calculated by a continued fraction method reported by Gautschi (1970) and was confirmed by comparing with the tables of Fried and Conte (1961).

γ_c, γ_L (both plotted by dotted lines) and γ ($= \gamma_c + \gamma_L$; dashed lines) represent the cyclotron instability, Landau damping ($\gamma_L < 0$) and the resultant approximated growth rate obtained by Eq. (4.8), respectively. γ_c is the sum of the terms multiplied by χ_1, ϕ_1, or ψ_1 of Eq. (4.10). This corresponds to the fundamental electron cyclotron resonance terms ($j = 1$ in Eq. (4.11)). Similarly, γ_L is the sum of the terms associated with χ_0, ϕ_0, and ψ_0 in Eq. (4.10). The electron temperature is adopted to be 25eV for a low temperature case and 2.5keV for a high temperature case as shown in Figs.4.1 and 4.2 respectively.

First we consider Fig.4.1. When $\theta < 30°$ or $ck < 20\Omega_e$, the approximation is accurate and approximated γ agrees with γ_{exact}. Therefore γ is not shown in the figure. When $\theta = 40°$, γ almost agrees with γ_{exact} if ck is less then $20\Omega_e$ and γ is still a good approximation if ck is less than $27\Omega_e$. When $\theta = 50°$, γ is not so exact because γ_c and γ_L have large absolute values of different signs. In Fig.4.2, γ agrees with γ_{exact} if $ck < 6\Omega_e$. The accuracy at large θ is later examined in section 4-5-3.

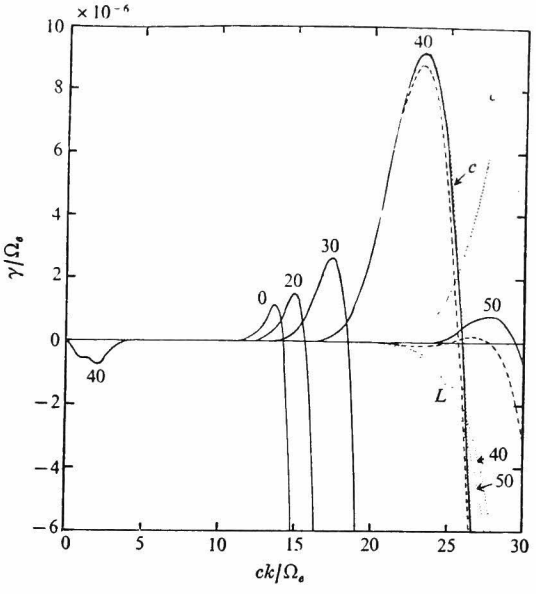

Fig. 4.1. Wave number vs. growth rate characteristics for a low temperature. The numbers 0, 20, etc., near the line indicate θ = 0°, 20°, etc. The letters L and c indicate γ_L and γ_c respectively. Π_c/Ω_e = 10; $T_\perp = 3T_{\parallel}$ (A = 2); $V_{T_{\parallel}}$ = 0.01c (25 eV); δ = 1%.

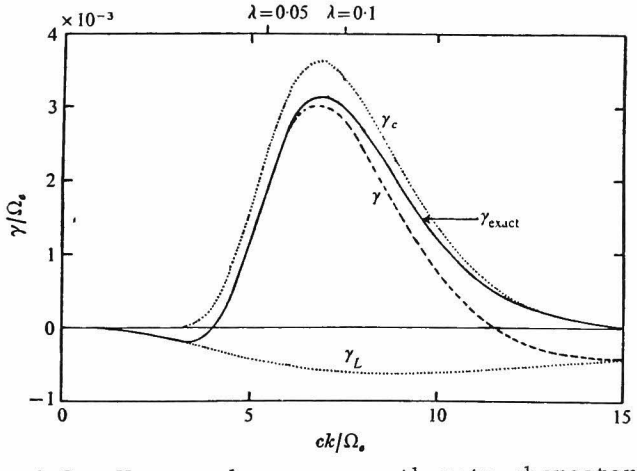

Fig. 4.2. Wave number vs. growth rate characteristics for a high temperature. Π_c/Ω_e = 10; $T_\perp = 3T_{\parallel}$ (A = 2); $V_{T_{\parallel}}$ = 0.1c (2.5 keV); δ = 1%; θ = 20°.

4-5 Growth Rate

4-5-1 Frequency or wavenumber dependence of the growth rate

We discuss Ladnau damping and cyclotron instability of oblique propagation separately. Figure 4.1 shows the wavenumber vs.growth rate characteristics for a low temperature case ($T_{\parallel}$ = 25eV). First we pay attention to the solution for $\theta = 40°$. When $ck < 5\Omega_e$, $\gamma = \gamma_{exact} = \gamma_L$ and $\gamma_c = 0$. This negative γ is due to the Landau damping which is caused by a slow phase velocity($\lesssim$ thermal velocity) and the presence of electric field components parallel to the wave vector. Landau damping rate ($-\gamma_L$) increases with increasing θ (not shown in the figure) and this tendency is the same as the results of Kennel (1966). When $5\Omega_e < ck < 15\Omega_e$, $\gamma \simeq 0$ where both γ_L and γ_c are nearly equal to zero. When $ck > 15\Omega_e$, γ begins to increase, then decreases and changes its sign at $ck \simeq 26\Omega_e$. A negative γ_c indicates cyclotron damping. The total damping ($-\gamma$) is larger than the cyclotron damping ($-\gamma_c$) because Landau damping is added to it, which is significant where $ck > 20\Omega_e$. This Landau damping is caused by a slow phase velocity of the whistler mode wave in the vicinity of the resonance cone angle. The peak value of γ is a maximum at $\theta = 40°$ in the figure. This fact means that γ is not always a muximum for the propagation along a static magnetic field line even in the bi-Maxwellian plasma.

Figure 4.2 is a high temperature case of $\theta = 20°$; then a maxumum in the positive γ occurs at the parallel propagation (i.e.$\theta = 0°$), although this case is not shown in the figure. In the figure, Landau damping γ_L reaches a blunt maximum at $ck = 9\Omega_e$ where the phase velocity shows a maximum, being closest to the thermal velocity which is larger than the phase velocity in this region. For a small k, γ is negative because Landau damping is larger than the growth due to the cyclotron instability.

4-5-2 Condition of minimal parallel growth

As was shown above, when either the wave frequency is low (i.e. k is small) or the temperature is high, the growth rate becomes a maximum for the parallel propagation ($\theta = 0°$). For a higher frequency as well as a lower temperature, the growth rate of the parallel propagation does not necessarily show a maximum.

The condition that the growth rate becomes a minimum for $\theta = 0°$ is called the minimal parallel growth and this condition is equivalent to $\gamma'' = d^2\gamma/d\theta^2 > 0$ at $\theta = 0°$ because $d\gamma/d\theta$ is always equal to zero for $\theta = 0°$. Brinca(1972) has discussed such a condition for the following hot plasma distribution function,

$$f(v_\perp, v_\parallel) = a v_\perp^{2p}/(v_\perp^2 + v_\parallel^2 + v_0^2)^q \qquad (4.12)$$

where a is a normalization factor, v_0 corresponds to thermal velocity and p corresponds to the anisotropy factor A. His results are that there exists minimal parallel growth for a high temperature case. We should note that the above distribution has a part of $\partial f/\partial v_\perp > 0$ when $p \neq 0$, whereas there is no such part for the bi-Maxwellian distribution used in the present paper.

Figure 4.3 shows the limiting condition of $\gamma''(0) = 0$; in other words the threshold value of the parallel temperature of a hot plasma in the bi-Maxwellian distribution as a function of ω_r. In this calculation, we differentiate Eq. (4.8) after setting λ equal to zero because θ is very close to zero and λ is the second order term in θ. Contrary to Brinca's case, the minimal parallel growth $\gamma''(0) > 0$(shown by '+' in the figure) occurs at a relatively lower temperature region in our case. $\gamma''(0)$ is always negative when ω_r is less than $0.5\Omega_e$. When the temperature anisotropy factor is greater than unity, $\gamma''(0)$ changes its sign near the frequency

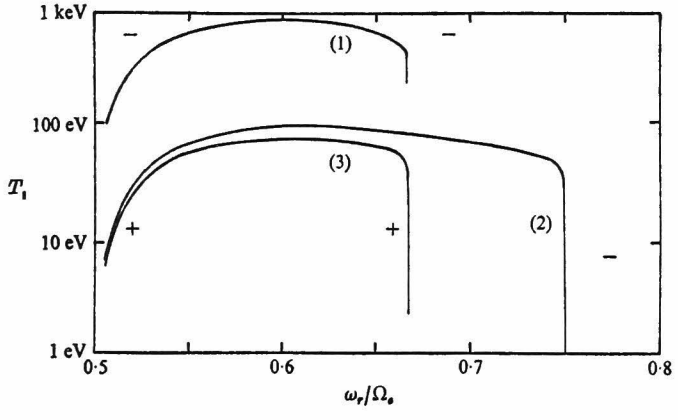

Fig. 4.3. Condition of the minimal parallel growth $\gamma''(0) = 0$. The signs + and - indicate the sign of $\gamma''(0)$. (1) $\Pi_c/\Omega_e = 3$; $T_\perp = 3T_\parallel$ (A = 2). (2) $\Pi_c/\Omega_e = 10$; $T_\perp = 4T_\parallel$ (A = 3). (3) $\Pi_c/\Omega_e = 10$; $T_\perp = 3T_\parallel$ (A = 2). $\delta = 1\%$.

$$\omega_r = A\Omega_e/(A+1) \qquad (4.13)$$

where γ also changes its sign. Thus A must be large enough for the existence of the minimal parallel growth. Though $\omega_r > 0.5\Omega_e$ and $T_\perp > 2T_\parallel$, in the case of Fig.4.2, $\gamma''(0) < 0$ because $T_\parallel$ is higher than 100eV.

4-5-3 Angular dependence

We discuss here the directional dependence of the growth rate for low and high frequencies at low temperatures for the same conditions as in Fig.4.1. Figure 4.4 shows the growth rate (actually a negative γ indicating damping rate) as a function of the wave normal angle for low frequencies. In this frequency region, γ is nearly equal to γ_L and so γ_c is not shown. When the frequency is very low ($\omega_r = 0.01\Omega_e$), the damping rate becomes large as θ increases. However when the frequency is low ($\omega_r = 0.1\Omega_e$), the damping rate has a peak at $\theta \simeq 30°$, and $|\gamma|$ becomes smaller at larger θ , because the Landau damping is a linear combination of the factors $\alpha_0\exp(-\alpha_0^2)$, $\alpha_0^2\exp(-\alpha_0^2)$ and $\alpha_0^3\exp(-\alpha_0^2)$. For such low frequencies, our approximation is valid.

At a higher frequency (e.g. $\omega_r = 0.62\Omega_e$), as shown in Fig.4.5, the Landau damping is small for θ less than 40° and is enhanced with increasing θ, whereas the growth rate due to cyclotron instability increases monotonically as θ increases. So the total growth rate becomes a maximum at $\theta \simeq 45°$ as the result of the combination of the growth due to the cyclotron instability and Landau damping. The exact solution γ_{exact} is also shown in the figure (dotted line). Our approximation is valid even for such large angles. It should be noticed that there exists a large growth rate near the resonance cone angle at low temperatures. At an angle in the vicinity of the resonance cone angle, however, our assumptions

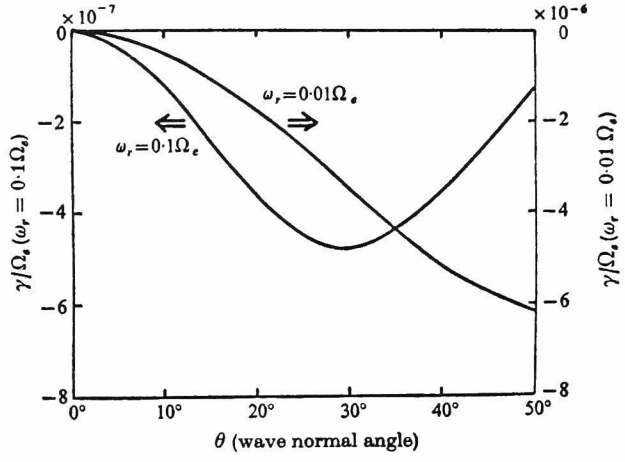

Fig. 4.4. Angular dependence of the growth rate (low frequencies). $\Pi_c/\Omega_e = 10$; $T_\perp = 3T_{||}$ (A = 2); $V_{T_{||}} = 0.01c$ (25 eV); $\delta = 1\%$.

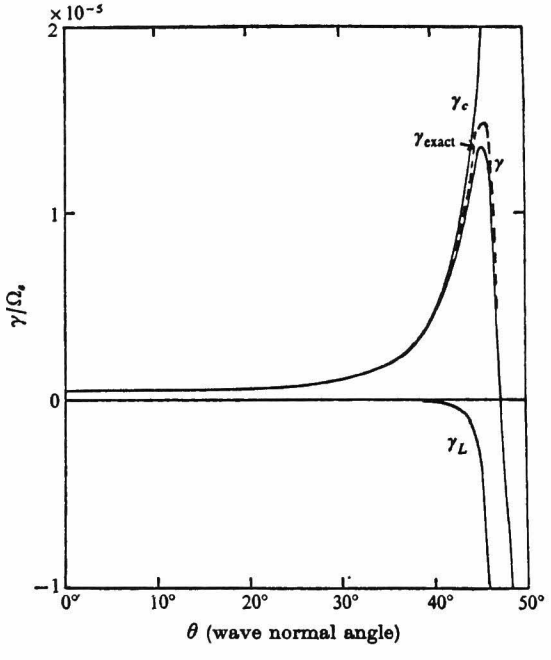

Fig. 4.5. Angular dependence of the growth rate (high frequency). $\Pi_c/\Omega_e = 10$; $T_\perp = 3T_{||}$ (A = 2); $V_{T_{||}} = 0.01c$ (25 eV); $\delta = 1\%$; $\omega_r = 0.62\Omega_e$.

no longer hold.

4-6 Calculation of the Net Growth along the Ray Path

For low frequencies ($\omega_r << \Omega_e$), Kennel and Thorne (1967) have evaluated the total amount of the growth along the path, combining a ray tracing of the whistlers (Thorne and Kennel,1967) with the growth rate due to instability of the obliquely propagating whistler mode (Kennel,1966).

In this section, we will calculate whistler mode ray paths by the ray tracing technique (Kimura,1966), and evaluate the net growth along the path by applying the method as stated in the preceding sections on the assumption that the paths are determined by the ray tracing in a cold plasma. The magnetospheric model stated in section 1-8 is used.

4-6-1 Net growth

We make the following assumptions about a hot plasma in the magnetosphere. Hot electrons are injected at the equator. The particles in the hot plasma move spirally along the geomagnetic field lines, whose energy and magnetic moment are conserved along the field lines. The injected electrons are of density 1% of that of the cold plasma. Their thermal characteristics are specified by a bi-Maxwellian distribution whose anisotropy factor is given at the equator. The density of the hot plasma is assumed to be constant along the field lines. Therefore γ becomes negligible at lower altitudes because δ is small. The mirror effect is neglected.

Based on these assumptions, we can define the equatorial distribution function of the hot plasma as

$$f(v_{\perp 0},\ v_{\parallel 0}) = C \exp\left(- \frac{v^2_{\perp 0}}{V^2_{T\perp 0}} - \frac{v^2_{\parallel 0}}{V^2_{T\parallel 0}} \right) \tag{4.14}$$

where $V_T = (2\kappa T/m)^{1/2}$, $C = \pi^{-3/2} V^{-2}_{T\perp 0} V^{-1}_{T\parallel 0}$

suffix 0 indicates equatorial value and the anisotropy at the equator is

$$A_0 = (V^2_{T\perp 0}/V^2_{T\parallel 0}) - 1. \tag{4.15}$$

The conservation of particle energy and magnetic moment are expressed as follows:

$$v^2_{\perp 0} + v^2_{\parallel 0} = v^2_{\perp} + v^2_{\parallel}, \tag{4.16}$$

$$v^2_{\perp 0}/B_0 = v^2_{\perp}/B \tag{4.17}$$

which are assumed to be satisfied along a geomagneitc field line. B is the strength of the geomagnetic field at the point of interest and B_0 is that of the equator of the same field line (the same value of L).

Substituting Eqs.(4.16) and (4.17) into (4.14), the distribution function at the point of interst is derived as

$$F(v_{\perp}, v_{\parallel}) = C \exp\left\{ - \frac{B_0 v^2_{\perp}}{B V^2_{T\perp 0}} - \left(1 - \frac{B_0}{B} \right) \frac{v^2_{\perp}}{V^2_{T\parallel 0}} - \frac{v^2_{\parallel}}{V^2_{T\parallel 0}} \right\}$$

$$= C \exp\left(- \frac{v^2_{\perp}}{V^2_{T\perp p}} - \frac{v^2_{\parallel}}{V^2_{T\parallel 0}} \right) \tag{4.18}$$

where $V_{T\perp p}$ is defined by the equation

$$\frac{V^2_{T\parallel 0}}{V^2_{T\perp p}} = 1 + \left(\frac{V^2_{T\parallel 0}}{V^2_{T\perp 0}} - 1 \right) \frac{B_0}{B} \tag{4.19}$$

Then, the temperature anisotropy A of Eq. (4.18) is given by

$$A = (V^2_{T\perp p}/V^2_{T\parallel 0})^2 - 1. \tag{4.20}$$

$V_{T\perp 0}$ of Eq. (4.14) is replaced by $V_{T\perp P}$ in Eq. (4.20) but $V_{T\parallel 0}$ remains unchenged. In other words, the parallel temperature $T_{\parallel}$ of the hot plasma is constant along the field lines.

Liemohn (1967) has represented the distribution function as a product of a pitch angle distribution and an energy distribution. Equation (4.16) shows that the energy distribution is invariant. On the other hand, the pitch angle distribution (30) of Liemohn (1967) can be derived from Eq.(4.17). These facts show that our assumptions are consistent with Liemohn's.

We calculate the growth rate at a given point using parameters obtained from the above model, and evaluate the net growth Γ by integrating the growth rate along a ray path:

$$\Gamma = -\int \vec{k}_i \cdot d\vec{s} = -\int \vec{k}_i \cdot \vec{v}_g dt = \int \gamma dt. \qquad (4.21)$$

In these equations we use the relation $\gamma = -\vec{k}_i \cdot \vec{v}_g$, where $\vec{k}_i$, $\vec{s}$, $\vec{v}_g$, and t are the imaginary part of the wavenumber, the path length, the group velocity, and the group delay time in the cold plasma.

4-6-2 Example of the growth rate accumulation

As an example, we discuss the net growth of non-ducted whistler mode waves which start from the equator of L = 4.5. The ray path and the wave normal angle vs.latitude characteristics of 4kHz waves with initial wave normal angles θ_0 = - 20°, -30°, and -40° (which point toward lower L shells) are shown in Figs.4.6 and 4.7. At such a frequency, the ray path can reach lower altitudes (e.g. less than 110km) only for a certain initial wave normal angle $\theta_0 \simeq -30°$. In this region, hot electrons of 2.5keV and anisotropy A_0 = 0 to 2 at the equator are assumed. The net growth along the path from 0° up to 20° (solid lines) or up to 30° (dashed lines) in latitude as a function of initial wave normal angles is shown in Fig.4.8. At this frequency, the growth rate is maximum

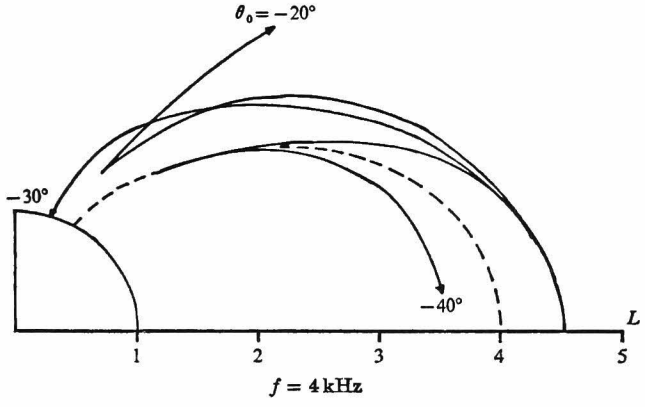

Fig. 4.6. Ray path for 4 kHz waves. (The cyclotron frequency is 9.5 kHz, and the plasma frequency is 49 kHz at the equator of L = 4.5).

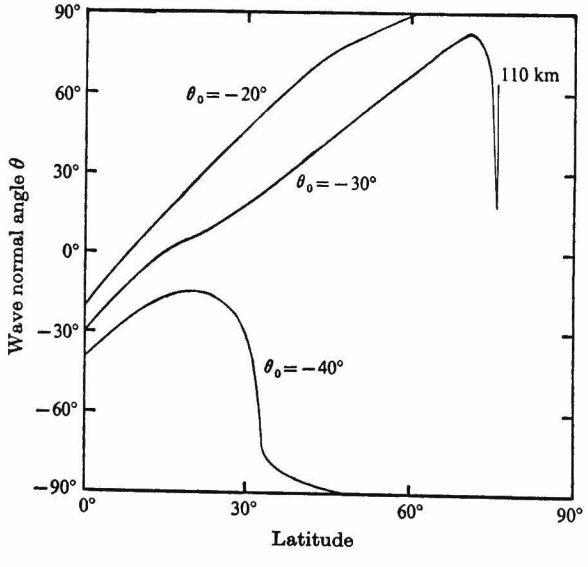

Fig. 4.7. Wave normal angle as a function of path latitude. L = 4.5; f = 4.5 kHz.

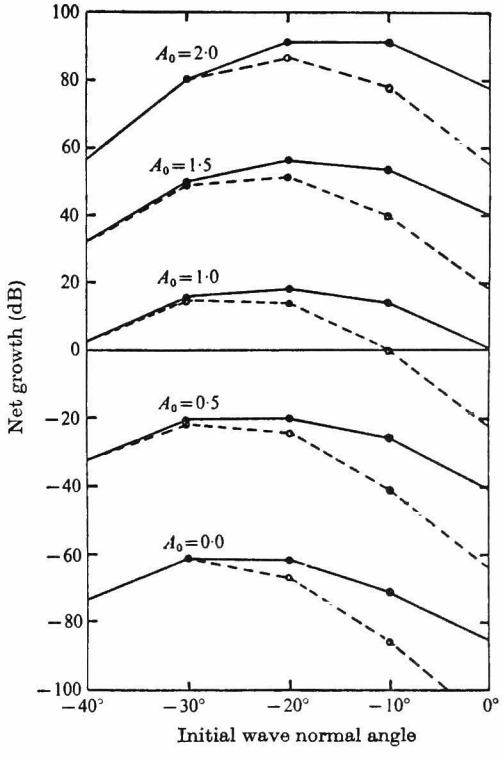

Fig. 4.8. Net growth vs. initial wave normal angles for various initial anisotropy factors A_0. L = 4.5; f = 4 kHz. ———, latitude = 20°, -----, latitude = 30°.

for parallel propagation. Therefore, it is clear from Fig.4.7 that the net growth is maximum at $\theta_0 \simeq -20°$, because the path length of nearly parallel propagation becomes maximum. In higher latitudes (lower altitudes) an additional accumulation becomes negligible. Equation (4.8) shows that the growth rate is in proportion to the hot electron density ratio δ .

This example shows propagation characteristics from the source region of ELF hiss. Though the wave is of course attenuated in an isotropic hot plasma ($A_0 = 0$), a small anisotropy causes slight amplification.

4-7 Discussion and Conclusion

We have shown that the growth rate of the oblique propagation can be calculated by very simple equations which are expressed explicitly by only elementary functions. The results of Figs.4.1 and 4.5 agree with the analytical expressions for γ_{max} ($\theta = 0°$) of Cuperman and Landau (1974). This method, for example, enables us easily to calculate the net growth along ray paths in a hot plasma.

It is found that at low temperatures and for wave frequencies not much lower than the electron cyclotron frequency, the Landau damping is relatively small and the growth rate is large for oblique propagation.

Our model calculation shows that non-ducted waves starting from outside the plasmapause can propagate with some growth. It would be valuable to adopt our method for more realistic various models. These results may be applied to the amplification mechanism of the non-ducted propagating waves.

We have shown in Fig.4.3 that the condition for the existence of minimal parallel growth depends very much on the distribution function of the hot plasma and actually our results are contrary to Brinca's (1972). In the space plasma, the condition for minimal parallel growth may not be easily

satisfied, if the hot plasma is bi-Maxwellian whose temperature anisotropy is less than unity. The necessary condition for minimal parallel growth is $A_0 > 1$ in a bi-Maxwellian plasma.

Cuperman and Sternlieb (1974) have performed a computer simulation of obliquely propagating whistler mode waves in a bi-Maxwellian hot plasma. They have confirmed that nonlinear effects do not alter the characteristic fact that the growth rate is not always maximum for parallel propagation.

CHAPTER 5

WARM PLASMA RAY TRACING AND ITS APPLICATION

5-1 Introduction

A satellite-borne "duct monitor" is designed for a Japanese eccentric satellite, EXOS-B. It detects field-aligned ionization ducts in the magnetosphere from the observation of a ground-based VLF signal. It is based on the Doppler shift of ducted waves propagating along the geomagnetic field being small, whereas the Doppler shift of non-ducted waves is generally large because their wave normal angle is large, and therefore the refractive index is also large.

The ray tracing technique has been widely used to calculate ray paths of non-ducted whistler mode waves in the magnetosphere. In these ray tracings, the plasma has been assumed to be cold. However, the propagation of whistler mode waves with large wave normal angles and/or with frequencies near the cyclotron frequency is affected by electron thermal motions. We have tried "ray tracing in a warm plasma" in order to estimate the anticipated Doppler shift in the deep plasmasphere to be observed by the above satellite. Bitoun et al. (1970) calculated ray paths by the warm-plasma approximation (Stenko and Stepanov, 1957) in a plane stratified ionosphere to interpret an upper hybrid resonance phenomenon observed by a topside sounder.

In section 5-2, we examine this warm plasma approximation for obliquely propagating whistler mode waves by comparing it with the exact solutions of the dispersion equation in a Maxwellian hot plasma (chapter 2) and find an allowable range of application of the approximation. A refractive index calculated from this warm plasma approximation is applied

to the ray tracing, and it is stated in section 5-3 that there are regions where no purely real refractive index for the whistler mode exists, and the ray tracing stops because of this thermal effect. In section 5-4, from the comparison with the exact solution in the hot plasma treatment, it is shown that the waves are highly damped. By taking account of such damping along the ray paths, we can estimate the electron temperature from the data on the Doppler shift and damping rate of the ground-based VLF signals observed in the magnetosphere by a satellite-borne instrument.

5-2 Warm Plasma Theory

We first consider the dispersion equation in order to deduce the refractive index in a usable form for ray tracing in a warm plasma. The well-known exact dispersion equation in a hot plasma (e.g. Stix, 1962) is very complex and not analytic. It is, therefore, not adequate for ray tracing, because it is not easy to calculate derivatives of the refractive index. Hereinafter, we refer to this solution as the hot plasma solution(Ch. 2). We have also examined the so-called CGL approximation (e.g. Allis et al., 1963, Chapter 5) and the warm plasma approximation (Allis et al., 1963, Chapter 6; Aubry et al.,1970). The former is not useful because this approximation is not sufficiently accurate for whislter mode waves.

We review the assumptions for the warm plasma approximation:

(1) Collisions are neglected.

(2) The hot electrons are Maxwellian.

(3) The electron temperature is so low that $\tau \equiv k^2 \kappa T/m\omega^2 \ll 1$, where κ, T, m, ω and k are, respectively, the Boltzmann constant, the electron temperature, the electron mass, the wave frequency and the wave number ($k = \omega n/c$; n and c are the refractive index and the speed of light in a

vacuum).

(4) The wavelength in the direction perpendicular to the constant magnetic field is much larger than the electron Larmor radius. This enable us to take only the Landau resonance and the cyclotron resonance into account.

The dielectric tensor derived from the warm plasma approximation is (Aubry et al., 1970);

$$\overleftrightarrow{K} = \overleftrightarrow{K}^{(0)} + \tau\overleftrightarrow{K}^{(1)}, \tag{5.1}$$

where $\overleftrightarrow{K}^{(0)}$ and $\overleftrightarrow{K}^{(1)}$ are the cold-plasma dielectric tensor and the warm plasma correction, respectively. Their elements are given in section 1-4. The dispersion equation derived from Eq. (5.1) is the first-order expansion in τ of the hot plasma dispersion and is a cubic equation in n^2. This equation gives only the real part of the refractive index: the imaginary part cannot be calculated, so a damping effect cannot be involved.

5-2-1 Refractive index for frequencies much below the cyclotron frequency

Figure 5.1 is an example of the refractive index n for plasmas at 10^3 and 10^4K as a function of wave normal angle θ near the resonance-cone angle when $f_p = 3f_H$ and $f = 0.3f_H$, where f_p, f_H and f are the plasma frequency, the cyclotron frequency and the wave frequency ($= \omega/2\pi$), respectively. The motions of the ions are neglected in this seciton. The solid, dashed and dotted lines in the above figure are the hot plasma solution, the approximate warm plasma solution and the cold plasma solution, respectively. The hot plasma solution is also used for the damping rate calculation in a later section. The characteristic features in this region can be summarized as follows:

(1) Thermal effect is not noticeable until the wave normal angle becomes

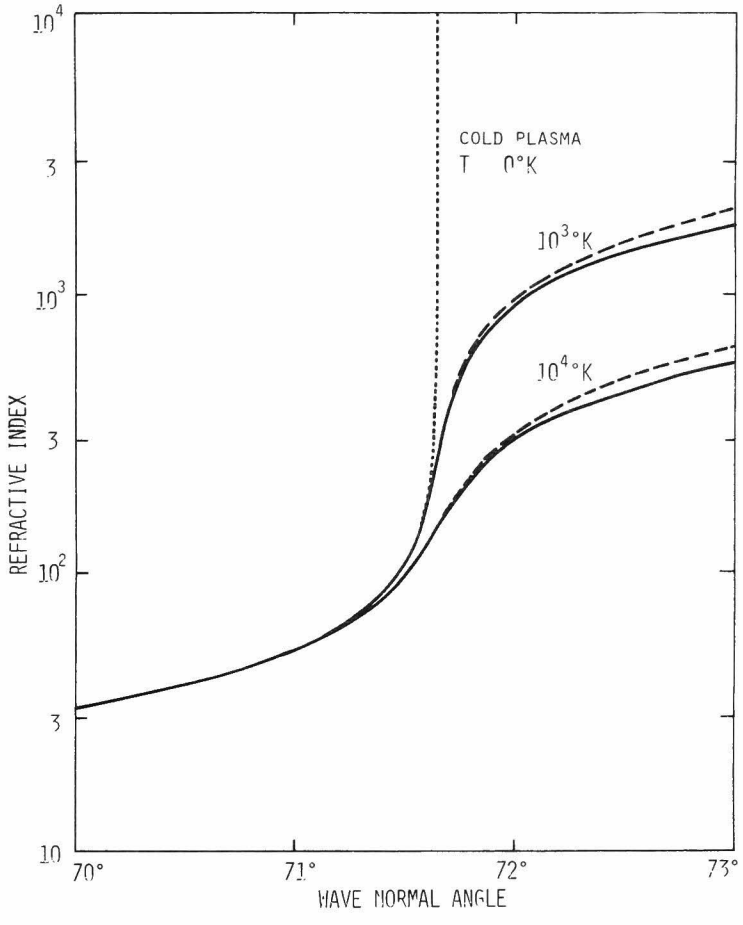

Fig. 5.1. Refractive index n vs. wave normal angle θ, for $f = 0.3f_H$ and $f_p = 3f_H$.

larger than the resonance cone angle θ_{res} (= 71.65° in this example).

(2) The waves can be propagated in the warm plasma even if the wave normal angle θ becomes larger than the resonance cone angle θ_{res}.

(3) The refractive index becomes smaller as temperature increases.

(4) The warm plasma approximation is relatively good. When θ = 73° in this example, the imaginary part of the refractive index $n_i \simeq -10^{-3} n_r$ at $T = 10^4$K, and therefore waves can be assumed as homogeneous (Kimura and Kawai, 1976) and the ray tracing using only the real part is valid.

(5) The ray direction becomes closer to the magnetic field direction as the temperature increases.

5-2-2 Refractive index for frequencies near the cyclotron frequency

Figure 5.2 is an example of the refractive index n for plasmas at 10^3 and 10^4K as a function of the wave normal angle near the cyclotron frequency when $f_p = 3f_H$ and $f = 0.88f_H$. Each line has the same meaning as Fig. 5.1. The characteristic features in this case are these:

(1) The thermal effect becomes marked at smaller wave normal angles, as compared with those in Fig.5.1.

(2) The refractive index becomes larger as the temperature increases.

(3) The approximate equation has no real solution for the whistler mode near the resonance cone angle (θ_{res} = 27.0° in this example), where it is already a poor approximation. For example, the point marked by a circle indicates the absence of any real solution for wave normal angles larger than the angle corresponding to this circled point, where the hot-plasma solution has a large imaginary part in the refractive index.

(4) The ray direction becomes closer to the magnetic field direction as the temperature decreases.

(5) When the wave normal angle is very close to or larger than the resonance cone angle, the refractive index becomes smaller as temperature

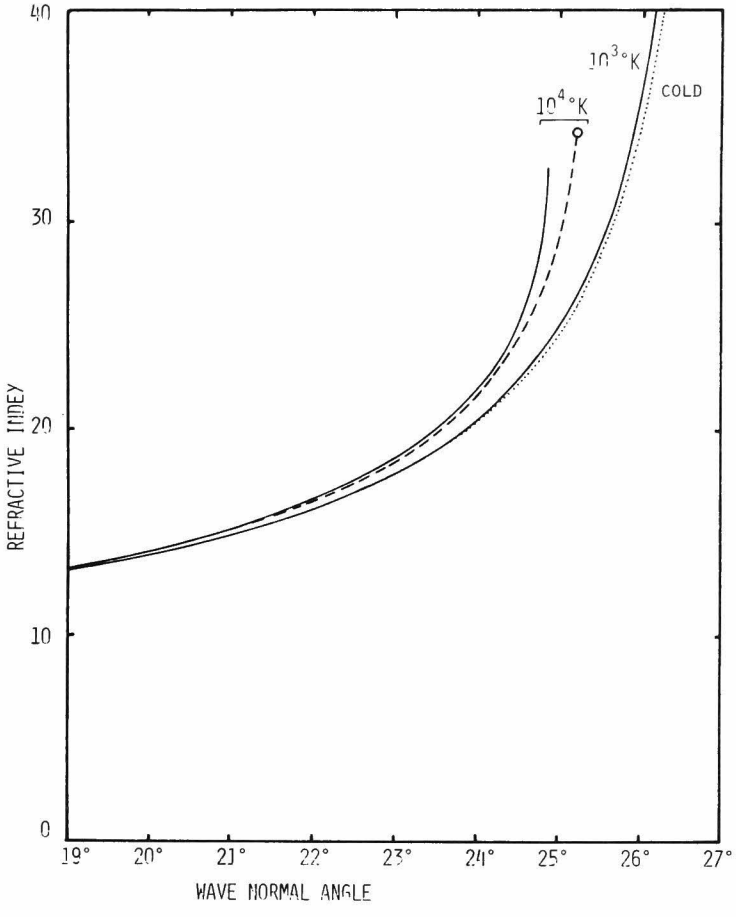

Fig. 5.2. Refractive index n vs. wave normal angle θ, for $f = 0.88f_H$ and $f_p = 3f_H$.

increases, as shown in Fig.5.1, though the hot plasma solution gives a large imaginary part to the refractive index. In any case, the $n(\theta)$ characteristics are topologically the same as those shown in Fig.5.1.

5-3 Ray Tracing in a Warm Plasma

We introduce the refractive index obtained by the warm plasma approximation into equations for ray tracing in section 1-7. The electromagnetic effects of the ions are taken into account but their thermal effects are neglected.

5-3-1 Example of ray paths

An example of the ray paths calculated for 22.3kHz is shown in Fig. 5.3. This frequency is that of the signal transmitted from the station NWC in Australia, which we observe by our satellite. The initial wave normal direction is set to be vertical and the wave starts at -60° in latitude and 500km in altitude. The ray paths are almost the same for the electron temperatures $T = 0$ (cold), 10^3 and 10^4K. At $T = 10^4$K, however, the refractive index has no purely real solution after passing through the point labeled x in the figure.

The refractive index as a function of latitude along the same path as in Fig.5.3 is shown in Fig.5.4. The dashed and dotted lines correspond to the case of $T = 10^4$K (warm plasma approximation) and to that of cold plasma, respectively. In the region labeled Δ, $f_p \cong 3.2f_H$, $f \cong 0.88f_H$ and $\theta \cong 26°$, which are almost the same parameters as used in Fig.5.2. If the wave normal angle were the same, the change of a refractive index due to the thermal effect should be noticeable. However, there is no significant difference between the two lines in Fig.5.4 because the wave

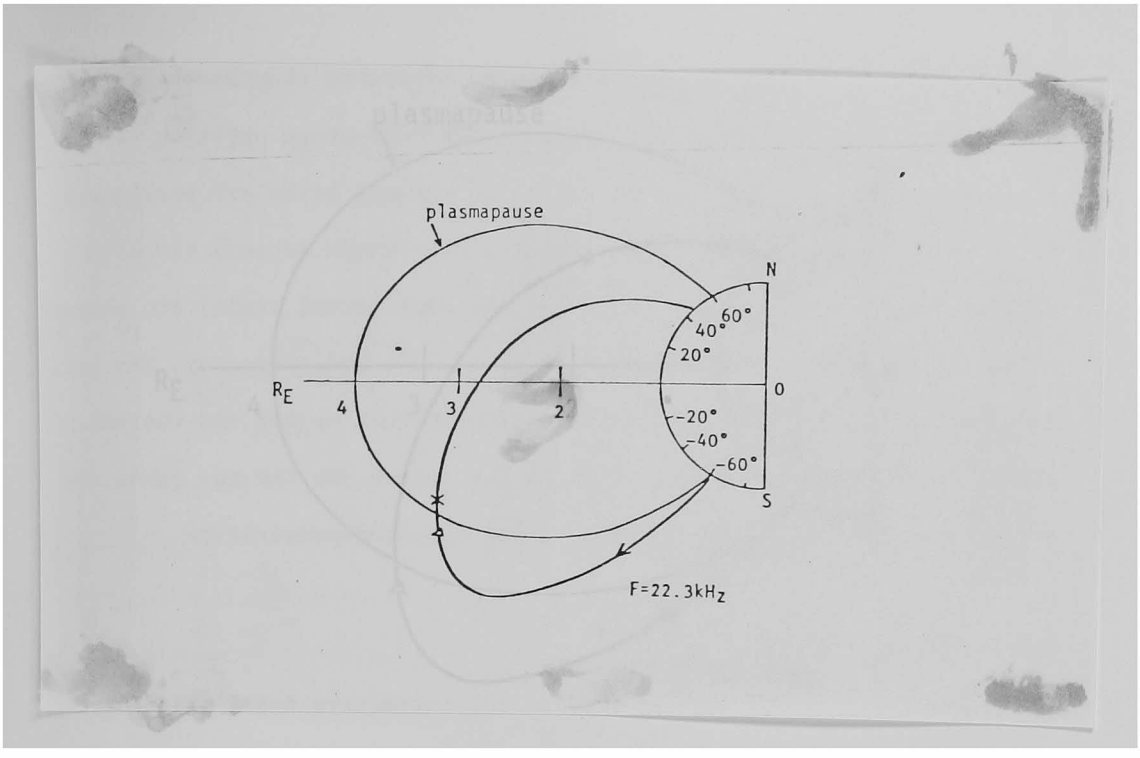

Fig. 5.3. A ray path of the 22.3 kHz wave starting at -60° in latitude.

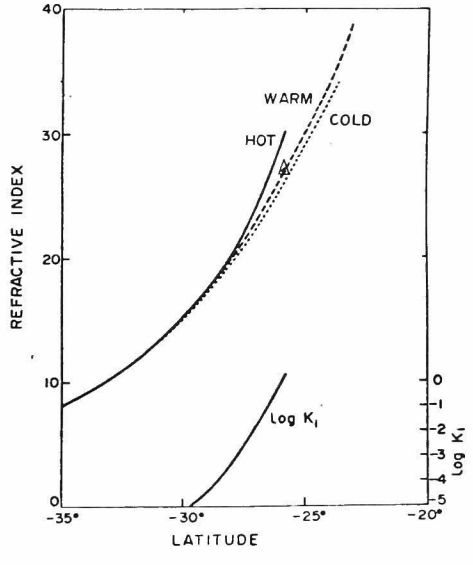

Fig. 5.4. Refractive index variation along the path of Fig. 5.3 at $T = 10^4$ K.

normal angle is smaller in the warm plasma treatment than in the cold plasma treatment. At lower altitudes in the hemisphere opposite to the starting points, the wave normal angles on the ray paths are very large, being close to 90°, because the resonance cone angle becomes close to 90° for $f/f_H \ll 1$. For such values of the wave normal angle, the thermal effect appears only in the very vicinity of 90°, and, moreover, the ray is directed along a geomagnetic field line whether or not the thermal effect is taken into account. This is the reason why the ray paths and refractive indices are insensitive to the electron temperature.

5-3-2 Damping characteristics

In Fig.5.4, the upper solid line is the refractive index calculated from the hot plasma dispersion equation, using the same parameters as those on the ray path traced by the 10^4K warm plasma treatment in Fig. 5.3. The lower solid line shows $\log K_i$ calculated by the hot plasma solution, where K_i is the damping rate and is equal to $ck_i/2\pi f_H$, where $k_i = -\gamma/v_{gk}$, $v_{gk} = \partial\omega_r/\partial k$ and $\omega = \omega_r + i\gamma$ which is the hot plasma solution for a real k (see Appendix A). The point labeled Δ in Fig.5.4 corresponds to that in Fig.5.3, where the warm plasma approximation is no longer valid. For example, at the point labeled Δ, $K_i = 1.8$ in the hot plasma solution, $f_H = 25$kHz, and therefore $k_i = 1$/km, that is, waves are attenuated by 8.7 dB (1 Neper) per 1 km. Though the ray paths around such a region are erroneous due to the thermal effects, it should be noted that the wave energy is damped there.

Figures 5.5 and 5.6 show ray paths for other values of the parameters. In Fig.5.5, the initial latitudes are different from those in Fig.5.3, while in Fig.5.6 the plasmapause position is different. The end of each path indicates the absence of the purely real solution where the ray tracing calculation stops. The points labeled Δ in each figure indicate the

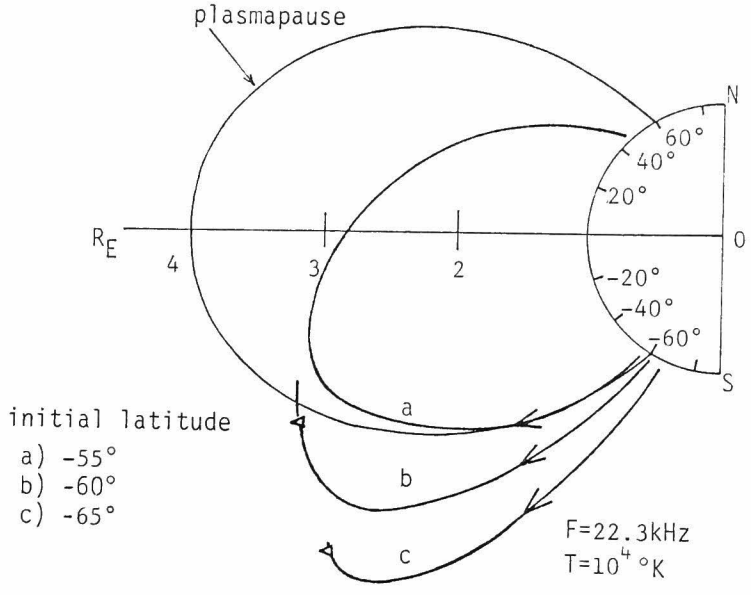

Fig. 5.5. Ray path for three initial latitudes.

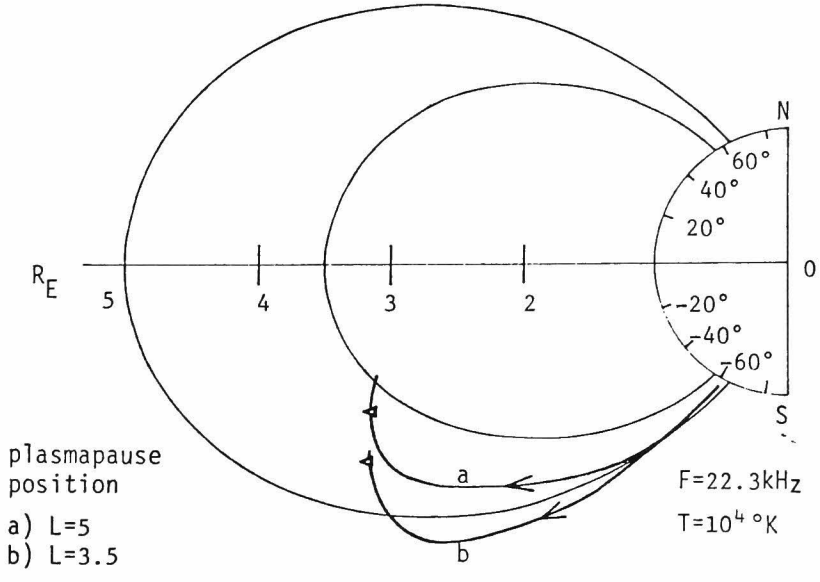

Fig. 5.6. Ray paths when the plasmapause position is different.

above-mentioned region where the waves are heavily damped. These points are calculated from the hot plasma solution with the same parameters as those along the path.

5-4 Estimation of Electron Temperature from Wave Damping Characteristics

We examine whether or not we can estimate the electron temperature by observing, with a satellite-borne receiver, the Doppler shift and damping of a ground-based VLF signal in the non-ducted mode of propagation. As an example, we will use the designed orbital elements of the Japanese eccentric satellite EXOS-B (the perigee and the apogee are 250 and 30,000 km, respectively, and the inclination is 30°), by which we will observe the Doppler shift and wave amplitude of a 22.3 kHz signal transmitted from the station NWC in Australia.

The signal is assumed to be vertically incident on the ionosphere at various latitudes. The plasmapause position is taken as L = 4. A ray path starting from an initial latitude LAT_0 is calculated by the warm plasma ray tracing. At different points along the ray path, the argument of perigee (ω) of the satellite orbit that intersects the ray path is determined. Then the instantaneous velocity of the satellite is calculated. This can be used to estimate the Doppler shift Δf by means of the following formula:

$$\Delta f = -fnV \cos\sigma/c, \tag{5.2}$$

where f, V and σ are the wave frequency, the satellite velocity and the angle between the wave normal direction and the satellite velocity direction. The damping rate (K_i) at each point on the ray path is calculated from the hot plasma solution as stated in section 5-3. Each solid line

in Fig. 5.7 shows the Doppler shifts on a ray path starting from the initial latitude (LAT_0) to be observed by different satellite orbits. The abscissa of the figure is the latitude of the observing point. Each dotted line in the figure indicates one satellite orbit (ω being the argument of perigee of the orbit) on which the signals having propagated along different ray paths are observed at each instant. The dashed lines are constant damping rate (K_i) lines, which are reproduced from K_i calculated along each ray path. In other words, the dotted lines show the Doppler shifts of the signal observed along a certain orbit and the intersections with the dashed lines indicate the damping rate of the signal.

When the Doppler shift of the nonducted signal is observed by an onboard receiver, the refractive index n at the observing point is determined by

$$n = -c\Delta f/(fV\cos\sigma), \tag{5.3}$$

where V is calculated from the orbital elements and σ can be estimated approximately by the ray tracing. The damping rate K_i is determined from the spatial variation of the signal amplitude. Now that the refractive index and the damping rate are known, the electron temperature can be estimated from figures like Fig.5.8, if the plasma frequency and the cyclotron frequency are also known from other measurements.

Even if the estimation of K_i differs by one order of magnitude from the true value due to experimental errors, the above process leads to errors of only about 30% in the estimation of electron temperature. Though the electron temperature is assumed to be isotropic in this figure, the effect of temperature anisotropy is negligible in the damping region.

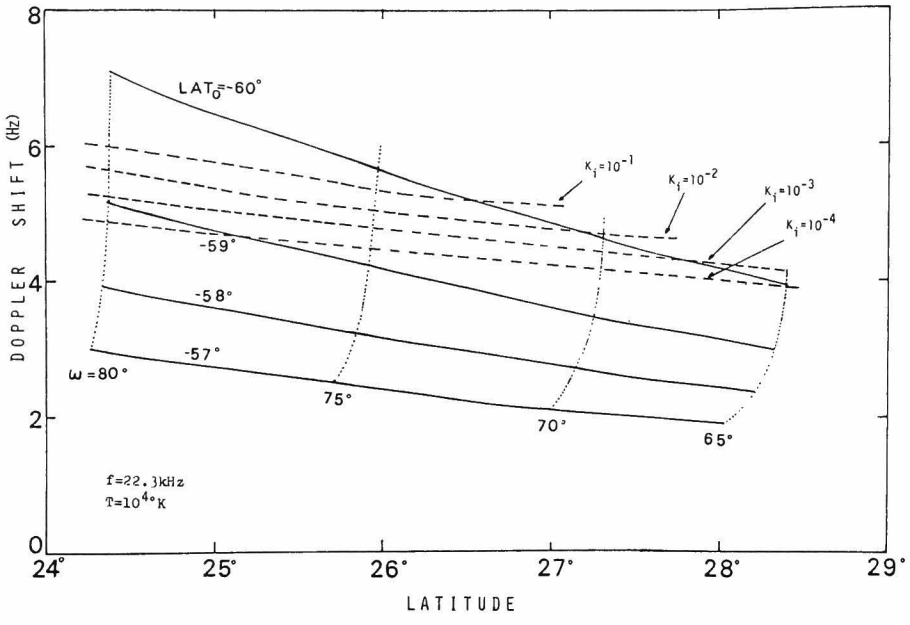

Fig. 5.7. Doppler shift as a function of latitude (see text).

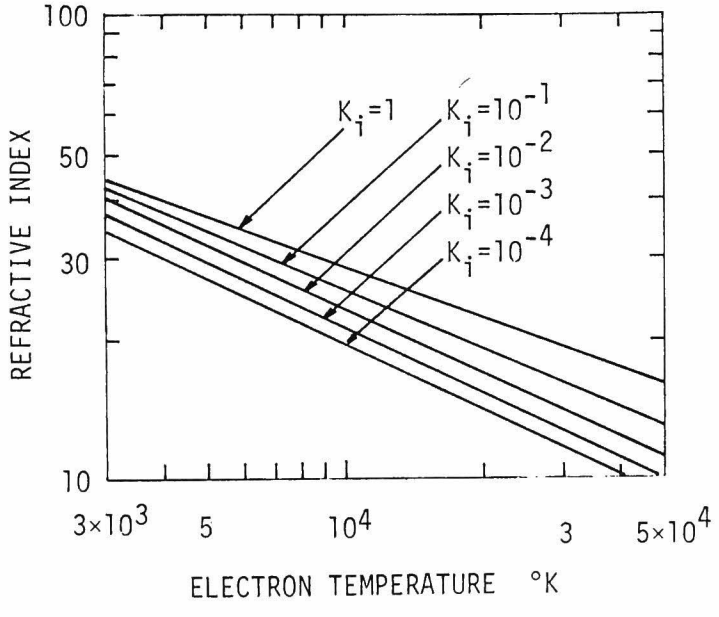

Fig. 5.8. A chart for obtaining the electron temperature from the refractive index and the damping rate K_i, where $f = 0.887f_H$ and $f_p = 3.088f_H$.

5-5 Discussion and Conclusion

We have developed a computer program for ray tracing in a warm plasma. It is demonstrated that in the warm plasma treatment the ray paths starting from the low altitudes in the ionosphere are generally identical to those calculated by the cold plasma treatment, except in highly damped regions. This is true even for a different magnetospheric plasma model, such as a constant density model. It is also expected to be true for two component (cold + hot) plasmas. The absence of purely real solutions of the dispersion equation in the warm plasma treatment indicates that wave damping occurs in the warm plasma when the wave frequency is near the cyclotron frequency. This damping can be calculated from the hot plasma solution. The warm plasma ray tracing is useful for locating these damping regions. For downgoing ray paths starting from, for instance, the equatorial plane with a wave normal angle larger than the resonance cone angle, the warm plasma ray tracing does not always yield a point where the purely real solution is absent, though the signal should be highly damped somewhere along the path.

A method for estimating the electron temperature from observation of the wave damping and Doppler shift of non-ducted signals is proposed. If the distribution function of the magnetosphere plasma is assumed as Maxwellian, the damping rate K_i is calculated as a function of the electron temperature. Therefore if the damping rate can be estimated from the observation of spatial amplitude variation of a signal, the electron temperature can also be estimated. If the distribution function is not Maxwellian and the actual distribution is known from the particle observation, the electron temperature can be estimated as before. If the distibution is not known, the temperature as the distribution is assumed to be Maxwellian is determined, as in the case of temperature determination by in situ probe technique.

The estimation of the damping rate K_i by the satellite observation may not be so simple, because the satellite does not always pass along a ray path. Though the estimation error of K_i results only in small errors on the electron temperature, the following points should be considered: (1) Whether or not we are able to know the equiamplitude plane? (2) How is the spatial amplitude profile modified by the ionospheric irregularity effects at the incident point and also along the ray paths?

Any in situ probe technique for electron temperature measurement is liable to suffer from the effects of potential fluctuations of the space vehicles. A different technique such as above may be valuable for comparison with the electron temperature determined by other techniques. Ducted signals propagated along the field-aligned ducts are easily distinguished from non-ducted signals, by the great difference in the Doppler shifts.

CHAPTER 6

TEMPERATURE ANISOTROPY AND BEAM TYPE WHISTLER INSTABILITIES

6-1 Introduction

Cyclotron instabilities of whistler mode waves propagating along an external magnetic field have been investigated separately for two different types. One is a temperature anisotropy type instability caused by an anisotropy of the velocity distribution of electrons (Stix. 1962, Sudan,1963, and Scharer and Trivelpiece, 1967). The other is a beam type instability caused by a beam-wave interaction between whistler mode waves and a counter-streaming electron beam (Bell and Buneman, 1964 and Matsumoto et al., 1970). The former has been treated for a hot plasma with a bi-Maxwellian velocity distribution function, while the latter has been dealt with for a cold plasma-beam system with a delta functional velocity distribution.

In this paper, we discuss a comparison between the two types in order to clarify an essential mechanism of whistler instabilities. This is an extension of the work by O'Neil and Malmberg (1968) which clarified the transition of electrostatic instabilities from a beam type to a Landau type.

We review the anisotropic type whistler instabilty in section 6-2. In section 6-3, we summarize the beam type whistler instability, paying special attention to an energy source of the instability. In section 6-4, to unify these two types of whistler instabilities, we consider a beam-plasma system composed of a cold plasma and a hot anisotropic beam with a shifted bi-Maxwellian distribution. A transition from the beam type to

the anisotropic type instability is examined by using a shifted Cauchy (Lorenzian) distribution function for the beam in section 6-5. Section 6-6 states the conclusions.

6-2 Temperature Anisotropy Type Whistler Instability

It is well known that a dispersion equation for whistler mode waves propagating along an external magnetic field is given by [see, Eq.(1.2)]

$$c^2k^2 - \omega^2 - \sum_s \Pi_s^2 \int_{-\infty}^{\infty} dv_{\parallel} \int_0^{\infty} dv_{\perp} \pi v_{\perp}^2 \times \left[\left(\omega - kv_{\parallel} \right) \frac{\partial f_s}{\partial v_{\perp}} + kv_{\perp} \frac{\partial f_s}{\partial v_{\parallel}} \right] \left(\omega - kv_{\parallel} - \Omega_e \right)^{-1} = 0, \tag{6.1}$$

where c,k, and ω are the light speed, the wavenumber, and the angular frequency and the ions are assumed to be a uniform background; Ω_e, f_s, and Π_s are the electron cyclotron frequency, the zero-order velocity distribution function, and the plasma frequency of the s-th electrons, respectively. The suffix s stands for species of electrons, i.e., s = c, h and b represent cold, hot, and beam electrons, respectively.

For a one-component hot plasma with a bi-Maxwellian distribution function (1.10), the dispersion equation (6.1) becomes (Stix, 1962, Sudan, 1963,and Scharer and Trivelpiece, 1967)

$$c^2k^2 - \omega^2 - \Pi_e^2 \left\{ \frac{\omega Z(\alpha)}{kV_{T_{\parallel}}} + A[1 + \alpha Z(\alpha)] \right\} = 0, \tag{6.2}$$

where

$$A = \left(T_{\perp}/T_{\parallel} \right) - 1, \qquad V_{T_{\parallel}} = (2\kappa T_{\parallel}/m)^{1/2},$$

$$Z(\alpha) = \frac{1}{\sqrt{\pi}} \int_{-\infty}^{\infty} \frac{\exp(-t^2)}{t - \alpha}\, dt, \qquad \alpha = \frac{\omega - \Omega_e}{kV_{T_\parallel}}, \tag{6.3}$$

in which m, v, T, subscripts $\perp$, and $\parallel$ denote electron mass, velocity, temperature, quantities in the perpendicular and parallel directions to the external magnetic field, respectively. The function $Z(\alpha)$ is the usual plasma dispersion function (Fried and Conte, 1961). The quantity A is a temperature anisotropy factor.

Under the assumptions that $V_{T_\parallel} << V_R$ and $|\gamma| << \omega_r$, where $V_R \equiv |(\omega_r - \Omega_e)/k|$ is a resonance velocity, γ and ω_r are the imaginary and real parts of a complex solution for a given real k of Eq.(6.2), the following explicit expression for γ is well known (Kennel and Petschek, 1966)

$$\gamma = \sqrt{\pi}\, \frac{\Omega_e}{kV_{T_\parallel}} \left(1 - \frac{\omega_r}{\Omega_e}\right)^2 [A\Omega_e - (A + 1)\omega_r] \exp\left[- \left(\frac{\omega_r - \Omega_e}{kV_{T_\parallel}} \right)^2 \right]. \tag{6.4}$$

A necessary condition for the instability ($\gamma > 0$) is, therefore, $A > 0$ or equivalently $T_\perp > T_\parallel$ for whistler mode waves.

For two-component electrons which consist of hot bi-Maxwellian and cold electrons, the dispersion equation (6.1) becomes

$$c^2k^2 - \omega^2 - \Pi_c^2 \frac{\omega}{\Omega_e - \omega} - \Pi_h^2 \left\{ \frac{\omega Z(\alpha)}{kV_{T_\parallel}} + A[1 + \alpha Z(\alpha)] \right\} = 0 \tag{6.5}$$

where Π_c and Π_h denote the plasma frequencies of cold and hot electrons, respectively. It is well known that the growth rate is increased by the addition of a cold plasma component (Jacquinot et al., 1969, Brice and Lucas, 1971, and Cuperman and Landau, 1974). Furthermore, it is noted that γ decreases to zero for large k in the two-component plasma in comparison with the case of damping for a one-component hot plasma. An example of numerical solutions of the dispersion Eq.(6.5) for a two-component plasma is shown by the solid lines in Figs.6.1(a) and (b). The real part of the dispersion

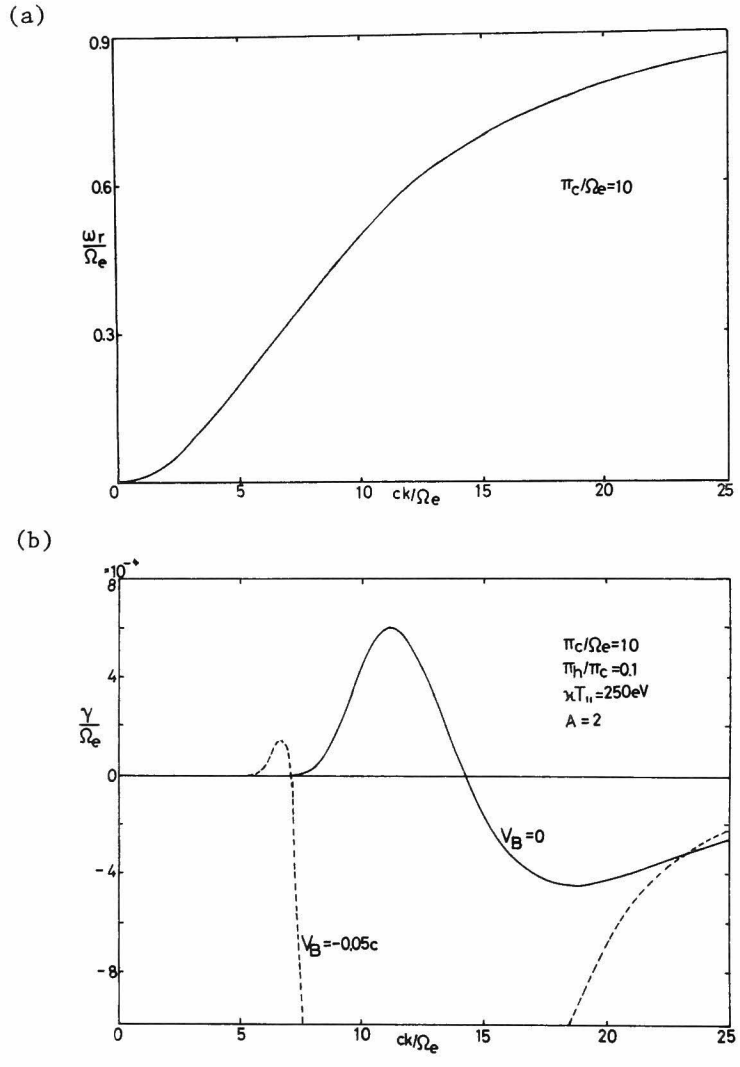

Fig. 6.1. Whistler dispersion in an anisptropic hot plasma. (a) Real part ω_r, (b) imaginary part γ.

is the same as that for the cold plasma case. Under the assumptions that $\Pi_h^2 << \Pi_c^2$ and $|\gamma| << \omega_r$, the real frequency ω_r is almost governed by the cold plasma component and determined approximately by

$$c^2k^2 - \omega_r^2 - [\Pi_c^2\omega_r/(\Omega_e - \omega_r)] = 0 \tag{6.6}$$

and γ is approximated by

$$\gamma = \sqrt{\pi}\,\frac{\Pi_h^2}{\Pi_c^2}\,\frac{\Omega_e}{kV_{T_{\parallel}}}\left(1 - \frac{\omega_r}{\Omega_e}\right)^2 [A\Omega_e - (A+1)\omega_r] \times \exp\left[-\left(\frac{\omega_r - \Omega_e}{kV_{T_{\parallel}}}\right)^2\right]. \tag{6.7}$$

It is noted that, in this case, the assumption $V_{T_{\parallel}} << V_R$ is not necessary, which is differnt from the case of Eq. (6.4). The unstable frequency range is determined for fixed A by Eq. (1.13).

6-3 Beam Type Whistler Instability

In this section we consider a beam-plasma system in which the plasma is cold and stationary and the beam is cold only in the parallel direction to an external magnetic field with a distribution function (1.14). For such a beam-plasma system, the dispersion equation (5.1) becomes an algebraic form of Eq. (1.15). The numerical solutions of Eq. (1.15) are shown in Fig.6.2 for two cases, where the solid, broken, and dotted lines are real solutions, real, and imaginary parts of complex solutions, respectively. The negative imaginary parts of the complex conjugate solutions are omitted. An oblique straight line shows a resonance condition $\omega_r - kV_B - \Omega_e = 0$. Cases (a) and (b) correspond to beam-plasma system with $\kappa T_\perp$ = 250 eV and $\kappa T_\perp$ =125 keV, respectively. The dispersion curves

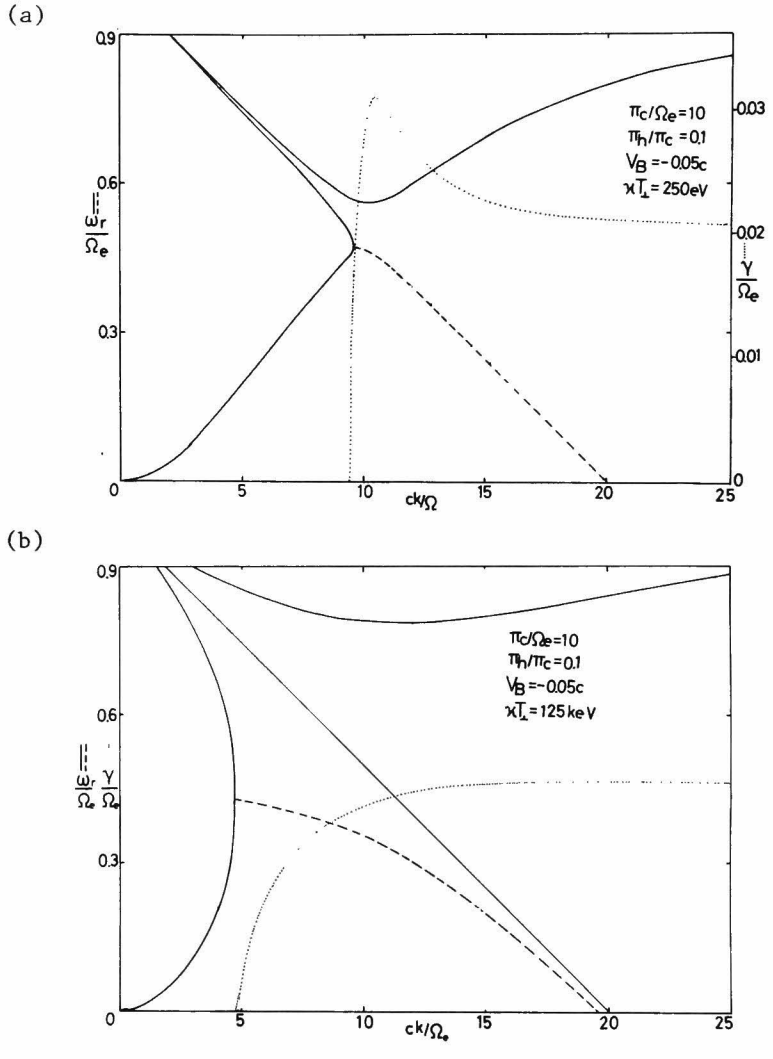

Fig.6.2. Whistler dispersion in a cold beam-plasma system. (a) $T_\perp$ = 250 eV, (b) $T_\perp$ = 125 keV.

for the case (b) with a large beam perpendicular temperature are deformed to some extent from the beamless whistler mode dispersion curves in Fig. 6.1 (a).

It should be noted that an energy source of this whistler mode instability is not a parallel kinetic energy, even though it is called a beam type whistler instability. The energy source is the perpendicular kinetic energy of the beam, since there is no instability when $\langle v_\perp^2 \rangle = 0$ (Kimura, 1961) and the instability takes place even if $V_B = 0$ when $\langle v_\perp^2 \rangle \neq 0$ (Lee and Crawford, 1970). On the contrary, energy sources of instabilities caused by interactions between whistler mode waves and an ion beam and between hydromagnetic waves (Alfven waves) and an electron beam are not the perpendicular energy but are the parallel kinetic energy of the beam.

6-4 Whistler Instability due to Anisotropic Hot Beam

As a transitional case between the previous anisotropic and beam type whistler instabillities, we consider a beam-plasma system composed of a cold stationary plasma and an anisotropic hot beam with a shifted bi-Maxwellian distribution function,

$$f_b(v_\perp, v_\parallel) = \frac{m}{2\pi\kappa T_\perp}\left(\frac{m}{2\pi\kappa T_\parallel}\right)^{1/2} \exp\left(- \frac{mv_\perp^2}{2\kappa T_\perp} - \frac{m(v_\parallel - V_B)^2}{2\kappa T_\parallel} \right) \tag{6.8}$$

The dispersion equation (6.1), then becomes

$$c^2k^2 - \omega^2 - \Pi_c^2 \frac{\omega}{\Omega_e - \omega} - \Pi_h^2 \left\{ \frac{\omega - kV_B}{kV_{T_\parallel}} Z(\alpha) + A[1 + \alpha Z(\alpha)] \right\} = 0, \tag{6.9}$$

where $\alpha = (\omega - kV_B - \Omega_e)/kV_{T_\parallel}$. The distribution function Eq.(6.8) tends

to that for anisotropic hot plasma i.e., Eq.(1.10) or that for a cold beam, i.e., Eq. (1.14) as $V_B \to 0$ or $T_{\parallel} \to 0$, respectively. When the temperature is low, Eq. (6.9) is approximated by an asymptotic expansion of the plasma dispersion function as

$$c^2k^2 - \omega^2 + \Pi_c^2 \frac{\omega}{\omega - \Omega_e} + \frac{\Pi_b^2}{\omega^2}\left[\frac{\omega - kV_B}{\omega - kV_B - \Omega_e} + \frac{\frac{1}{2} k^2 \langle v_{\perp}^2 \rangle}{(\omega - kV_B - \Omega_e)^2} + \frac{\frac{1}{2} k^2 \langle v_{\parallel}^2 \rangle \Omega_e}{(\omega - kV_B - \Omega_e)^3} \right] = 0 \tag{6.10}$$

where we used the relation $Z(\alpha) \simeq -\alpha^{-1}(1 + 1/2\alpha^2)$. This equation becomes identical to Eq. (1.15) when the parallel temperature of the beam is zero, i.e., $\langle v_{\parallel}^2 \rangle = 0$.

Under an assumption that $|\gamma| \ll \omega_r$, an approximate expression for γ in this beam-plasma system can be obtained. The result is

$$\gamma = \frac{\Pi_h^2 Z_i}{kV_{T_{\parallel}}} \frac{\Omega_e A - (A+1)(\omega_r - kV_B)}{\Pi_c^2 \Omega_e / (\omega_r - \Omega_e)^2 + \Pi_h^2 (A+1) Z_r / kV_{T_{\parallel}} + 2\omega_r}, \tag{6.11}$$

where

$$Z(\alpha) \equiv Z_r + iZ_i. \tag{6.12}$$

If $\Pi_h^2 \ll \Pi_c^2$ so that the second and the third terms in the denominator of Eq.(6.11) can be neglected, then Eq.(6.11) becomes

$$\gamma \simeq \sqrt{\pi} \frac{\Pi_h^2}{\Pi_c^2} \frac{\Omega_e}{kV_{T_{\parallel}}} \left(1 - \frac{\omega_r}{\Omega_e}\right)^2 [A\Omega_e - (A+1)(\omega_r - kV_B)]$$

$$\times \exp[-(\omega_r - kV_B - \Omega_e)^2 (kV_{T_{\parallel}})^{-2}], \tag{6.13}$$

where an approximation

$$Z_i \simeq \sqrt{\pi} \exp(-\alpha_r^2) \tag{6.14}$$

is used in which $\alpha \equiv \alpha_r + i\alpha_i$.

It is interesting to note that Eq.(6.13) coincides with Eq.(6.4) formally if $V_B \to 0$ and $\Pi_h = \Pi_c$ although the latter condition violates the previous assumption for the derivation of Eq.(6.13). The unstable frequency range for this case is determined by Eq.(6.13) as

$$\omega_r < kV_B + \frac{A}{A+1}\Omega_e \tag{6.15}$$

which is modified from Eq.(1.13) only by the amount of the Doppler shift, kV_B. In case of $V_B = -0.05c$ in Fig.6.1, the imaginary part of the solutions are modified as broken lines in Fig.6.1(b).

Examples of the numerical solutions for the real k of Eq.(6.9) are illustrated in Figs.6.3 and 6.4. The numerical evalution of the Z function, Eq. (6.3), was performed by a continued fraction method reported by Gautschi (1970). A fixed parameter in Fig.6.3 is $T_\perp$, while $T_{||}$ is a fixed parameter in Fig.6.4. These fixed parameters, $T_\perp$ and $T_{||}$, are chosen so that the calculation parameters coincide with each other when A = 0. It should be noted that the branches which are labeled H in both figures,have no counterpart in the cold beam system.

In Fig.6.3, we see that the dispersion curves for $A = \infty$ coincide with those in the cold beam-plasma system shown in Fig.6.2(a). This fact can be explained by Eq.(6.10). As A decreases from infinity, i.e., as a parallel temperature of the beam increases from $T_{||} = 0$ to a finite value, the growing range of wavenumbers becomes narrower with decreasing magnitude of the growth rate. Correspondingly, the unstable frequency range with a comparatively large growth rate becomes limited. At the same time, a wavenumber k_{max} of the maximum growth range shifts to a smaller k value as A decreases (or $T_{||}$ increases).

In Fig.6.4, the perpendicular temperature $T_\perp$ is changed. As A is increased, the dispersion curves for the real part of the solutions become very similar to those in the case of the cold beam-plasma system shown by

(a)

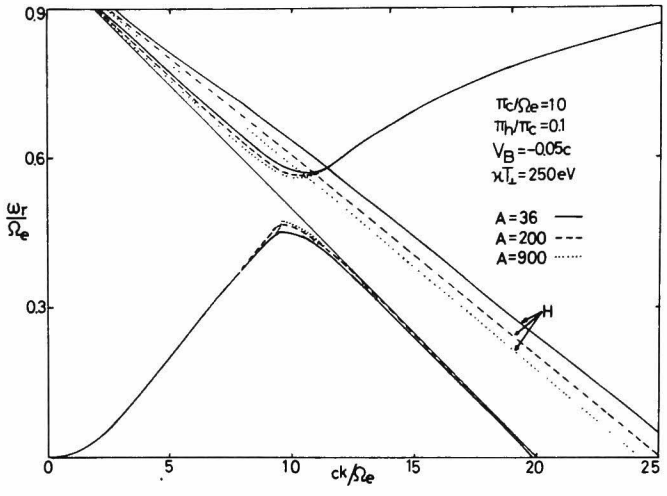

(b)

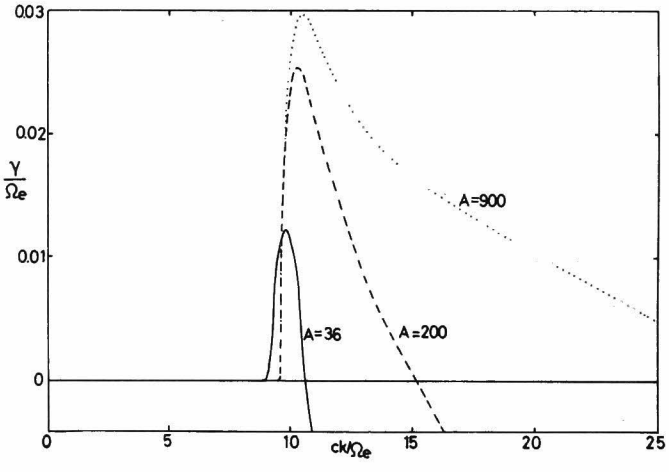

Fig. 6.3. Whistler dispersion in an anisotropic hot beam-plasma system. $T_\perp$ = constant. (a) Real part ω_r, (b) imaginary part γ.

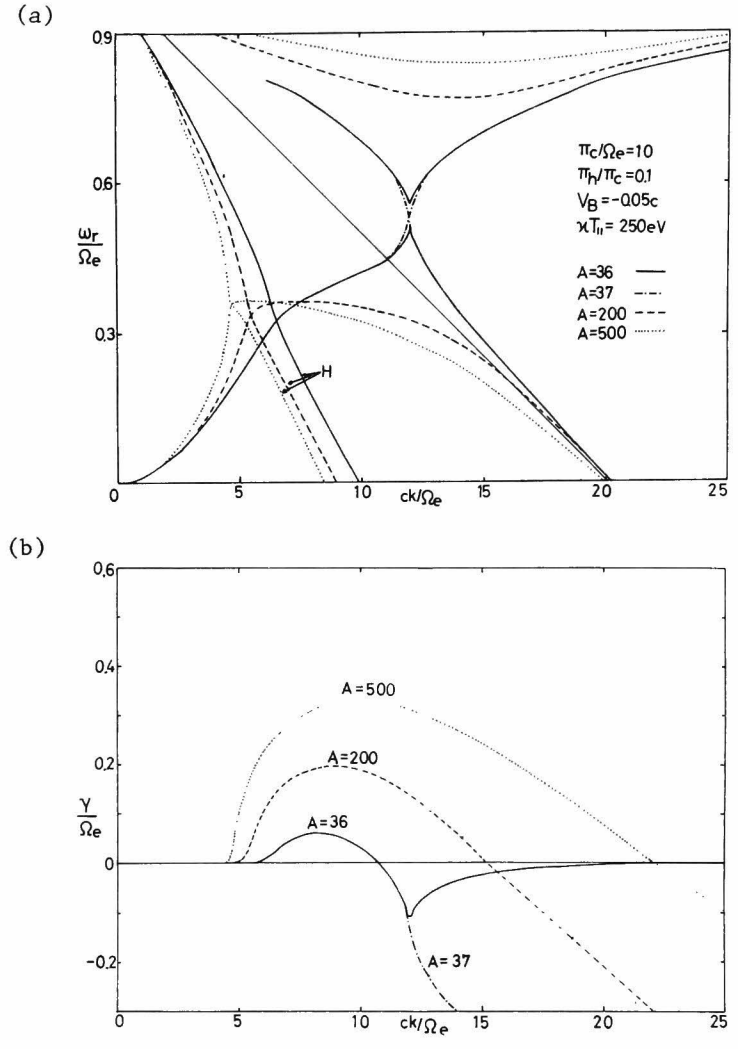

Fig. 6.4. Whistler dispersion in an anisotropic hot beam-plasma system. $T_{||}$ = constant. (a) Real part ω_r, imaginary part γ.

Fig.6.2(b). It is noted that the perpendicular thermal energy of the beam in both cases of Fig.6.2(b) and A = 500 in Fig.6.4 are the same, i.e., both $kT_{\perp}$ = 125 keV. The corresponding growth rate, however, is clearly different in the hot and cold beam cases. Comparing Fig.6.2(b) and Fig. 6.4, we can observe that the growth rate for large wavenumber is suppressed by a cyclotron damping effect due to a finite temperature in the case of the hot beam (Fig.6.4).

Figure 6.4 is useful in considering a transition of the instability characteristics between the temperature anisotropy type and beam type whistler instabilities. For small A such as A = 2, the real and imaginary dispersion curves resemble those for an anisotropic hot but stationary plasma which are shown in Fig.6.1. It should be noted that, different from the beamless case, the beam mode appears in an anisotropic hot beam-plasma system which does not, however, couple with the whistler mode for small A.

On the contrary, for large A such as A = 500, the dispersion curves of both real and imaginary solutions become similar to those for the cold beam type whistler instability as shwon in Fig.6.2(b) except for the previously mentioned cyclotron damping effect for large k. A transition between the two types is clearly observed for A = 36 and 37 using the present parameters.

6-5 Transition

In the previous section , we examined the transition from a cold beam to a hot anisotropic beam by assuming a bi-Maxwellian distribution for the beam. It is, however, difficult to observe the trasition in detail for the bi-Maxwellian beam due to the difficulty in searching for all

solutions of the disperison equation by Newton's method. Therefore, we discuss the transition by assuming a Cauchy (Lorentzian) distribution function for the beam, which enables us to obtain all the solutions of the dispersion equation. Such a transitional calculation from a cold beam case to a gentle bump case for an electrostatic mode instability was performed by O'Neil and Malmberg (1968).

The shifted Cauchy distribution function is given by

$$f_b(v_\perp, v_\parallel) = \frac{V_{T_\parallel}}{\pi} h_\perp(v_\perp)[(v_\parallel - V_B)^2 + V_{T_\parallel}^2]^{-1}, \tag{6.16}$$

where $V_{T_\parallel}$ is an effective parallel velocity. Substituting Eq. (6.16) into Eq. (6.1) and integrating over $v_\perp$ and $v_\parallel$, we obtain

$$c^2k^2 - \omega^2 + \frac{\Pi_c^2\omega}{\omega - \Omega_e} + \Pi_b^2\left[\frac{\omega - kV_B + i|k|V_{T_\parallel}}{\omega - kV_B - \Omega_e + i|k|V_{T_\parallel}}\right.$$

$$\left. + \frac{\frac{1}{2}k^2\langle v_\perp^2\rangle}{(\omega - kV_B - \Omega_e + i|k|V_{T_\parallel})^2}\right] = 0 \tag{6.17}$$

which is reduced to a fifth order polynomial of ω for a given k.

In order to see the transition of characteristics of the whistler mode instability from the beam type coupling to the temperature anisotropy type coupling, we present several detailed dispersion curves around a coupling region in the $\omega - k$ diagram for various parallel temperatures. The numerical results are shown in Fig.6.5 in succession in ascending order of $V_{T_\parallel}$ of the beam. A solid or dashed line indicates that the absolute value of the imaginary part of the solution is less or greater than $10^{-2}\Omega_e$, respectively.

In Fig.6.5(a), dispersion curves for a cold beam are shown. Degenerated complex conjugate solutions are seen in the beam branch. Figure 6.5(b) shows the case for $V_{T_\parallel} = 10^{-4}c$. The introduction of a small amount of

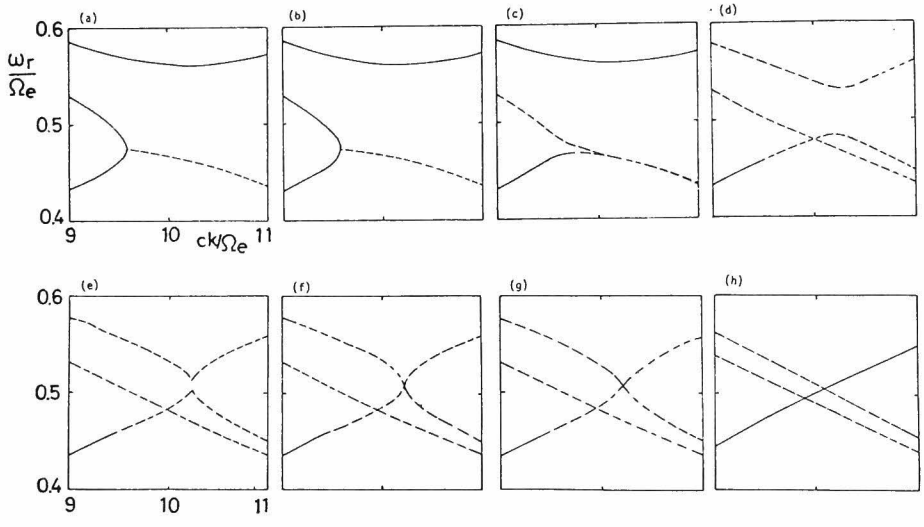

Fig. 6.5. Transition of a whistler dispersion from $V_{T\parallel} = 0$ to $V_{T\parallel} = 0.03c$. $V_{T\parallel}$ are (a) 0.0c, (b) $10^{-4}c$, (c) $10^{-3}c$, (d) 0.01c, (e) 0.011c, (f) 0.0111c, (g) 0.012c, and (h) 0.03c, respectively. Dashed lines indicate an absolute value of imaginary portion of the solution is greater than 0.01 Ω_e.

parallel temperature spread removes the degeneration of the complex conjugate solutions. An increase in $V_{T_{\parallel}}$ causes an intersection of the two beam modes as seen in Fig.6.5(c) which is for the case where $V_{T_{\parallel}} = 10^{-3}c$. As $V_{T_{\parallel}}$ is increased, a separation of the two beam modes becomes more conspicuous and, at the same time, the upper branch of the dispersion curves becomes closer to one of the beam modes [see Figs.6.5(d) and (e)]. At last these two approaching branches merge at a critical value $V_{T_{\parallel}c}$ ($V_{T_{\parallel}c}$ = 0.0111c) as shown in Fig.6.5(f). For $V_{T_{\parallel}}$ larger than $V_{T_{\parallel}c}$, one can see that the whistler mode branch exists continuously for a continuous change in ω although it is affected by the beam modes [see Figs. 6.5(f) and (g)]. For much larger values of $V_{T_{\parallel}}$, the whistler mode becomes uncoupled from the beam mode as seen in Fig.6.5(h).

It is interesting to note that the transition is topologically very similar to the case of electrostatic instabilities, although their coupling mechanism is quite different from the present whistler mode coupling.

6-6 Conclusions

We have compared the dispersion characteristics of the two types of whistler mode instabilities, i.e., the beam type and the temperature anisotropy type. A transition from one to the other is investigated by observing the change in dispersion characteristics for various temperature anisotropies of the anisotropic hot electron beam. It is clarified that both types mentioned here are only the two extreme special cases of the anisotropic hot beam case. When $V_B = 0$, the temperature anisotropy type instability occurs, while the beam type instability is realized when $T_{\parallel} = 0$ (or $A \to \infty$). Therefore, the energy source of the whistler instability is not the beam kinetic energy, but the perpendicular kinetic energy (i.e.,

thermal anisotropy) in any case. The beam velocity V_B only gives the effect of the Doppler shift of the unstable frequency.

Although this point has been understood since the work of Brice (1964), we have arrived at the same conclusion by examining the dispersion characteristics of whistler mode waves under various conditions. It is noted, however, that a rigorous necessary condition for instability of parallel propagating whistler waves is not the thermal (or temperature) anisotropy which is determined by the average characteristics of the distribution function. Instead, the most general statement of the whistler instability criterion is that the averaged distribution function only over $v_\perp$ has a slope of appropriate sign on the local surfaces defined by a resonance condition $V_R \equiv (\omega - \Omega_e)/k$. This condition is also applied to the quasilinear regime of whistler mode instability (Kennel and Engelman, 1966 and Matsumoto and Kimura, 1971)

Although the present analysis is limited to parallel propagation, any oblique propagation allows the possibility of the true beam instability.

CHAPTER 7

CONCLUDING REMARKS

In this thesis, propagation and instabilities of obliquely propagating whistler mode waves in a hot magnetospheric plasma are analysed.

In chapter 2, an instability with a large growth rate of obliquely propagating whistler mode waves is shown to exist in a transition between electrostatic and electromagnetic modes. This instability is a kind of the Harris type electrostatic instability and is considered as an extention of the whistler mode. The dependence of this instability on parameters, i.e., electron density and temparature anisotropy, is also discussed. It is expected that some types of VLF emissions can be accounted for by this instability.

Chapter 3 is an application of the instability clarified in chapter 2. Narrow-band hiss emissions observed by satellites are interpreted by this mechanism. The limited growth region at $f > f_H/2$ and sufficient spatial growth rate at an anisotropy $A = 2$ are clarified. It is noted from a calculation of the wave polarization that the emissions caused by this instability has a weak magnetic field component.

In chapter 4, analytical and approximated equations of growth rate in a 2-component (cold + bi-Maxwellian hot) plasma are derived. It is clarified that Landau damping in the oblique propagation does not always become larger even if the wave normal angle increases. Conditions for the growth rate to be minimal at $\theta = 0$ are obtained in the 2-component plasma. The necessary conditions are $f > f_H/2$ and $T_\perp > 2T_\parallel$. These equations are used to calculate the net growth along the ray paths of obliquely propagating non-ducted whistler mode waves in a model magnetosphere.

In chapter 5, a ray tracing algorithm in a warm plasma in the magnetosphere is established. It is demonstrated that the ray paths do not depend appreciably on electron temperature. However, it is clarified that there are regions where the waves are heavily damped by the Landau damping due to thermal effects. By making use of this damping, a possibility of estimation of the electron temperature in the magnetospheric plasma by satellite observation of Doppler shift and damping of a ground-based VLF signal is proposed.

In chapter 6, the dispersion characteristics of the two types of whistler mode instabilities, i.e., the temperature anisotropy type and the beam type and a transition between the two are investigated for a propagation along a magnetic field. It is clarified that both types are only the two extreme cases of the anisotropic hot beam case. The energy source of the whistler instability is the perpendicular kinetic energy (i.e., thermal anisotropy) in any case. The beam velocity only gives the effect of the Doppler shift. It is interesting to extend this analysis to those of obliquely propagating waves.

As a test of our theories, it is to be desired that a polarization of narrow band hiss stated in chapter 3 is measured and damping phenomena predicted in chapter 5 are observed. In order to calculate ray paths in the growing region or highly damped region, ray tracing in a hot plasma should be performed. Evaluation of the accumulated net growth along the path may also be interesting.

In conclusion, several dispersion and propagation characteristics of obliquely propagating whistler mode waves are clarified and applied to the interpretation of hiss emissions in the magnetosphere. A new technique to obtain ray paths in a warm plasma is developed. It is hoped that the results of this thesis are useful to the analysis of data observed by the EXOS-B and other satellites. It is also interesting to investigate

characteristics of obliquely propagating waves in nonlinear region.

APPENDIX A

Damping Rate Calculation

The hot plasma dispersion equation for a real k (i.e. k_r), namely

$$D(\omega, k_r) = 0 \tag{A.1}$$

can be written explicitly as $\omega(k_r)$. To obtain γ for a given frequency ω_o, we solve the equation

$$\mathrm{Re}[\ \omega(k_r)\ ] - \omega_o = 0 \tag{A.2}$$

by the method regula falsi (Hildebrand, 1956). When a solution of Eq.(A.2) is obtained, we can get $\partial\omega_r/\partial k_r$ approxiamtely as a by-product. The group velocity $\vec{v}_g$ is defined as

$$\vec{v}_g = (\partial\omega_r/\partial k_r)[\hat{k} - \hat{\theta}(1/k_r)(\partial k_r/\partial\theta)] \tag{A.3}$$

$$= (\partial\omega_r/\partial k_r)[\hat{k} + \hat{\theta}\tan\alpha], \tag{A.4}$$

where $\hat{k}$, $\hat{\theta}$ and α are the unit vector in the wave normal direction, the unit vector normal to $\hat{k}$ and coplanar with $\vec{v}_g$ and $\hat{k}$, and the angle between $\hat{k}$ and $\vec{v}_g$. On the other hand

$$\gamma = \mathrm{Im}[\ \omega(k_r)\ ] = -\vec{k}_i\cdot\vec{v}_g = -k_i(\partial\omega_r/\partial k_r) \equiv -k_i v_{gk}. \tag{A.5}$$

Therefore

$$k_i = -\gamma/v_{gk} = -\mathrm{Im}[\ \omega(k_r)\ ](\partial k_r/\partial\omega_r). \tag{A.6}$$

REFERENCES

Aikyo, K. and T. Ondoh, Propagation of nonducted VLF waves in the vicinity of the plasmapause, J. Radio Res. Lab., 18, 153, 1971.

Allis, W.P., S.J. Buchsbaum, and A. Bers, Waves in anisotropic plasmas, M.I.T. Press, Cambridge, 1963.

Anderson, R.R. and K. Maeda, VLF emission associated with enhanced magnetospheric electrons, J. Geophys. Res., 82, 135, 1977.

Angerami, J.J. and J.O. Thomas, Studies of planetary atmospheres: I-the distribution of electrons and ions in the earth's exosphere, J. Geophys. Res., 69, 4537, 1964.

Angerami, J.J., Whistler duct properties deduced from VLF observations made with the OGO-3 satellite near the magnetic equator, J. Geophys. Res., 75, 6115, 1970.

Aubry, M.P., J.Bitoun and Ph. Graff, Propagation and group velocity in a warm magnetoplasma, Radio Sci., 5, 635, 1970.

Bell, T.F. and O. Buneman, Plasma instability in the whistler mode caused by a gyrating electron stream, Phys. Rev., 133, A1300, 1964.

Bernstein, I.B. Waves in a plasma in a magnetic field, Phys. Rev., 109, 79, 1958.

Bitoun, J., Ph. Graff, and M. Aubry, Ray tracing in warm magnetoplasma and applications to topside resonances, Radio Sci., 5, 1341, 1970.

Brice, N., Fundamentals of very low frequency emission generation mechanisms, J. Geophys. Res., 69, 4515, 1964.

Brice, N. and C. Lucas, Influence of magnetospheric convection and polar wind on loss of electrons from the outer radiation belt, J. Geophys. Res., 76, 900, 1971.

Brinca, A. L., On the stability of obliquely propagating whistlers, J. Geophys. Res., 77, 3495, 1972.

Budden, K.G., Radio waves in the ionosphere, Ch. 14, Cambridge University Press, London, 1961.

Burtis, W.J. and R.A. Helliwell, Magnetospheric chorus: occurence patterns and normalized frequency, Planet. Space Sci., 24, 1007, 1976.

Burton, R.K. and R.E. Holzer, The origin and propagation of chorus in the outer magnetosphere, J. Geophys. Res., 79, 1014, 1974.

Coroniti, F.V., R.W. Fredricks, C.F. Kennel, and F.L.Scarf, Fast time resolved spectral analysis of VLF banded emissions, J. Geophys. Res., 76,2366,1971.

Coroniti, F.V., F.L.Scarf, C.F. Kennel, W.S. Kurth, and D.A. Gurnett, Detection of Jovian whistler mode chorus: Implication for the Io torus aurora, Geophys. Res., Lett., 7, 45, 1980.

Crawford, F.W., Cyclotron harmonic waves in warm plasmas, Radio Sci., 69D, 789, 1965.

Cuperman, S. and W. Landau, On the enhancement of the whistler mode instability in the magnetosphere by cold plasma injection, J. Geophys. Res., 79, 128, 1974.

Cuperman, S. and A. Sternlieb, Obliquely propagating unstable whistler waves: a computer simulation, J. Plasma Phys., 11, 175, 1974.

Decreau, P.M.E., J. Etcheto, K. Knott, A. Pedersen, G.L. Wrenn, and D.T. Young, Multi-experiment determination of plasma density and temperature, Space Sci. Rev., 22, 633, 1978.

Dory, R.A., G.E. Guest, and E.G. Harris, Unstable electrostatic plasma waves propagating perpendicular to a magnetic field, Phys. Rev. Lett., 14, 131, 1965.

Eviatar, A., A.M. Lenchek, and S.F. Singer, Distribution of density in an ion-exospehre of a nonrotating planet, Phys. Fluids, 7, 1775, 1964.

Fried, B.D. and S.D. Conte, The plasma dispersion function, Academic Press, New York , 1961.

Gautschi, W., Efficient computation of the complex error function, SIAM J. Number. Anal., 7, 187, 1970.

Gitomer, S.J., D.W. Forslund, and L. Rudsinski, Numerical simulation of the Harris instability in two dimension, Phys. Fluids, 15, 1570, 1972.

Guest, G.E. and R.A. Dory, Microinstability of a mirror-confined plasma, Phys. Fluids, 8, 1853, 1965.

Guest, G.E. and D.J. Sigmar, Stability of microwave-heated plasmas, Nucl. Fusion, 11, 151, 1971.

Hamelin, M. and C. Beghin, Electromagnetic and electrostatic waves in a multicomponent plasma near the lower hybrid frequency, J. Plasma Phys., 15, 115, 1976.

Harris, E.G., Unstable plasma oscillations in a magnetic field, Phys. Rev. Lett., 2, 34, 1959.

Harris, E.G., Plasma instabilities associated with anisotropic velocity distibutions, J. Nucl. Energy, Part C, 2, 138, 1961.

Haselgrove, J., Ray theory and a new method for ray tracing, Proc. Cambridge Conf. Phys. Ionosphere, Phys. Soc. London, 355, 1954.

Helliwell, R.A., Whistlers and related ionospheric phenomena, Stanford Univ. Press, Stanford,Carifornia, 1965.

Hashimoto, K. and I. Kimura, Oblique whistler mode propagation in a hot plasma, Rept. Ionos. Space Res. Japan, 27, 73, 1973.

Hildebrand, F.B., Introduction to Numerical Analysis, p. 446, McGraw-Hill, New York, 1956.

Hashimoto, K. and H. Matsumoto, Temperature anisotropy and beam type whistler instabilities, Phys. Fluids, 19, 1507, 1976.

Hashimoto, K. and I. Kimura, Obliquely propagating whistler mode waves in cold plasmas permeated by dilute low-β anisotropic plasmas, J. Plasma Phys., 18, 1, 1977.

Hashimoto, K., I. Kimura, and H. Kumagai, Estimation of electron temperature by VLF waves propagating in directions near the resonance cone, Planet. Space Sci., 25, 871, 1977.

Hashimoto, K. and I. Kimura, A generation mechanism of narrow band hiss emissions above one half the electron cyclotron frequency in the outer magnetosphere, submitted to J. Geophys. Res., 1980.

Jacquinot, J., C. Leloup, J.P. Poffe, M. de Pretis, F. Waelbroeck, P.Evrard, and J. Ripault, Etude de microinstabilites dans un plasma d'electrons chauds confine, Plasma Physics and Controlled Nuclear Fusion Research, Vol. II, 347, IAEA, Vienna, 1969.

Jacquinot, J. and C. Leloup, Growth rate calculations for electron-electron modes with pressure anisotropy and cold plasma, Phys. Fluids, 13, 2332, 1970.

Kennel, C., Low-frequency whistler mode, Phys. Fluids, 9, 2190, 1966.

Kennel, C.F. and F. Engelmann,Velocity space diffustion from weak plasma turbulence in a magnetic field, Phys. Fluids, 9, 2377, 1966.

Kennel, C.F. and H. E. Petscheck, Limit on stably trapped particle fluxes, J. Geophys. Res., 71, 1, 1966.

Kennel, C.F. and R.M. Thorne, Unstable growth of unducted whistlers propagating at an angle to the geomagnetic field, J. Geophys. Res., 72, 871, 1967.

Kimura, I., Amplification of the VLF electromagnetic wave by a proton beam through the exosphere -an origin of the VLF emissions-, Rept. Ionos. Space Res. Japan, 15, 171, 1961.

Kimura, I., Effect of ions on whistler-mode ray tracing, Radio Sci., 1, 269, 1966.

Kimura, I., On observations and theories of the VLF emissions, Planet. Space Sci., 15, 1427, 1967.

Kimura, I. and M. Kawai, Ray path in a stratified absorbing medium, IEEE Trans. Antenna and Propagation, AP-24, 515, 1976.

Lee, J.C. and F.W. Crawford, Stability analysis of whistler amplification, J. Geophys. Res., 75, 85, 1970.

Lewis, R.M. and J.B. Keller, Conductivity tensor and dispersion equation for a plasma, Phys. Fluids, 5, 1248, 1962.

Liemohn, H.B., Cyclotron - resonance amplification of VLF and ULF whistlers, J. Geophys. Res., 72, 39, 1967.

Maeda, K. and I. Kimura, A theoretical investigation on the propagation path of the whistling atmospherics, Rept. Ionos. Space Res. Japan, 10, 105, 1956.

Maeda, K., Cyclotron side-band emissions from ring-current electrons, Planet. Space Sci., 24, 341, 1976.

Maeda, K., P.H. Smith, and R.R. Anderson, V.L.F. emission from ring-current electrons, Nature, 263, 37, 1976.

Matsumoto, H., S. Miyatake, and I. Kimura, Convective beam cyclotron instability and discrete VLF emissions in the magnetosphere, Rept. Ionos. Space Res. Japan, 24, 207, 1970.

Matsumoto, H. and I. Kimura, Linear and nonlinear cyclotron instability and VLF emissions in the magnetospehre, Planet. Space Sci., 19, 567, 1971.

Muldrew, D.B. and M.F. Estabrooks, Computation of dispersion curves for a hot magnetoplasma with application to the upper-hybrid and cyclotron frequencies, Radio Sci., 7, 579, 1972.

Muldrew, D.B. and A. Gonfalone, Resonance cone and Bernstein wave interference patterns in a magnetoplasma, Radio Sci., 9, 873, 1974.

O'Neil, T.M. and J.H. Malmberg, Transition of the dispersion roots from beam-type to Landau-type solutions, Phys. Fluids, 11, 1754, 1968.

Oya, H., Conversion of electrostatic plasma waves into electromagnetic waves: numberical calculation of the dispersion relation for all wavelengths, Radio Sci., 6, 1131, 1971a.

Oya, H., Verification of theory on weak turbulence relating to the sequence of diffuse plasma resonances in space, Phys. Fluids, 14, 2487, 1971b.

Ozawa, Y., I. Kaji, and M. Kito, Stability criterion for longitudinal plasma waves in a magnetic field, Plasma Phys., 4, 271, 1962.

Scharer, J.E. amd A.W. Trivelpiece, Cyclotron wave instabilities in a plasma, Phys. Fluids, 10, 591, 1967.

Serbu, G.P. and E.J.R. Maier, Low-energy electrons measured on IMP 2, J. Geophys. Res., 71, 3755, 1966.

Shima, Y. and L.S. Hall, Electrostatic instabilities in a plasma with anisotropic velocity distibution, Phys. Rev., 139, A1115, 1965.

Sitenko, A.G. and K.N. Stepanov, On the oscillation of a electron plasma in a magnetic field, Soviet Phys. J.E.T.P., 4, 512, 1957.

Smith, R.L., R.A. Helliwell, and I.W. Yabroff, A theory of trapping of whistlers in field-aligned columns of enhanced ionization, J. Geophys. Res., 65, 815, 1960.

Stix,T.H., The theory of plasma waves, McGraw-Hill, New York, 1962.

Sudan, R.N., Plasma electromagnetic instabilities, Phys. Fluids, 6, 57, 1963.

Taylor, W.W.L., and S.D. Shawhan, A test of incoherent Cerenkov radiation for VLF hiss and other magnetospheric emissions, 79, 105, 1974.

Thorne, R.M. and C.F. Kennel, Quasi-trapped VLF propagation in the outer magnetosphere, J. Geophys. Res., 72, 857, 1967.

Thorne, R.M., E.J. Smith, R.K. Burton, R.E. Holzer, Plasmaspheric hiss, J. Geophys. Res., 78, 1581, 1973.

Yabroff, I., Computation of whistler ray paths, J. Res., N.B.S., 65D, 485, 1961.

Young, T.S.T., J.D. Callen, and J.E. McCune, Flute-like instabilities in mirror-confined plasmas with broad $v_\perp$-distributions, Phys. Fluids, 14, 2783, 1971.

Young, T.S.T., J.D. Callen, and J.E. McCune, High-frequency electrostatic waves in the magnetosphere, J. Geophys. Res., 78, 1082.,1973.

Young, T.S.T., Electrostatic waves at half electron gyrofrequency, J. Geophys. Res., 79, 1985, 1974.